Investigation of Structure-Property Relationships of Polythiophenes through Rational Molecular Design

Chunhui Zhao

August 2016

Investigation of Structure-Property Relationships of Polythiophenes through Rational Molecular Design

Chunhui Zhao
Doctoral Program in Materials Science and Engineering

Submitted to the Graduate School of
Pure and Applied Sciences
in Partial Fulfillment of the Requirements
for the Degree of Doctor of Philosophy in
Engineering

at the
University of Tsukuba

Contents

Chapter 1 General introduction

1.1 Conjugated polymers

Polymers, which are generally referred to as plastics, are insulated materials. As is well known, plastics have been wildly used due to its attractive mechanical and insulated properties, which means plastics do not conduct electricity. However, in 1977, Shirakawa, MacDiarmid and Heeger discovered that oxidation with halogen vapor, such as chlorine, bromine, or iodine vapor, made polyacetylene (PA) film 10^9 times more conductive than it was originally.[1)] In analogous with the "doping" of semiconductor, the oxidation process for polymer was also called "doping". The resulted doped PA showed a conductivity of 10^5 S/m, which was higher than that of any previously reported polymer. This result was a surprising discovery because it indicated that polymers can conduct "plastic electricity". From then on, entirely a new scientific field of research on conductive polymers have been generated. Huge efforts were devoted to the development of conductive polymers in the past decades, such as constructing new conductive polymers, investigating the mechanism of charge carrier conduction, applying polymers to new devices and so on.

Conductive polymers, which are also referred to as conjugated polymers (CPs), are organic macromolecules consisting of alternating double- and single-bonds along the polymer main chain. Through chemical synthetic methods, a large number of different CPs and their derivatives and copolymers were synthesized, such as polyacetylene (**PA**), polyaniline (**PANI**), polypyrrole (**PPy**), polythiophene (**PT**), polyphenylene (**PPP**) and so on (Figure 1-1). Such unique structure creates a system of delocalized π-electrons, which can result in interesting and useful optical, magnetic and electronic properties.

Due to the contribution on the discovery and development of conducting polymers, Heeger, MacDiamid, and Shirakawa earned Nobel Prize in Chemistry in 2000.

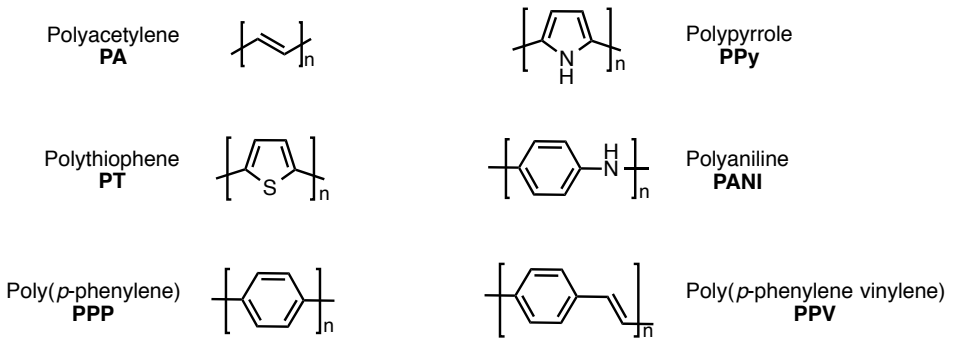

Figure 1-1. Some examples of conjugated polymers (CPs).

1.2 Structure and charge conduction

The structure of CPs plays a dominant role in determining their physical properties. Understanding the delocalized π-electrons, which created by the unique structure of CPs, is important to the development of CPs and their physical properties. Here, we use PA as an example to introduce π-electrons. CPs have the backbone of contiguous sp^2 hybridized carbon centers. Each carbon in backbone uses three sp^2 hybrid atomic orbitals couple with two hydrogens and two other carbons forming three sigma bonds. Then, one valence electron resides in the remaining p_z orbital on each carbon center of PA backbone (Figure 1-2a-c). It is well known that two p_z orbitals can overlap and couple to each other forming a π bond (Figure 1-2d). If the backbone of PA without any distortion or twist, all p_z orbitals could well overlap and couple to each other forming a long one dimensional (1D) or molecule wide delocalized set of orbital. However, in reality, due to the well-known Peierls distortion mechanism in all 1-D metals, every adjacent p_z orbitals are paired on PA backbone forming π bonding orbitals (Figure 1-2e-g).[2] The electrons in these delocalized π orbitals were so-called π-electrons. But, π-electrons are not enough to make CPs conductive. Through "doping", charge carriers in the form of "holes" were generated by removing some of these delocalized electrons. When an electron is missing, a hole is generated, which, after filling by another neighbouring electron, giving rise to a new hole. In such a way, the charge is able to migrate for a long distance.[3] As a result, CPs can conduct "plastic electricity".

Charge conduction is the most important property of CPs, owing to which, CPs have received an increasing amount of attention as functional materials that are applicable to a variety of optoelectronic devices. However, despite the practical applications developed so far, the mechanism of charge carrier conduction through the polymeric materials is still a subject of great controversy. There have had two reasons. First, σ-dimers, π-dimers, and polaron pairs have been proposed as the charge carrying species, in addition to the simple polaron-bipolaron model. These charge carriers usually coexist at a given doping level but are often indistinguishable, which makes elucidation of the conduction mechanism difficult. Second, there are two conceivable charge carrier transport pathways in the polymeric materials, namely, intrawire and interwire processes. Chain conformational changes (relevant to the *intra*wire process) and π-stacking formation (*inter*wire process) are simultaneously affected by self-assembly in conventional CPs. Therefore, in practice, the contributions of these two processes to electrical conductivity cannot be assessed independently.[4]

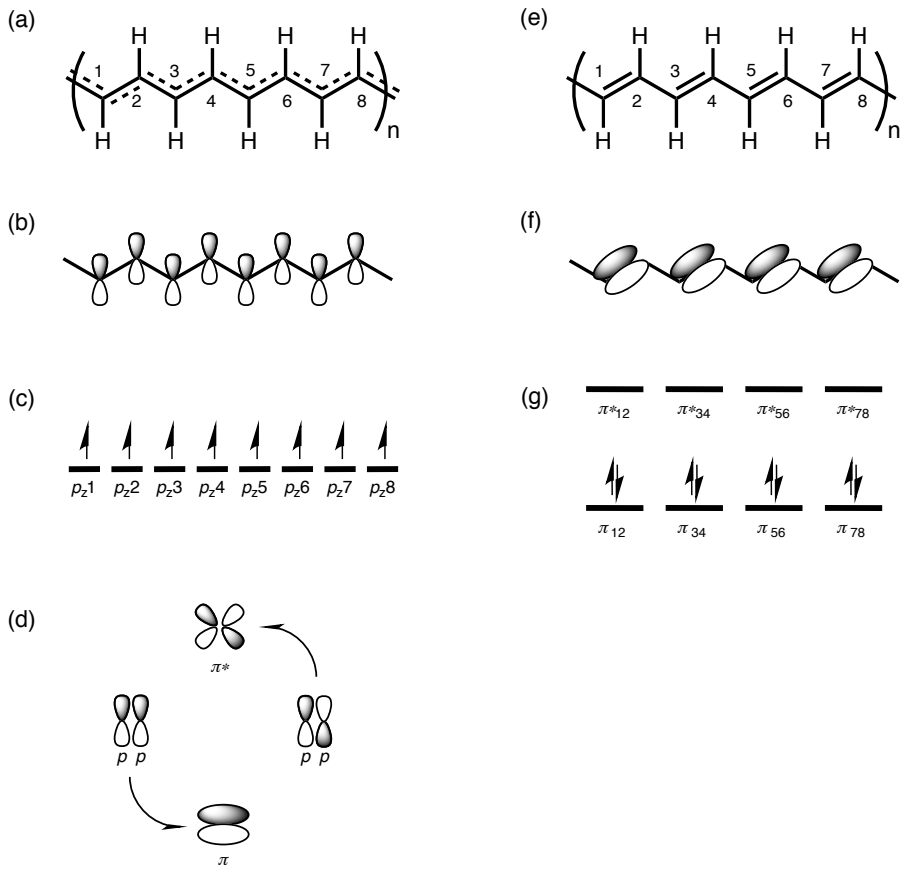

Figure 1-2. Schematic representation of C-C double π bonds, represented in (a) chemical structure of PA assuming no 1-D Peierls distortion; (b) atomic p_z orbital of PA backbone; (c) scheme of frontier orbitals and valence electron of PA assuming no 1-D Peierls distortion; (d) scheme of a pair of π-type molecular orbitals formed form the overlap of two vertically aligned parallel *p* atomic orbitals; (e) chemical structure of PA assuming 1-D Peierls distortion applicable; (f) scheme of PA conjugated backbone showing π bonding orbitals; (g) scheme of frontier orbitals and valence electron of PA assuming 1-D Peierls distortion.

1.3 Practical applications

CPs have attracted large amount of attentions, not only because of their charge carrier conductive properties but also their mechanical properties. In fact, the biggest advantage of CPs is their processability from polymer solution at room temperature, which mainly as a result of dispersion. They are generally not thermosoftening plastic, which means they are not thermoformable. They are organic materials, like insulating polymers. Therefore, CPs become the promising candidates as materials used in various flexible and printable organic electronics and optoelectronics, such as organic lighting-emitting diode (OLED), organic field-effect transistor (OFET), organic solar cell (OSC), chemical sensors, and so on.[5)]

However, it is still difficult to find CPs which can leads to commercialized applications. At the same time, CPs still have few large-scale applications. They have many limitations, including the manufacturing cost, toxicity, inability to directly melt process, material inconsistencies and so on. Therefore, construing new CPs is important to the development of organic electronics and optoelectronics.

1.4 Molecular design

As stated above, although CPs become the promising candidates as materials used in various devices, but CPs still did not go to real applications. Further more, the mechanism of charge transport and the nature of charge carriers are not revealed. Therefore, there have a plenty of room for research in conjugated polymer system, especially design and synthesis of CPs.

The structure of CPs plays a dominant role in determining their physical properties, and thus affects the performance of organic devices. Thus, it is essential to clarify the relationship between structures and properties. Those relationships could pave the way to new design principle of polymers, better performance of devices and deeper understanding on the nature of charge.

1.5 Polythiophenes (PTs)

Among the various CPs, polythiophenes (PTs) display the most unique properties due to the best combination of three advantages. First one is the incredible synthetic versatility. PTs have been synthesized and modified easily by transition metal-catalyzed cross-coupling reactions,[6] with which the electronic properties can be tuned in a wide range. Second one is the high chemical stability; PTs are stable both in doped state and undoped state. Accordingly, their unique optical, electronic and redox properties in solution can be characterized by many methods, as well as those in the solid state. Third one is efficient conjugation length. Applications in organic and molecular electronics call for stabilization of the conjugated chain and excellent charge transport properties, both of which are facilitated by the high polarization of sulfur atoms in thiophene rings.[7] Although many different type of PTs have been designed and synthesized, also it is still difficult to find one PT which can leads to excellent performance of electronics and optoelectronics. While, the mechanism of charge transport and the nature of charge carriers are still unclear. Therefore, molecular design for new PTs are necessary for understanding the relationships between structures and properties. To this end, we have focused on structural parameters of polythiophenes such as dihedral angle, dielectric constant, and regioregularity and established rational molecular design to investigate the structure-property relationships.

1.6 Molecular design for PTs

1.6.1 Poly(3-alkylthiophenes)

There are many different structural parameters in macromolecules, such as molecular weight, polydispersity, regioregularity, planarity and so on. Through molecular design and synthetic scheme, the structural parameters can be controlled. With the controlled structure parameters, the physical properties of polymer can be discussed. Poly(3-alkylthiophene)s (P3AT) have been widely investigated, and their well-defined structures and good morphologies through π-stackings among polymer backbones leads to the enhanced performance in many devices.[2,5,8-10)]

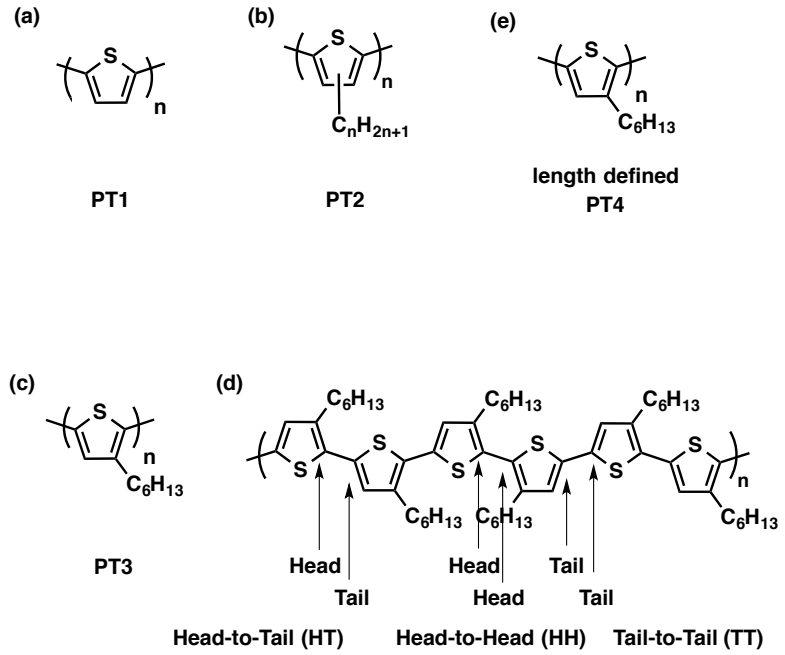

Figure 1-3. Chemical structure of poly(3-alkylthiophenes) (P3AT): (a) **PT1**[11-12)] (b) **PT2**[13)] (c) **PT3**[14)], (e) **PT4**[15-16)]. And (d) Regiochemcial coupling in poly(3-hexylthiophene) (P3HT): Head-to-Tail (HT) coupling, Head-to-Head (HH) coupling, Tail-to-Tail (TT) coupling.

In 1980, unsubstituted polythiophene (**PT1**, Figure 1-3a) was synthesized successfully through chemical preparation method for the first time. Yamamoto *et al.*[11)] and Lin *et al.*[12)] reported the synthetic scheme through metal-catalyzed polycondensation polymerization using 2,5-dibromothiophene as starting material. The obtained **PT1** has planar backbone. However due to the planarity of backbone, **PT1** has inherently poor solubility in common organic solvents, which limits the formation of **PT1** with higher molecular weight. Even **PT1** with low molecular weight is insoluble in tetrahydrofuran (THF). In 1985, Elsenbaumer *et al.*[13)] reported environmentally stable and soluble poly(3-alkyl-thiophene) (**PT2**, Figure 1-3b)

for the first time. Although the backbones of **PT2** are not planar, **PT2** still showed reasonably high electrical conductivity after doping. So far, regardless many efforts have devoted to synthesize P3AT, the regioregularity of PTs can't be controlled. The regiochemical control over coupling between adjacent thiophene ring is very important because it can significantly affect the packing of polymer chains. As shown in Figure 1-3d, there are three different coupling types: head-to-tail (HT) coupling, head-to-head (HH) coupling and tail-to-tail (TT) coupling. HT-coupled P3AT were expected to have more planar conformation leading to better conjugation. HH coupling and TT coupling, which are referred to as structural defect in P3AT, are unfavorable coupling because they cause damage to the packing among polymer chains. In 1992, McCullough *et al.*[14] first synthesized regioregular P3AT (**PT3**, Figure 1-3c) having ~ 100% HT couplings through Kumada cross-coupling reaction using 2-bromo-5-(bromomagnesio)-3-alkyl-thiophene as starting materials.

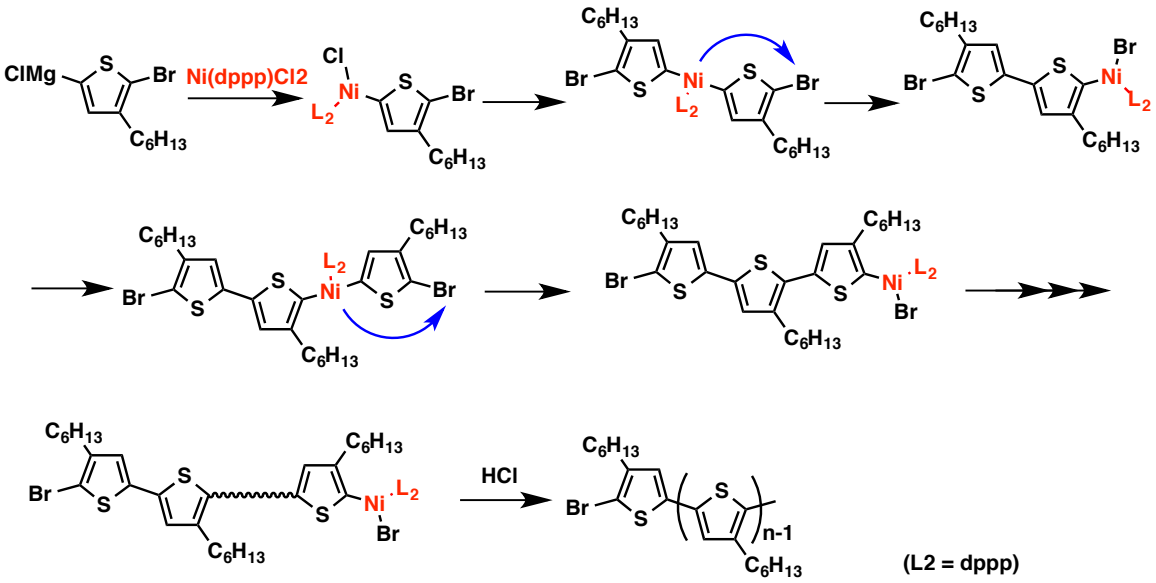

Figure 1-4. Proposed mechanism of catalyst transfer polymerization method.[17]

In 2004, McCullough *et al.*[15] and Yokozawa *et al.*[16] independently reported regioregular poly(3-hexylthiophene) (P3HT) with defined length. They simultaneously developed catalyst transfer polymerization (CTP) method using Nickel (Ni) catalyst system. The defined length and low polydispersity indicated that the monomer were polymerized in a chain growth manner. As shown in Figure 1-4, the mechanism of this chain growth polymerization was proposed.[17] The well-defined P3HT is one of most important polythiophene reported so far because through defined structural parameters, the structure-

properties relationships were studied, especially, the relationship between packing structure and charge mobility has been clarified.[9)]

1.6.2 Poly(3,4-ethylene-dioxythiophene) (PEDOT)

Poly(3,4-Ethylene-dioxythiophene) (PEDOT) (**PT5**, Figure 1-5a) was developed by scientists at Bayer AG research laboratories in 1980s in Germany.[18)] However, **PT5** encounter the solubility issues which hinder the applications. Jonas *et al.*[19)] reported that the problem can be circumvented by using poly(styrenesulfonic acid) (PSS). An aqueous solution was observed when PSS was introduced during the polymerization of EDOT. PSS was considered as charge-balancing dopant in the aqueous PEDOT/PSS blend (Figure 1-5b). The resulted PEDOT/PSS blend formed good films which showed high conductivity and stability.[18)] Now, PEDOT/PSS blend is an important PT-based material because of this unsurpassed stability and high electronic conductivity. Alemán *et al.*[20)] found that the attractive S – O intramolecular interactions (Figure 1-5a, dotted line) and π-conjugation, geometric restrictions and electron donating effects in **PT5** are responsible for the planarity of backbone. More importantly, PEDOT shows low bandgap between highest occupied molecular orbital (HOMO) and lowest unoccupied molecular orbital (LUMO). HOMO-LUMO bandgap is one key factor to evaluate new CPs. As a result, PEDOT complex with poly(styrenesulfonic acid) (PSS) becomes one of the most useful PT-based materials in industry. The complex showed good properties in many applications including antistatic and conductive coatings, electronic components, OLED, OSC and so on.[5)]

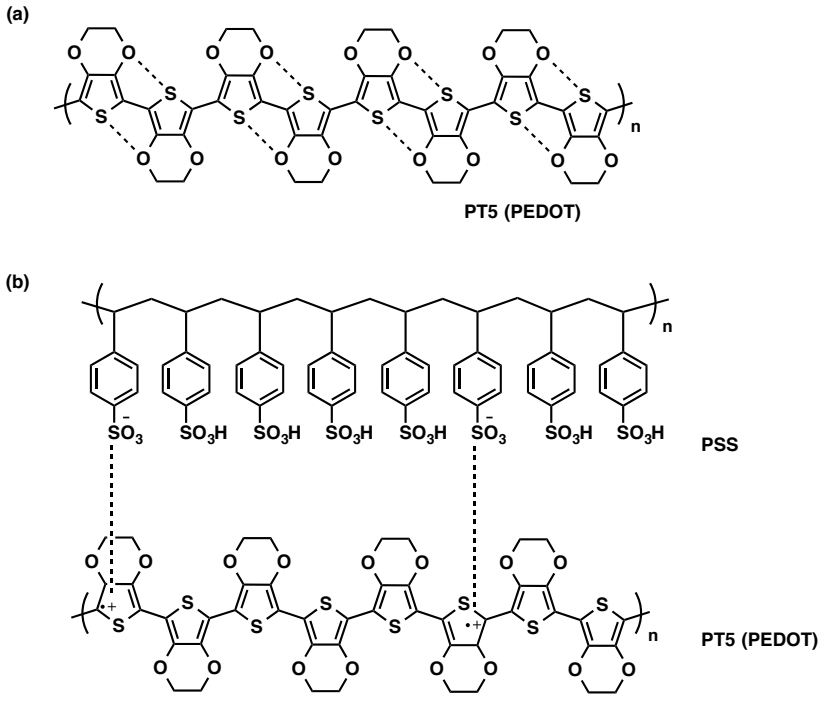

Figure 1-5. Chemical structure of (a) poly(3,4-ethylene-dioxythiophene) (PEDOT) (**PT5**), S – O intramolecular interactions (dotted line) (b) PEDOT/poly(styrenesulfonic acid) (PSS) blend.

1.6.3 PTs for OFET

CPs have recently become the key component in OFETs and often determined the performance of OFETs. As one of the most studied CPs, P3AT having well-defined structure has been applied for OFETs, however due to the relatively low charge carrier mobility, new design strategies has been explored so far. By molecular design, planarity and side chain density can be tuned. General strategies of the molecular design for OFET application of CPs as following: (1) introducing long alkyl side chains on polymer backbone for better solubility and self-assembly, (2) introducing more planar thiophene segment for the planarity of polymer backbone, (3) introducing some functional group in the polymer backbone for decreasing HOMO level and enhancing π- π interaction among polymer chains.

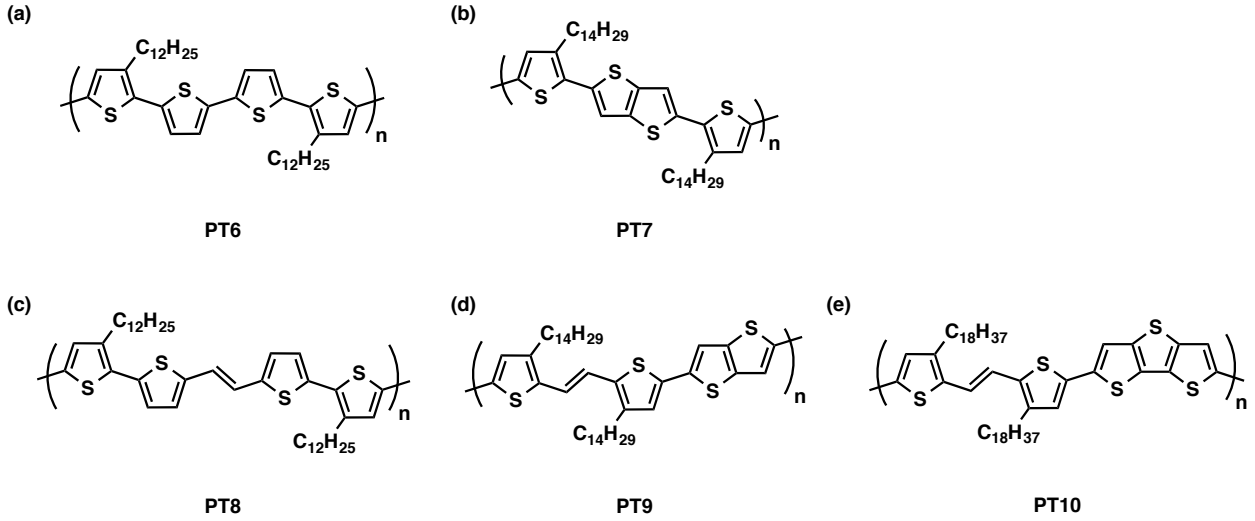

Figure 1-6. Chemical structures of p-type PTs for OFET: (a) **PT6**[21-22], (b) **PT7**[23], (c) **PT8**[24], (d) **PT9**[25], (e) **PT10**[26].

Ong *et al.*[21-22] designed and synthesized **PT6**, in which unsubstituted bithiopthene as segment was introduced into monomer (Figure 1-6a). **PT6** showed better stability due to the decreased density of side chains. The charge carrier mobility reached 0.14 $cm^2V^{-1}s^{-1}$ while I_{on}:I_{off} ratio reached 10^7. However with increased air humidity, the performance of OFET decreased. In 2006, McCulloch *et al.*[23] designed and synthesized **PT7**. (Figure 1-6b) The HOMO level of **PT7** decreased 0.3 eV compared with that of P3HT. More importantly, it was revealed that **PT7** forms relatively large domein size in its liquid crystalline phase, the area of which reached about ~ 200 nm and the charge carrier mobility reached 0.72 $cm^2V^{-1}s^{-1}$. Poly(thiophene vinylene) (PTV) is another class of CP, which wildly used in electronics. In 2009, Kim *et al.*[24] designed and synthesized **PT8** (Figure 1-6c). With introduced vinylene group, **PT8** showed high charge

carrier mobility of 0.15 $cm^2V^{-1}s^{-1}$ in OFET. In 2014, Fei *et al.*[25] designed and synthesized **PT9** (Figure 1-6d). **PT9** based OFET showed high charge carrier mobility due to the planarity of polymer backbone. The OFET charge carrier mobility of **PT9** reached 4.6 $cm^2V^{-1}s^{-1}$. Later, Kim *et al.*[26] designed and synthesized **PT10** based on the previously research (Figure 1-6e). The charge carrier mobility of **PT10** based OFET reached 3.91 $cm^2V^{-1}s^{-1}$. Those CPs are all p-type PTs.

The number of n-type PTs is still limited. In 2008, Facchetti *et al.*[27] designed and synthesized **PT11** through Stille coupling reaction (Figure 1-7a). The electron mobility of **PT11** based OFET reached 0.002 $cm^2V^{-1}s^{-1}$. At the same time, they also designed and synthesized **PT12** (Figure 1-7b). The electron mobility reached 0.06 $cm^2V^{-1}s^{-1}$, which is 30 times higher than that of **PT11**. This difference was contributed to the different packing nature of two polymers in solid state. With higher ordered structure, higher electron mobility can be obtained. In 2008, Marks *et al.*[28] designed and synthesized **PT13**. The LUMO level of **PT13** reached -3.47 eV, while its mobility in OFET was determined to be 0.011 $cm^2V^{-1}s^{-1}$.

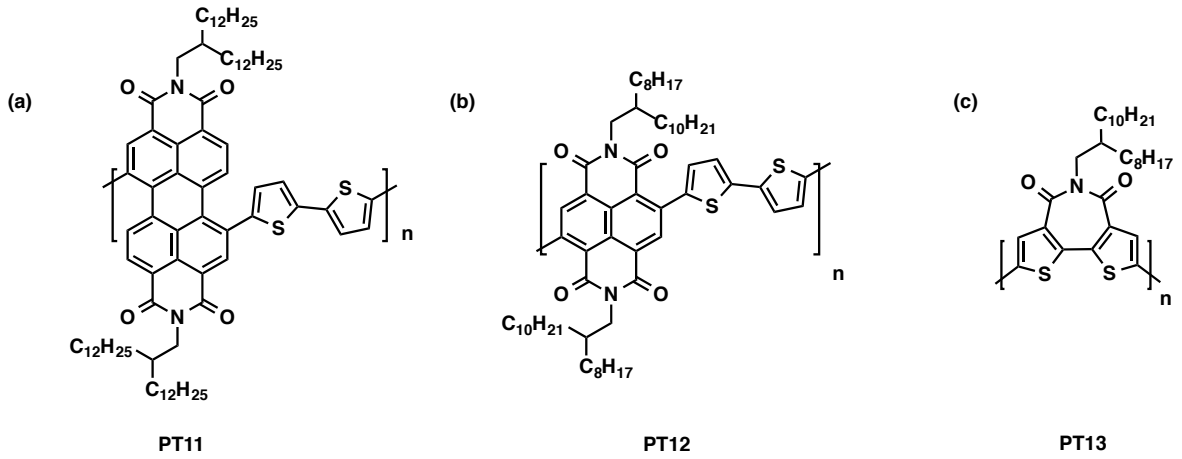

Figure 1-7. Chemical structures of n-type PTs for OFET: (a) **PT11**[27], (b) **PT12**[27], (c) **PT13**[28].

1.6.4 PTs for OLED

PTs have been also used as key materials in OLED. Their incredible synthetic versatility makes polymer have different HOMO-LUMO level through tuning functional groups on the backbone. This indicates that PTs can show various colors in OLED. However, the luminescence efficiency of most PTs in the solid state is relative low. This may due to the strong interactions among polymer main chains.[5] Here, we showed some examples of PTs, whose HOMO-LUMO level and twisted angle of thiophenes are considered in molecular design.

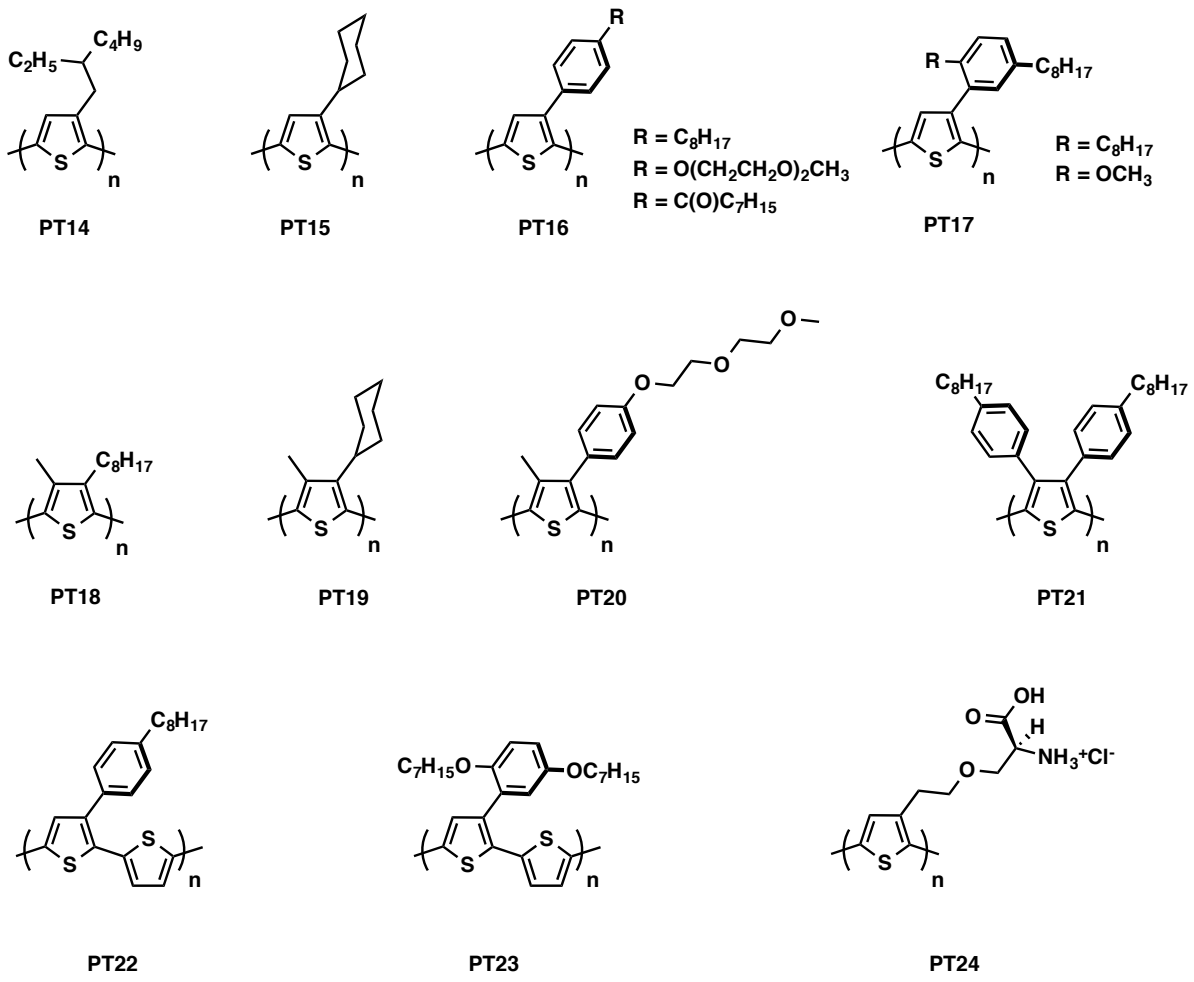

Figure 1-8. Chemical structures of PTs for OLED: **PT14** – **PT24**.

In 1991, Ohmori *et al.*[29-30] reported the first PT based OLEDs. Red – orange – emitting color was observed by using P3ATs as materials. From then on, a large number of PTs exhibitiing emissions covering the full visible region was developed through tuning functional group in PTs. Inganäs *et al.*[31-35] designed and synthesized a wide range of PTs (**PT18** – **PT24**). Those PTs (Figure 1-8) showed full visible range of light emitting from red to blue. It was found that although the structures of PTs are similar, the light emitting property is not predictable because many factors such as dihedral angle, regioregularity, steric hindrance and so on should be taken into consideration.

1.6.5 PTs for sensors

When introducing molecular recognition moieties on the CPs through molecular design, the changes in photophysical properties of CPs upon recognition events can be utilized for the creation of chemosensor.

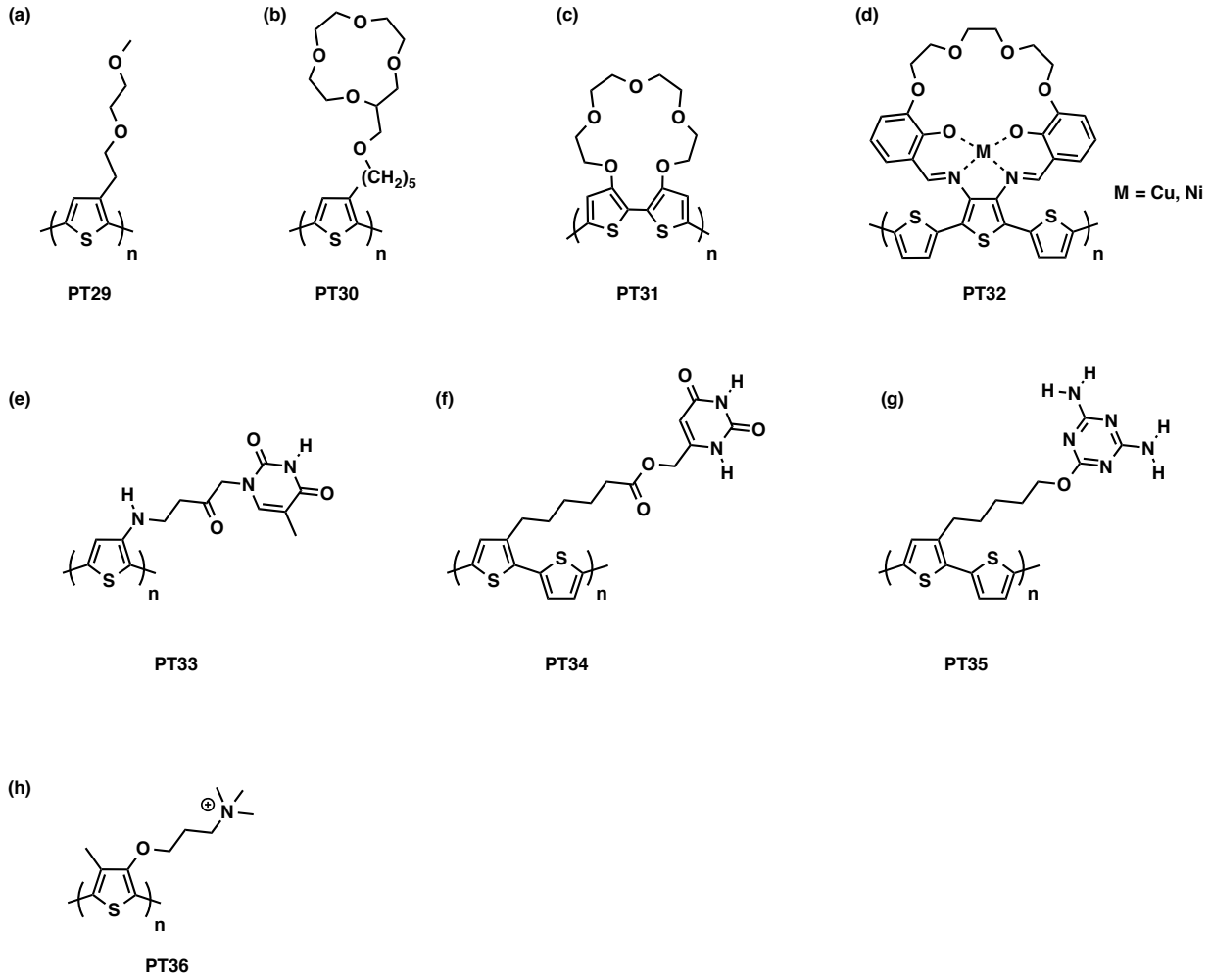

Figure 1-9. Chemical structures of PTs for host gust chemistry: (a) **PT29**[36], (b) **PT30**[37], (c) **PT31**[38], (d) **PT32**[39], (e) **PT33**[40], (f) **PT34**[41], (g) **PT35**[42].

In 1989, Roncali *et al.*[36] designed and synthesized **PT29** (Figure 1-9a). **PT29** undergoes a specific interaction with lithium cation. In 1993, Bäuerle *et al.*[37] designed and synthesized **PT30** (Figure1-9b). 12-Crown-4 was introduced on the side chain of PT, which makes **PT30** attract ions. Also in 1993, Swager *et al.*[38] designed and synthesized **PT31** (Figure 1-9c). **PT31** showed an ion-specific UV-Vis response. In 2004, Reynolds *et al.*[39] designed and synthesized **PT32** (Figure 1-9d). **PT32** having Schiff base moiety showed the ability simultaneously to coordinate and respond to metal ions and non-ionic molecules. In 2006, Wang *et al.*[40] designed and synthesized **PT33** (Figure 1-9e). **PT33** showed fluorescence quenching selectively in response to Hg^{2+} because of the aggregation. While, some PTs can be applied for the detection of biological molecules. In 1998, Bäuerle *et al.*[41] designed and synthesized **PT34** and **PT35** (Figure 1-9f-g), which can detect the purine or pyrimidine. In 2005, Shinkai *et al.*[42] also designed and synthesized **PT36** (Figure 1-9h). **PT36** showed the detection ability of adenosine triphosphate (ATP).

1.6.6 PTs as single molecular wire

CPs are often referred to as molecular wires because of their quasi one dimensional electronic wavefunctions delocalized along the polymer chains. However, in the solid state, CPs tend to self-assemble through π-stacking, which greatly attenuates the one dimensional nature. By molecular design, CPs can be molecularly insulated just like electric power cords, resulting in so-called "insulated" molecular wires (IMWs).[43)]

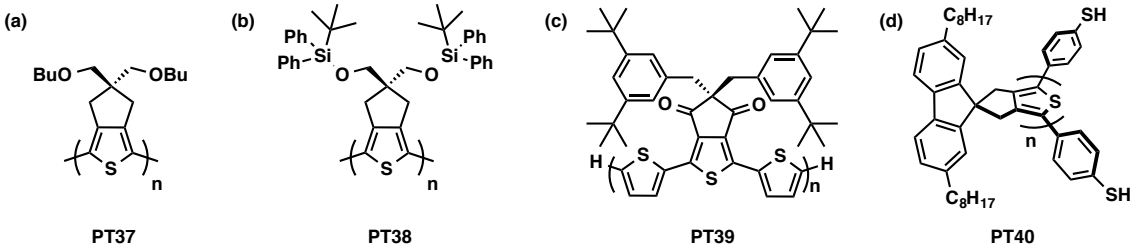

Figure 1-10. Chemical structures of Insulated Molecular Wires (IMWs): (a) **PT37**[44)], (b) **PT38**[45)], (c) **PT39**[47)], and (d) **PT40**[48)].

In 2003, Aso *et al.*[44)] reported structurally well-defined π-conjugated oligothiophenes (**PT37**) (Figure 1-10a). The elegant molecular design, which makes use of a five-membered ring to protect the considerably reactive *β*-positions, allowed stepwise synthesis of very long oligothiophenes, up to 96-mer. In addition, solubilizing side chains could be substituted with minimal steric hindrance, thus achieving a long effective conjugation length. In 2009, they[45)] reported IMWs based on this molecular design where the *n*-butyl groups in **PT37** were replaced with bulky *tert*-butyldiphenylsilyl (TBDPS) groups to insulate the oligothiophene backbone (Figure 1-10b). Interestingly, the effective conjugation was preserved despite the bulky side chains. In addition, doped **PT38** (i.e., **PT38**$^{\bullet+}$) was unable to form π-dimers in solution, even at very low temperatures (223 K), demonstrating the effective insulation. Further doping to the dicationic state (i.e., **PT38**$^{2+}$) results in either a polaron pair or bipolaron depending on how the cationic charges are delocalized on the oligothiophene backbone. Navarrete, Casado *et al.*[46)] investigated the Raman spectra of **PT38**$^{2+}$. They found that there is a given length at which the stabilization energy gained by thiophene aromatization overcomes the energy required to break a double bond; namely, the polaron pair prevails over the bipolaron. Extrapolation from such systematic oligomer studies can give insight into the charge carrying species in PTs. Aso *et al.*[47)] reported insulated oligothiophenes with an electron-deficient character (**PT39**) (figure 1-10c). Similar to **PT38**, **PT39** consists of a five-membered ring, but has a large electron affinity owing to the

carbonyl groups. Tada *et al.*[48] also investigated the insulated oligothiophene (**PT40**) designed by Aso *et al.* (Figure 1-10d), by scanning tunneling microscopy (STM) break junction technique.

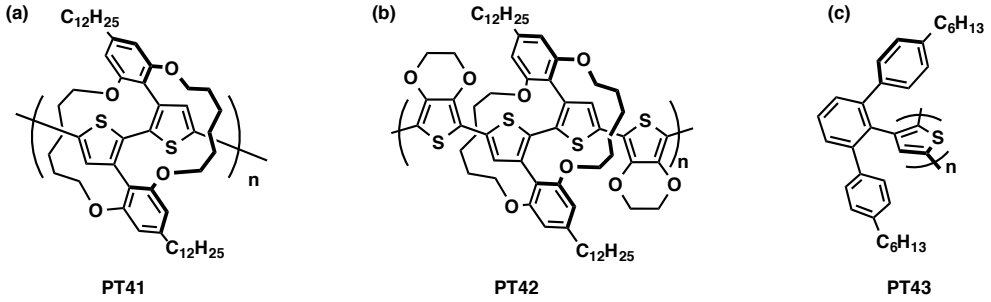

Figure 1-11. Chemical structures of Insulated Molecular Wires (IMWs): (a) **PT41**[49], (b) **PT42**[50], and (c) **PT43**[51].

In 2010, Sugiyasu and Takeuchi *et al.*[49] designed and synthesized insulated Polythiophene wire (**PT41**, Figure 1-11a). The three dimensional (3D) structure of **PT41** resembles a polyrotaxane as the CP backbone is threaded through macrocycles. However, the ring and axis are covalently linked; accordingly, all the repeating units are completely encapsulated without any "short-circuits". As a result, the generated charge carrier can transport only along the polymer backbone. Flash-photolysis time-resolved microwave conductivity (FP-TRMC) method can monitor kinetic trances of transient changes of power of microwaves from a resonant cavity after generation of photo charge with a time constant of ~ 10 ns, resulting in dynamic observation of charge carrier species.[52] For the first time, in determining the charge carrier mobility along a single planar polythiophene wire: 0.9 cm^2/Vs TRMC method. In 2012, Sugiyasu and Takeuchi *et al.*[50] also designed and synthesized new IMWs (**PT42**, figure 1-11b). By applying a controlled electrochemical potential (i.e., through electrochemical doping), charge carrying species were generated within the isolated polythiophene wire of **PT42**, which were simultaneously assessed by ESR, Raman, and UV-vis-NIR spectroscopy. The spectral data were plotted as a function of the electrochemical potential (or doping level), and clearly showed the transformation of the charge carrying species from a polaron to a polaron pair, and eventually to a bipolaron. The charge carrier transformations were found to occur at defined doping levels. In 2014, Sugiyasu and Takeuchi *et al.*[51] also designed and synthesized new IMWs (**PT43**, Figure 1-11c). PT39, which are block copolymer, was synthesized through catalyst-transfer polycondensation (CTP) method. The unsheathed P3AT block self-assembled through π-stacking into a crystalline structure, whereas the picket-fence polythiophene was. Accordingly, these two blocks underwent phase separation, and they succeeded for

the first time in creating a microphase separation comprising an ensemble of stacked and isolated polythiophenes in a single polymeric film. Such sophisticated control over π-stacking will extend the use of these materials to various unexplored applications owing to the synergy of the contrasting properties of the two blocks.

1.7 Structure of thesis

As introduced, the structure of CPs plays a dominant role in determining their physical properties, and thus affects the performance of organic devices. Therefore, it is essential to clarify the relationship between structures and properties. We have focused on structural parameters of polythiophenes such as dihedral angle, dielectric constant, and regioregularity and established rational molecular design to investigate the structure-property relationships. In this thesis, a series of thiophene-based conjugated polymers were described: (1) twisted poly(3-substituted thiophene)s; (2) picket-fence polythiophenes; and (3) self-threading polythiophenes. Through those molecular design, we attempt to establish and control the structural parameters: dihedral angle, dielectric constant, and regioregularity. Upon extensive characterization of the physical and electrical properties of these unique polymers, the structure-properties relationships were clearly demonstrated.

Chapter 2, Molecular design: *twisted poly(3-substituted thiophene)s*; Structural parameter: *dihedral angle*.

In this chapter, twisted poly(3-substituted thiophene)s were synthesized through cyclopolymerization. This is the first attempt of polythiophene synthesis through cyclopolymerization. One important structural parameter, the dihedral angle, can also be dictated by monomer design. As a consequence, photophysical properties of polythiophene could be modulated.

Chapter 3, Molecular design: *picket-fence polythiophenes*; Structural parameter: *dielectric constant*.

In this chapter, new picket fence polythiophenes based on a 7-spiro(9-fluorenyl)-cyclopentadithiophene (SFT) framework were synthesized. Despite the bulky side chains, well-developed conjugation was achieved as demonstrated by the oligomer studies. The dielectric sheaths can be altered in this new molecular design, thereby allowing the properties of the charge carriers generated in IMWs to be modulated. A highly doped state of insulated polythiophene can be stabilized using sheaths with a high dielectric constant even in the absence of interchain delocalization.

Chapter 4, Molecular design: *self-threading polythiophenes*; Structural parameter: *regioregularity*.

In this chapter, new self-threading polythiophenes in which the structural defect was intentionally introduced were synthesized. The defect copolymer backbone was isolated and interchain π–π interaction was effectively prevented. Even 1% structural defect deteriorates the electronic property of polythiophene, which lead to the decrease of the effective conjugation length. Block copolymers were obtained despite using the polycondensation reaction.

Our study on thiophene-based materials not only improves the understanding on the nature of charge carriers, but also paves the way to new molecular design around polythiophene backbone for device application.

1.5 Reference

[1] Shirakawa, H.; Louis, E. J.; MacDiarmid, A. G.; Chiang, C. K.; Heeger, A. J. *J. Chem. Soc. Chem. Commun.* **1977**, 16, 578.

[2] Sun, S.-S.; Dalton, L. R. *Introduction to Organic Electronic and Optoelectronic Materials and Devices*, **2008**, CRC Press, Taylor & Francis Group, 6000Broken Sound Paekway NW, Suite 300 Boca Raton.

[3] *The Nobel Prize in Chemistry, 2000: Conductive polymers*. Kungl Vetenskapsakademien, Royal Swedish Academy.

[4] Pan, C.; Zhao, C.; Takeuchi, M.; Sugiyasu, K. *Chem. Asian J.* **2015**, 10, 1820.

[5] Perepichka, F., Perepichka, D. F. (eds), *Handbook of Thiophene-based materials: Applications in Organic Electronics and Photonics*, **2009**, John Wiley & Sons, Ltd, Chichester, UK.

[6] Skotheim, T. A.; Reynolds, J. R. *Conjugated Polymers: Theory, Synthesis, Properties, and Characterization*, **2007**, CRC Press, Taylor & Francis Group, 6000Broken Sound Paekway NW, Suite 300 Boca Raton.

[7] Mishra, A.; Ma, C.-Q.; Bäuerle, P. *Chem. Rev.* **2009**, 109, 1141.

[8] McCullough, R. D. *Adv. Mater.* **1998**, 10, 93.

[9] Sirringhaus, H.; Brown, P. J.; Friend, R. H.; Nielsen, M. M.; Bechgaard, K.; Langeveld-Voss, B. M. W.; Spiering, A. J. H.; Janssen, R. A. J.; Meijer, E. W.; Herwig, P.; de Leeuw, D. M. *Nature* **1999**, 401, 685.

[10] Kim, Y.; Cook, S.; Tuladhar, S. M.; Choulis, S. A.; Nelson, J.; Durrant, J. R.; Bradley, D. D. C.; Giles, M.; McCulloch, I.; Ha, C. S.; Ree, M. *Nature Mater.* **2006**, 5, 197.

[11] Yamammoto, T.; Sanechika, K.; Yamamoto, A. *J. Polym. Sci., Polym Lett. Ed.* **1980**, 18, 9.

[12] Lin, J. W. P.; Dudek L. P. *J. Polym. Sci., Polym Lett. Ed.* **1980**, 18, 2869.

[13] Jen, K. Y.; Oboodi, R.; Elsenbaumer, R. L. *Polym. Mater. Sci. Eng.* **1985**, 53, 79.

[14] McCullough, R. D.; Lowe, R. D. *J. Chem. Soc., Chem. Commun.* **1992**, 70.

[15] Sheina, E. E.; Liu, J.; Iovu, M. C.; Laird, D. W.; McCullough, R. D. *Macromolecules* **2004**, 37, 3526.

[16] Yokoyama, A.; Miyakoshi, R.; Yokozawa, T. *Macromolecules* **2004**, 37, 1169.

[17] Miyakoshi, R.; Yokoyama, A.; Yokozawa, T. *J. Am. Chem. Soc.* **2005**, 127, 17542.

[18] Groenendaal, L. B.; Jonas, F.; Freitag, D.; Pielartzik, H.; Reynolds, J. R. *Adv. Mater.* **2000**, 12, 481.

[19] Jonas, F; Krafft, W.; Muys, B. *Macromol. Symp.* **1995**, 100, 169.

[20] Poater, J.; Casanovas, J.; Solà, M.; Alemán, C. *J. Phys. Chem. A* **2010**, 114, 1023.

[21] Ong, B. S.; Wu, Y.; Liu, P.; Gardner, S. *J. Am. Chem. Soc.* **2004**, 126, 3378.

[22] Chabinyc, M. L.; Endicott, F.; Vogt, B. D.; DeLongchamp, D. M.; Lin, E. K.; Wu, Y.; Liu, P.; Ing, B. S. *Appl. Phys. Lett.* **2006**, 88, 113514/1.

[23] McCulloch, I.; Heeney, M.; Bailey, C.; Genevicius, K.; MacDonald, I.; Shkunov, M.; Sparrowe, D.; Tierney, S.; Wagner, R.; Zhang, W.; Chabinyc, M. L.; Kline, R. J.; McGehee, M. D.; Toney, M. F. *Nature Mater.* **2006**, 5, 328.

[24] Lim, B.; Baeg, K. J.; Jeong, H. G.; Jo, J.; Kim, H.; park, J. W.; Noh, Y. Y.; Vak, D.; Park J. H.; Park, J. W.; Kim, D. Y. *Adv. Mater.* **2009**, 21, 2808.

[25] Fei, Z.; Pattanasattayavong, P.; Han, Y.; Schroeder, B.; Yan, F.; Kline, R.; Anthopoulos, T.; Heeney, M. *J. Am. Chem. Soc.* **2014**, 136, 15154.

[26] Jang, S.; Kim, I.; Kim, J.; Khim, D.; Jung, E.; Kang, B.; Lim, B.; Kim, Y.; Jang, Y.; Cho, K.; Kim, D. *Chem. Mater.* **2014**, 26, 6907.

[27] Chen, Z.; Zheng, Y.; Yan, H.; Facchetti, A. *J. Am. Chem. Soc.* **2008**, 131, 8.

[28] Letizia, J. A.; Salata, M. R.; Tribout, C. M.; Facchetti, A.; Ratner, M. A.; Marks, T. J. *J. Am. Chem. Soc.* **2008**, 130, 9679.

[29] Ohmori, Y.; Uchida, M.; Muro, K.; Yoshino, K. *Jpn. J. Appl. Phys. Part 2* **1991**, 30, L1938.

[30] Ohmori, Y.; Uchida, M.; Muro, K.; Yoshino, K. *Solid State Commun.* **1991**, 80, 605.

[31] Andersson, M. R.; Selse, D.; Berggren, M.; Järvinen, H.; Hjertberg, T., Inganäs O.; Wennerström, O.; Österholm, J. E. *Macromolecules* **1994**, 27, 6503.

[32] Andersson, M. R.; Berggren, M.; Inganäs O.; Gustafsson, G.; Gustaffson-Carlberg, J. C.; Selse, D.; Hjertberg, T., Wennerström, O. *Macromolecules* **1995**, 28, 7525.

[33] Andersson, M. R.; Mammo, W.; Olinga, T.; Svensson, M.; Theander, M.; Inganäs O. *Synth. Met.* **1999**, 101, 11.

[34] Pei, Q.; Järvinen, H.; Österholm, J. E.; Inganäs O. *macromolecules* **1992**, 25, 4297.

[35] Berggren, M.; Gustafsson, G.; Inganäs O.; Andersson, M. R.; Wennerström, O. *Adv. Mater.* **1994**, 6, 488.

[36] Roncali, P.; Garreau, R.; Delabouglise, D.; Garnier, F.; Lemaire, M. *J. Chem. Soc., Chem. Commun.* **1989**, 679.

[37] Bäuerle, P.; Scheib, S. *Adv. Mater.* **1993**, 5, 848.

[38] Marsella, M. J.; Swager, T. M. *J. Am. Chem. Soc.* **1993**, 115, 12214.

[39] Reddinger, J. L.; Reynolds, J. R. *Chem. Mater.* **1998**, 10, 3.

[40] Tang, Y.; He, F.; Yu, M.; Feng, F.; An, L.; Sun, H.; Wang, S.; Li, Y.; Zhu, D. *Macromol. Rapid Commun.* **2006**, 27, 389.

[41] Bäuerle, P.; Emge, A. *Adv. Mater.* **1998**, 3, 324.

[42] Li, C.; Numata, M.; Takeuchi, M.; Shinkai, S. *Angew. Chem. Int. Ed.* **2005**, 44, 6371.

[43] Frampton, F, M.; Anderson, H. L. *Angew. Chem. Int. Ed.* **2007**, 46, 1028.

[44] Izumi, T.; Kobashi, S.; Takimiya, K.; Aso, T.; Otsubo, T. *J. Am. Chem. Soc.* **2003**, 125, 5286.

[45] Ie, Y.; Han, A.; Otsubo, T.; Aso, Y. *Chem. Commun.* **2009**, 3020.

[46] Gonzµlez, S. R.; Ie, Y.; Aso, Y.; Navarrete, J. T. L.; Casado, J. *J. Am. Chem. Soc.* **2011**, 133, 16350.

[47] Endou, M.; Ie, Y.; Aso, Y. *Chem. Commun,* **2012**, 48, 540.

[48] Ie, Y.; Endou, M.; Lee,S. K.; Yamada, R.; Tada, H.; Aso, Y. *Angew. Chem. Int. Ed.* **2011**, 50, 11980.

[49] Sugiyasu, K.; Honsho, Y.; Harrison, R. M.; Sato, A.; Yasuda, T.; Seki, S.; Takeuchi, M. *J. Am. Chem. Soc.* **2010**, 132, 14754.

[50] Shomura, R.; Sugiyasu, K.; Yasuda, T.; Sato, A.; Takeuchi M. *Macromolecules* **2012**, 45, 3759.

[51] Pan, C.; Sugiyasu, K.; Aimi, J.; Sato, A.; Takeuchi M. *Angew. Chem. Int. Ed.* **2014**, 53, 8870.

[52] Seki, S.; Saeki, A.; Sakurai, T.; Sakamaki, D. *Phys. Chem. Chem. Phys.* **2014**, 16, 11093.

Chapter 2. Twisting Poly(3-substituted thiophene)s: Cyclopolymerization of Gemini Thiophene Monomers through Catalyst-Transfer Polycondensation

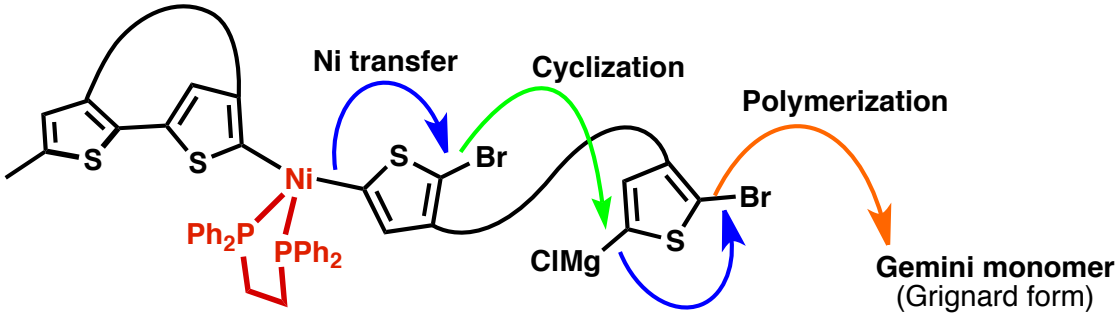

Abstract:

Polythiophenes are an important class of materials in the field of organic electronics. The molecular structures of polythiophenes play a critical role in determining device performance; therefore, tremendous effort has been devoted to controlling regioregularity, molecular weight, and polydispersity. Herein, we demonstrate a new approach to control another structural parameter, the dihedral angle. To achieve this, we exploited the unique polymerization mechanism of cyclopolymerization: an alternating intramolecular-intermolecular chain propagation that produces a series of cyclic molecules along the polythiophene chain. We designed gemini thiophene monomers, in which two thiophene monomers are tethered by an alkylene strap, and processed the monomers using the catalyst-transfer polycondensation method. We found that the dihedral angle in the polythiophene can be dictated by the size of the macrocycle formed.

2.1 Introduction:

In general, polymerization of a monomer that has two polymerizable moieties results in insoluble cross-linked polymer networks. However, with an appropriate monomer design and under optimized polymerization conditions, a soluble polymer can be obtained through a process called cyclopolymerization in which an alternating intramolecular-intermolecular chain propagation produces a series of cyclic molecules along the polymer chain.[1,2] To achieve this, monomers are generally designed such that thermodynamically favored five or six membered rings are formed. However, with an elaborate monomer design, large macrocycles can be produced, leading to polymeric materials applicable to host–guest chemistry.[3-8] In addition, the alternating propagation process can be exploited for the sequence control in a polymer main chain.[9,10] As such, cyclopolymerization is an intriguing polymerization methodology that allows access to unprecedented polymer structures. The aim of the present study was to apply cyclopolymerization to the synthesis of poly(3-substituted thiophene)s.

Poly(3-substituted thiophene)s, abbreviated as P3XT in which 'X' represents the substituents, are semiconducting polymers and widely used in various organic electronic devices.[11,12] Synthetic methodologies that achieve well-defined P3XT structures have been developed in the last two decades and have contributed to understanding structure-property relationships.[13,14] The structural parameters regarding P3XT include regioregularity (head-to-tail selectivity), molecular weight, and polydispersity, which are currently controllable owing to recent advances in nickel catalyst-transfer polycondensation (CTP).[15-20] In this study, we focus our attention on another structural parameter, specifically, the dihedral angle of the conjugated backbone as it governs the effective conjugation length along the polymer chain.[21,22] Dihedral angle indeed plays an important role in device performance. For instance, Bao and co-workers,[23] reported that a twisted polythiophene backbone achieved larger open-circuit voltages in bulk heterojunction solar cells in comparison with a planar polymer. Given the chain growth nature, the CTP method would enable cyclopolymerization of thiophenes (Scheme 2-1a). We can then envisage that the dihedral angle of P3XT is dictated by the size of the macrocycles formed (Scheme 2-1b). To date, cyclopolymerization that affords -conjugated polymers has been limited to the synthesis of polyacetylene based on ring-closing metathesis;[24-26] to the best of our knowledge, this is the first attempt of polythiophene synthesis through cyclopolymerization.

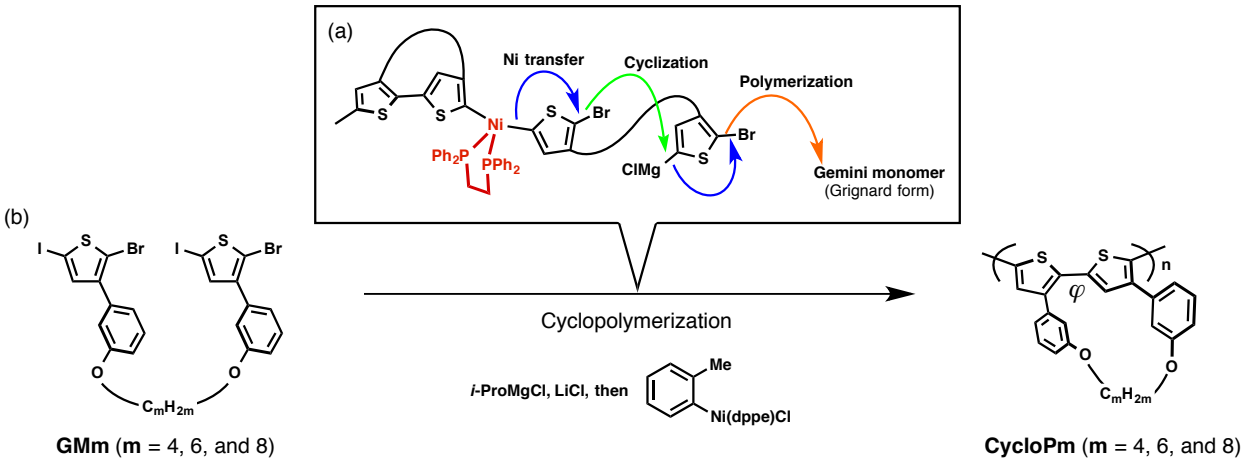

Scheme 2-1. (a) Proposed cyclopolymerization mechanism based on catalyst-transfer polycondensation. (b) Cyclopolymerization of **GMm**s.

2.2 Results and discussions

2.2.1 Synthesis of monomers

We designed and synthesized gemini thiophene monomers in which 2-bromo-5-iodo-thiophenes, which is processable by CTP,[17-19] are tethered by alkylene straps (Scheme 2-1b: **GMm**, where **GM** stands for "gemini monomer" and **m** represents the strap length). These monomers were synthesized in 7 steps as shown in Scheme 2-2a. Kumada–Tamao–Corriu cross coupling between 3-methoxyphenylmagnesium bromide and 3-bromothiophene afforded compound **1**. We first conducted bromination of thiophene in **1** using *N*-bromosuccinimide; however, the reaction was not selective, and the anisole moiety was also brominated. We thus replaced the methoxy group with acetoxy group to alter the reactivity. With **3**, bromination and subsequent iodination proceeded in good yield, thereby producing the 2-bromo-5-iodo-thiophene skeleton, **5**. Deprotection of the acetoxy group followed by Williamson ether synthesis produced gemini thiophene monomers, **GMm**. **M8** and **7** were also synthesized as a reference monomer and a model compound for a "pendant" defect, respectively (Scheme 2-2b). All the compounds were ambiguously characterized as discussed in the Experimental Section.

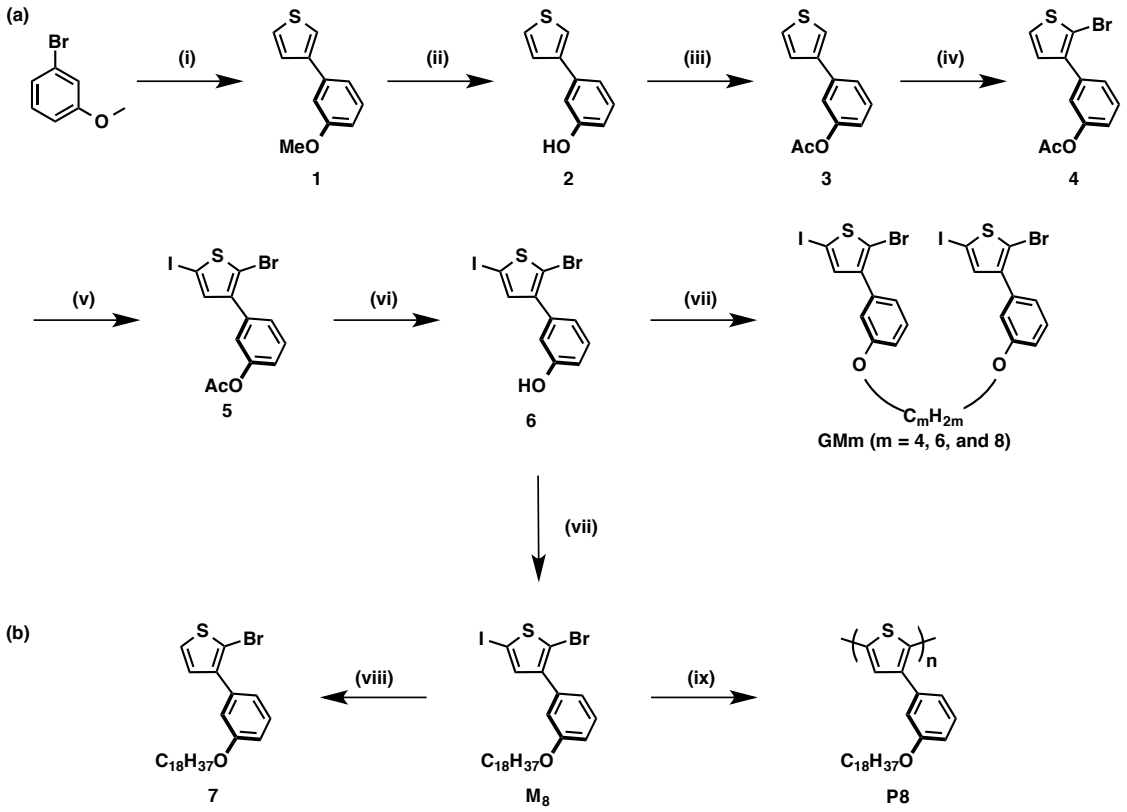

Scheme 2-2. Synthetic scheme of the gemini thiophene monomer, (a) **GMm**, (b) **7**, **M8** and reference polymer **P8**: (i) 3-methoxyphenylmagnesium bromide, Dichloro[1,3-bis(diphenylphosphino)propane]nickel ($Ni(dppp)Cl_2$) , THF, reflux; (ii) BBr_3, DCM, 0 °C; (iii) $(AcO)_2O$, NaOH, THF; (iv) NBS, $CHCl_3$, AcOH; (v) I_2, $PhI(OAc)_2$, DCM; (vi) NaOH aq.; and (vii) $Br(C_mH_{2m})Br$, Cs_2CO_3, DMF; (viii) octylbromide, Cs_2CO_3, DMF; (ix) *iso*-propylmagnesium chloride and lithium chloride, then the external catalyst; (x) *iso*-propylmagnesium chloride and lithium chloride, then quenched with methanol.

2.2.2 Cyclopolymerization of gemini thiophene monomers

CTP of **GMm**s under common conditions ([**GMm**] = 100 mM, $Ni(dppp)Cl_2$, THF, room temperature) resulted in insoluble orange precipitates, while **M8** yielded a soluble regioregular polythiophene (**P8**), suggesting that gemini monomers underwent cross-linking. We thus optimized the concentrations and catalyst systems. Under diluted concentration conditions (6 mM) and using an external catalyst ((*o*-tolyl)(1,2-bis(diphenylphosphino)ethane)nickel bromide[30,31]), we obtained polythiophenes that were soluble in common organic solvents, briefly implying the success of cyclopolymerization. We performed MALDI-TOF MS spectral measurements using several matrices and additives (such as sodium trifluoroacetate); however unfortunately, we could not observe the peaks of polymeric species. Size exclusion chromatography revealed that the number average molecular weights (M_ns) of the obtained polymers were in the range of 6K

to 9K with PDI values of 1.4 to 1.6 (Table 2-1). These values are not strong indicators of controlled polymerization; yet it is known that cyclopolymerization often results in a relatively large PDI value, especially when a large macrocycle is designed.

Table 2-1. Cyclopolymeriation of **GMm** and CTP of **M8**.

	M_n	M_w	**PDI**	**DP**
CycloP4	6.6 k	10.0 k	1.51	16
CycloP6	8.9 k	14.2 k	1.58	20
CycloP8	7.0 k	9.6 k	1.36	15
P8	6.8 k	7.5 k	1.10	23

^{1}H-NMR spectra of **CycloP4**, **CycloP6**, and **CycloP8** together with those of **P8** and **7** are shown in Figure 2-1. Though rather complicated to interpret, all the **CycloPm**s showed similar spectra to each other. The integral ratios of the aromatic peaks (6.5–7.5 ppm) to that of the OCH_2 peak in the straps (around 3.9 ppm) were in agreement with the expected ratio (10H:4H). In comparison with **P8**, **CycloPm**s showed broad peaks most likely due to the slow molecular motion restricted by the strap. In addition, sharp peaks that represent compound **7** were not clearly observed in **CycloPm**s, suggesting that pendant defect, which would be formed by the failure of cyclization, is negligible.

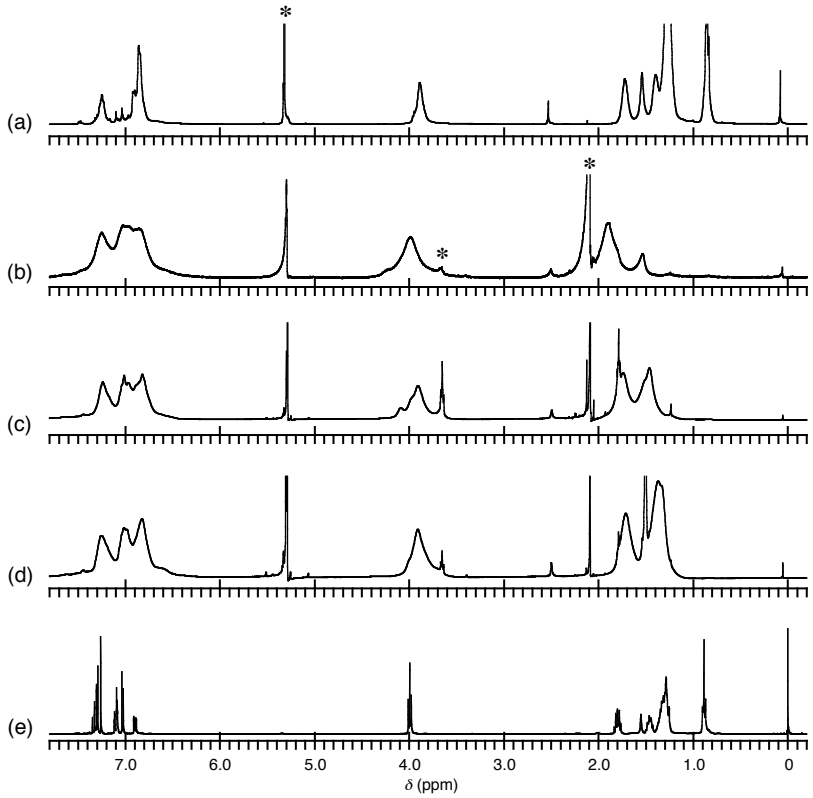

Figure 2-1. ^{1}H-NMR spectra of (a)**P8**, (b) **CycloP4**, (c) **CycloP6**, (d) **CycloP8**, and (e) **7**. The marks * indicate the solvent peaks: deuterated DCM for polymers and chloroform for **7**.

^{13}C-NMR spectra were simpler than the ^{1}H-NMR spectra, thus allowing for further characterization. Although the ^{13}C-NMR spectra of **M8** and **GM8** monomers are virtually the same (Figure 2-2), the spectra of **P8** and **CycloP8** do not overlap (Figure 2-3b,c), indicating that these two polymers have distinct structures. ^{13}C-NMR distortionless enhancement by polarization transfer (DEPT) experiments distinguishes tertiary and quaternary carbons in the aromatic moiety. In **P8** (**M8** and **GM8** as well, see Figure 2-4), five tertiary carbons are observed as anticipated (Figure 2-3d), while **CycloP8** showed one additional tertiary carbon at 126.24 ppm (as indicated by the arrow in Figure 2-3e). Note that the two equivalent thiophenes in the gemini monomer become dissimilar after the cyclopolymerization in the linear sequence along the polymer chain (Scheme 2-1b). Taking the ring-current effect by the anisole moiety into account,[32] we attribute the new peak to the tertiary carbon of thiophene that locates inside the macrocycle.

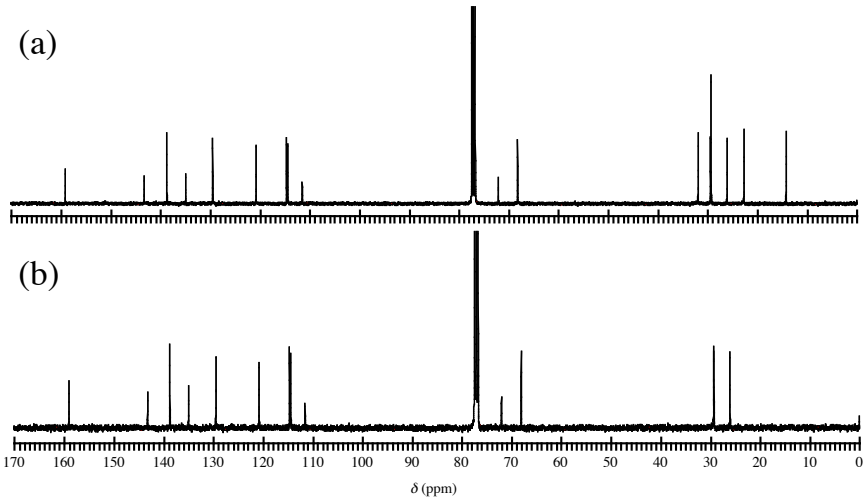

Figure 2-2. ^{13}C-NMR spectra of (a) **M8** and (b) **GM8**

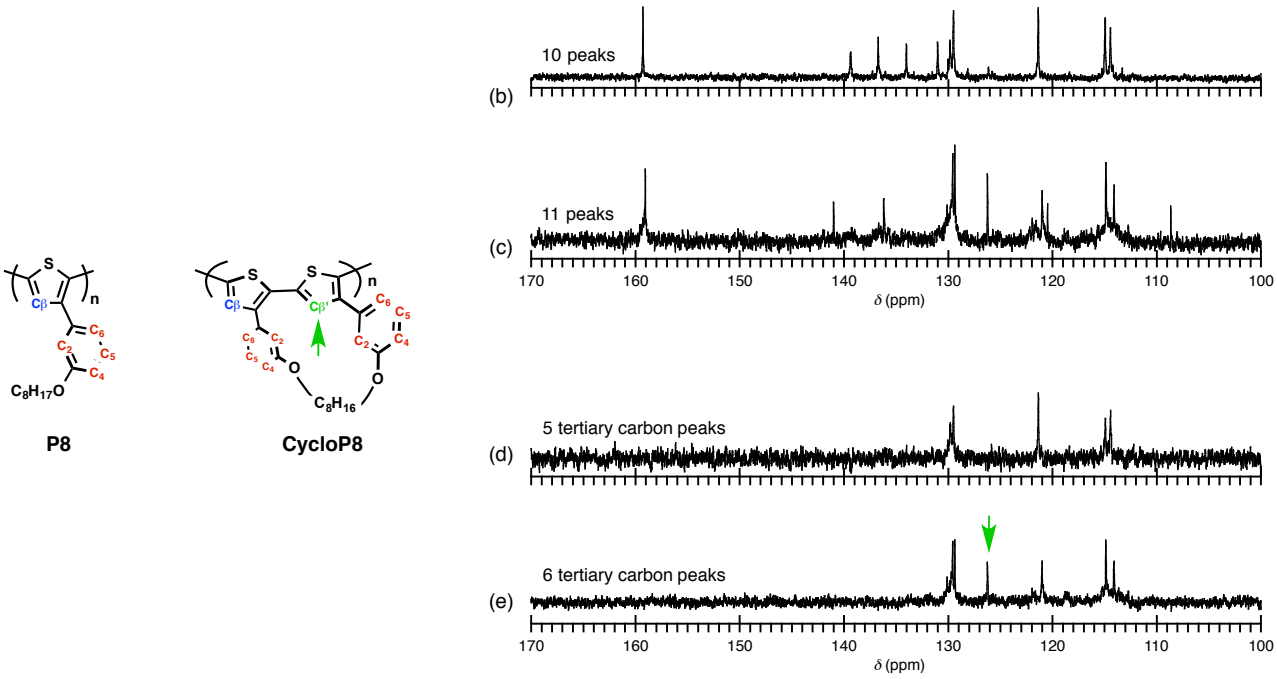

Figure 2-3. (a) Structures of **P8** and **CycloP8**. ^{13}C-NMR spectra of (b) **P8** and (c) **CycloP8**, and ^{13}C-NMR DEPT spectra of (d) **P8** and (e) **CycloP8**.

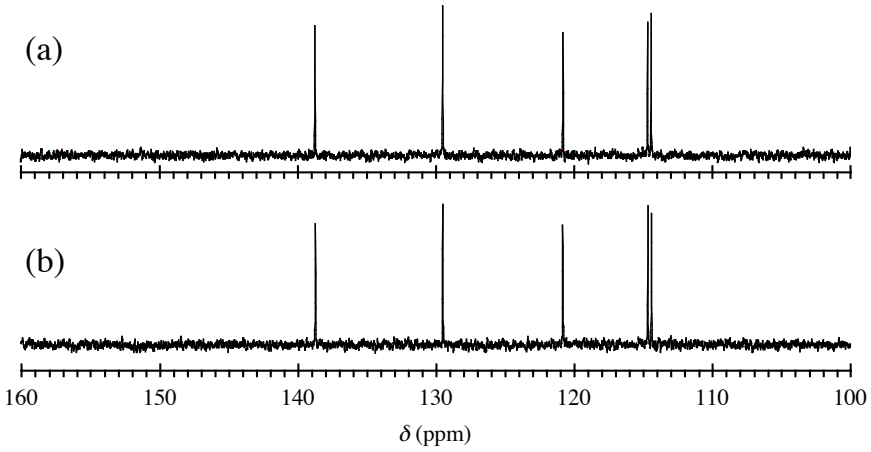

Figure 2-4. ^{13}C-NMR DEPT Spectra of (a) **M8** and (b) **GM8**

To further corroborate the cyclic structure, we synthesized **GM6′** in which the strap contains an olefin. **GM6′** was polymerized under the optimized conditions, and we obtained a cyclopolymer **CycloP6′** (M_n = 6.4K , PDI = 1.4). Except the olefin moiety, **CycloP6′** showed similar ^{1}H- and ^{13}C-NMR spectra to those of **CycloP6**. However, treating **CycloP6′** with butyl acrylate in the presence of 2nd-generation Grubbs catalyst significantly changed the spectra; as shown in Figure 2-5c, the ^{1}H-NMR spectrum became sharper, suggesting that conformational restriction was released. The peak of tertiary carbon at 126 ppm, which is characteristic of the cyclic structure (see above), disappeared after the metathesis reaction (Figure 2-5c,d). In addition, ^{1}H- and ^{13}C-NMR spectra of **CycloP6′** after the cross-metathesis reaction resemble those of **P8**. These results indicate that the cross-metathesis reaction opened the macrocycles, thus producing **P6′** (Figure 2-5e). Importantly, the molecular weight did not change significantly after the metathesis reaction (M_n = 5.3K, PDI = 1.9), suggesting that the cross-link defect in **CycloP6′** was insignificant if any. These results indirectly evidence the proposed structure of the cyclopolymers.

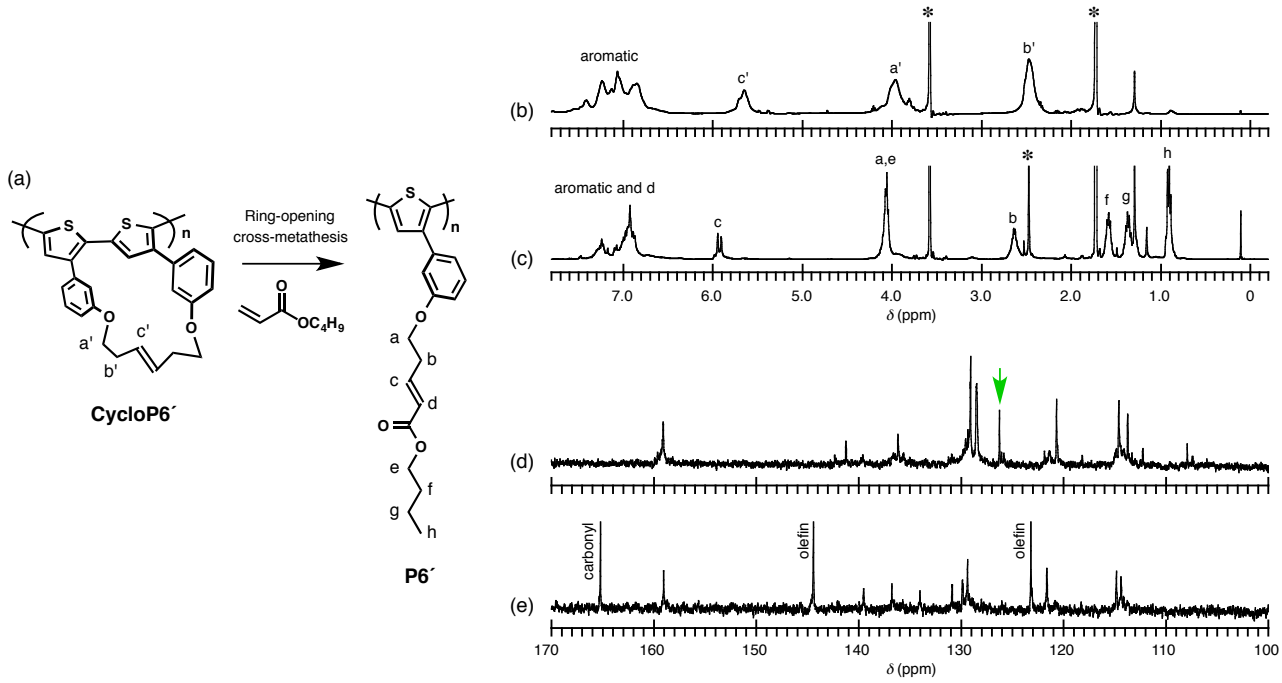

Figure 2-5. (a) Ring-opening cross-metathesis reaction of **CycloP6′** with butyl acrylate. (b,c) ^{1}H- and (d,e) ^{13}C-NMR of **CycloP6′**(a,d) before and (c,e) after the metathesis reaction. Note that the peak indicated by arrow in (d) disappears after the metathesis reaction. The marks * indicate the solvent and residual water peaks in deuterated THF.

2.2.3 Structure-property relationship of cyclopolymers

Figure 2-6a compares absorption spectra of **CycloP4**, **CycloP6**, **CycloP8**, and **P8**. Interestingly, absorption maxima gradually blue-shifted as the strap length increased. Although the peak shift was not significant, we also observed a similar tendency in the fluorescence spectra (Figure 2-6b,c). Absorption spectra of **CycloPm**s in the film state were similar to those measured in solution, which we believe corroborates the cyclic structure as it should prohibit the conformational changes upon the film formation. To gain an insight into the structure-property relationship, we performed DFT calculations (B3LYP/6-31+G(d,p)) for the repeating units of **CycloPm**: cyclized bithiophenes (**CBTm**s) (Figure 2-7). With increasing the strap length, the dihedral angle was found to become larger. By using the energy minimized structures of **CBTm**s (Figures 2-7 and 2-8), we further conducted time-dependent (TD) DFT calculations for their trimers (i.e., sexithiophene conjugation) (B3LYP/6-31G(d)//B3LYP/6-31(d)). Though the excitation energies were slightly overestimated, HOMO-LUMO gap was found to increase with increasing the strap length: a tendency that agrees well with the experimental result (Figure 2-9).[33)]

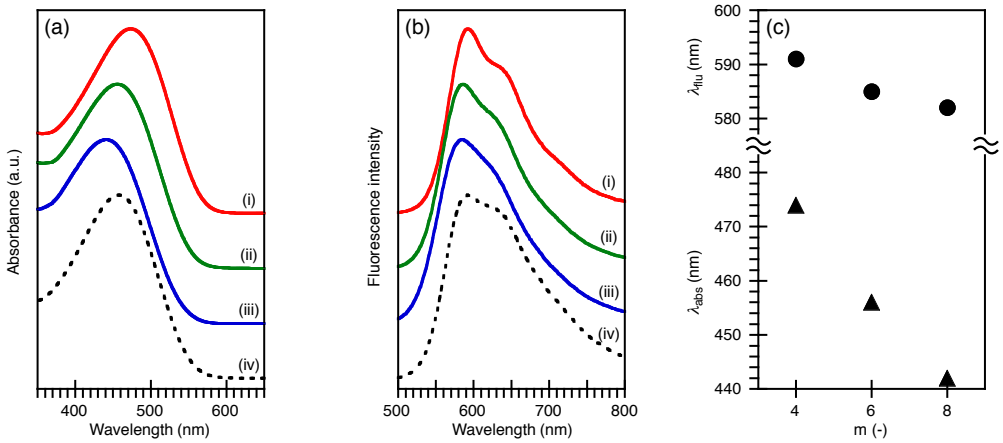

Figure 2-6. (a) Absorption and (b) fluorescence spectra of **CycloP4** (i), **CycloP6** (ii), **CP8** (iii), and **P8** (iv). (c) Plots of (triangle) absorption maxima and (circle) fluorescence maxima as a function of the strap length.

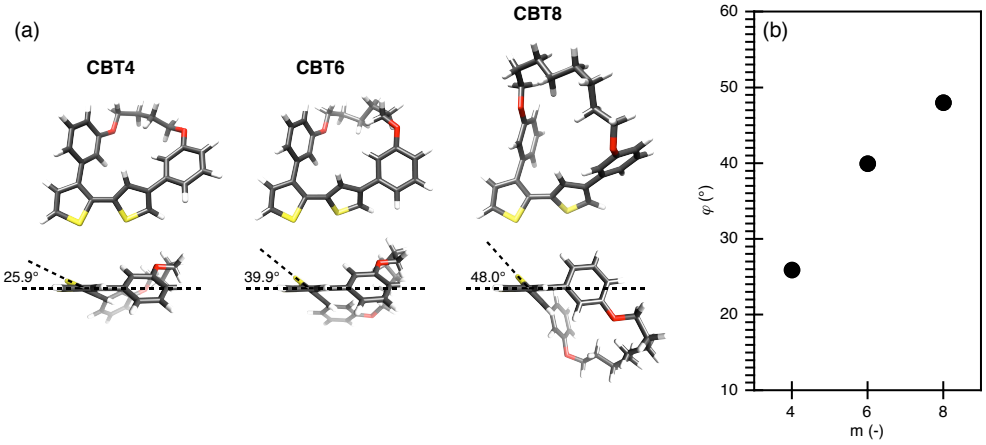

Figure 2-7. (a) Top and side views of the optimized structures of cyclic bihtiophenes at the B3LYP/6-31+G(d,p) level. (b) Plot of the dihedral angle of the bithiophene unit as a function of the strap length.

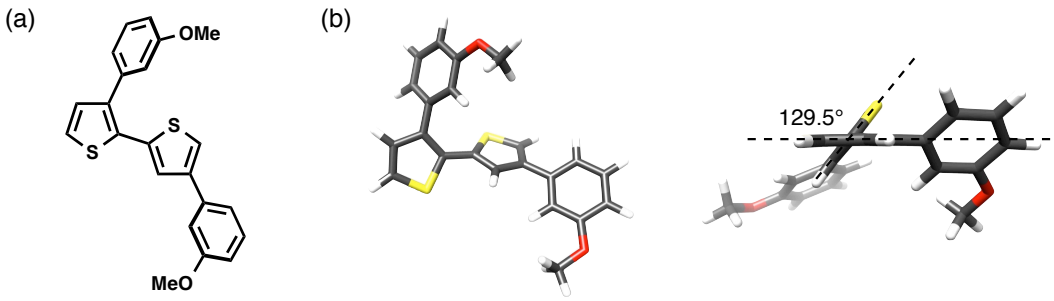

Figure 2-8. (a) Molecular structure and (b) top and side views of optimized structure of acyclic bithiophene **ABT** at the B3LYP/6-31+G(d,p) level.

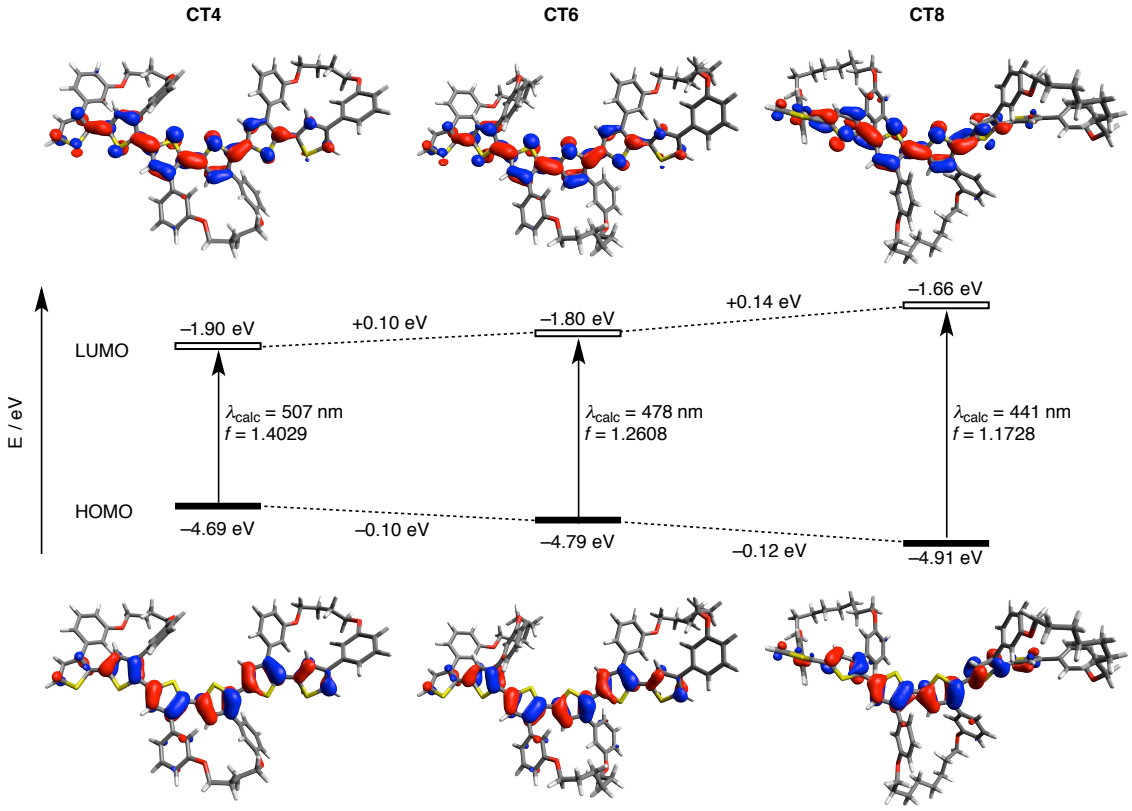

Figure 2-9. Kohn–Sham Molecular orbitals and electronic transitions of trimers of **CBT4**, **CBT6**, and **CBT8** at the B3LYP/6-31G(d)// B3LYP/6-31G(d) level of theory.

Conceptually related to the present study was previously reported by our group, in which the dihedral angle of bithiophene can be affected by cyclic side chains.[34-37] In **STBm/n** (Scheme 2-3), the movable range of the dihedral angle of the bithiophene backbone was defined by the length of the strap. Namely, the longer the strap was, the lager the fluctuation of the dihedral angle became (Scheme 2-3c). However, the absorption spectral change induced by this approach was not very significant.[36] The present study adds another example of "strapped" polythiophenes, which appeared to be more effective than our previous molecular design concept in terms of controlling the dihedral angle.

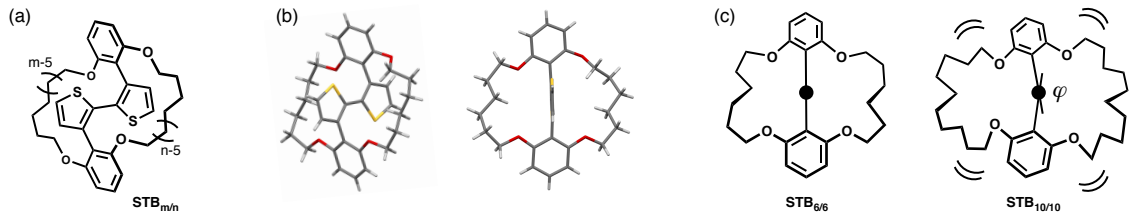

Scheme 2-3. (a) Structure of **STB$_{m/n}$**. (b) X-ray crystallographic structure of **STB$_{6/6}$**. (c) Schematic illustration of the side views of **STB$_{6/6}$** and **STB$_{10/10}$**, representing the control of the dihedral angle of the bithiophene backbone by changing the length of the straps.

2.3 Conclusions

In conclusion, we presented a proof-of-concept example of the synthesis of polythiophene through cyclopolymerization. To date, structural parameters such as regioregularity, molecular weight, and polydispersity have been controlled using CTP method. We demonstrated that another important structural parameter, the dihedral angle, can also be dictated by monomer design. As a consequence, photophysical properties of polythiophene could be modulated.

The present study expanded the scope of the CTP method in terms of the *intramonomer* condensation process; such an acrobatic CTP is expected to lead to unprecedented conjugated polymer structures.[38,39] Although the concept is still primitive, optimization of the monomer structure as well as the polymerization conditions (e.g. catalyst systems) will improve the controllability of quasi-living CTP, allowing the access to block and gradient polymers.[30,40-42] We are also interested in controlling the axial chirality regarding the bithiophene dihedral angle by using a chiral ligand; this research is now in progress in this laboratory.

2.4 Experimental section

2.4.1 General

Reagents and solvents were purchased from commercial suppliers and used without further purification. Air- and/or water-sensitive reactions were conducted under argon using dry solvents. Nuclear magnetic resonance (NMR) spectra were recorded on a JEOL ECS-400 (400 MHz) spectrometer. Matrix-assisted laser desorption ionization time-of-flight (MALDI-TOF) mass spectra were measured by using a Shimadzu AXIMA-CFR Plus station. Melting points were determined with a Yanako NP-500P micro melting point apparatus. Ultraviolet–visible absorption and fluorescence spectra were recorded on a JASCO V-630 spectrophotometer and JASCO FP-8500 spectrofluorometer, respectively. The molecular weight distribution M_n and M_w/M_n (polydispersity index: PDI) values of the polymers were determined in THF at 40 °C (polystyrene standard for **CycloPm**s and **P8**, and PMMA standard for **P6′**; where **CycloP** stands for cyclopolymer) using a TOSHO GPC system (HLC-8320GPC EcoSEC) equipped with two TSK gel super-multipore HZ-M columns and an ultraviolet detector (254 nm).

2.4.2 Synthesis of Gemini monomers

Synthesis of compound 1: A 100 mL two-neck round-bottom flask was charged with magnesium turnings (176.7 mg, 7.36 mmol) and a small piece of iodine. The flask was evacuated and refilled with argon three times. After addition of dry THF (30 mL), 3-bromoanisole (1.26 g, 6.75 mmol) was slowly added. The reaction mixture was stirred at room temperature for 3 hours, resulting in a Grignard solution. In another 250 mL two-neck round-bottom flask, 3-bromothiophene (1.0 g 6.14 mmol) and Ni(dppp)Cl_2 (166.3 mg, 0.31 mmol) were placed, and the flask was evacuated and refilled with argon three times. After addition of THF (40 mL), the Grignard solution was slowly transferred to this flask. The mixture was stirred at 80 ºC overnight. Then, methanol was slowly added to quench the reaction. The mixture was washed with water and extracted with EtOAc three times. The organic layer was washed with brine and dried over $MgSO_4$. After solvent was evaporated, product was purified by column chromatography (silica gel, DCM / hexane = 1 / 9). Compound **1** was obtained as colorless oil (1.16 g, 96 %).

^{1}H NMR ($CDCl_3$, 400 MHz, TMS, 298 K): δ 3.87 (s, 3H), 6.86 (dd, J = 8.0 & 2.0 Hz, 1H), 7.15 (m, 1H), 7.21 (d, J = 8.0 Hz, 1H), 7.33 (t, J = 8.0 Hz, 1H), 7.47 (m, 1H). ^{13}C NMR ($CDCl_3$, 100 MHz, TMS, 298 K): δ 55.39, 112.39, 112.53, 119.14, 120.63, 126.28, 126.53, 129.91, 137.35, 142.31, 160.03.

Synthesis of compound 2: A 100 mL two-neck round-bottom flask was charged with compound **1** (200 mg, 1.05 mmol). After addition of dry DCM (10 mL), BBr_3 (1.05 mL, 1 mol/L, 1.05 mmol) was added slowly at 0 ºC. The resulting mixture was stirred at room temperature for 3 hours, and then, washed with water and extracted with DCM. The organic layer was washed with brine and dried over $MgSO_4$. After solvent was

evaporated, product was purified by column chromatography (silica gel, DCM / hexane = 1 / 1). Compound **2** was obtained as white solid quantitatively (185 mg).

M. p.: 95.3 ºC . ^{1}H NMR ($CDCl_3$, 400 MHz, TMS, 298 K): δ 4.82 (s, 1H), 6.77 (m, 1H), 7.08 (m, 1H), 7.19 (m, 1H), 7.28 (t, J = 8.0 Hz, 1H), 7.36 – 7.40 (m, 2H), 7.44 (m, 1H). ^{13}C NMR ($CDCl_3$, 100 MHz, TMS, 298 K): δ. 113.44, 114.14, 119.24, 120.70, 126.33, 126.40, 130.14, 137.59, 141.94, 155.88.

Synthesis of compound 3: A 100 mL two-neck flask was charge with compound **2** (100 mg, 0.57 mmol), THF (3 mL) and acetic anhydride (2 mL) . After addition of NaOH solution at 0 ºC, mixture was stirred at room temperature for 1 hour, and then, washed with water two times, $NaHCO_3$ solution three times and extracted with DCM three times. The combined organic layer was washed with brine and dried over $MgSO_4$. After solvent was evaporated, product was purified by column chromatography (silica gel, DCM / hexane = 1 / 2) and reprecipitation (hexane). Compound **3** was obtained as white solid quantitatively (128 mg).

M. p.: 56.9 ºC . ^{1}H NMR ($CDCl_3$, 400 MHz, TMS, 298 K): δ 2.33 (s, 3H), 7.03 (m, 1H), 7.32 (m, 1H), 7.36 – 7.42 (m, 3H), 7.44 – 7.48 (m, 2H). ^{13}C NMR ($CDCl_3$, 100 MHz, TMS, 298 K): δ 21.28, 119.71, 120.31, 121.03, 124.02, 126.34, 126.48, 129.85, 151.17, 169.60.

Synthesis of compound 4: A 1 L flask was charged with compound **3** (9.0 g, 41.3 mmol). After addition of CH_3COOH (200 mL) and $CHCl_3$ (200 mL), NBS (7.35 g, 41.3 mmol) was added at 0 ºC. The resulting mixture was stirred at room temperature for 3 hours, and then, washed with water and extracted with DCM. The organic layer was washed with brine and dried over $MgSO_4$. After solvent was evaporated, product was purified by column chromatography (silica gel, DCM / hexane = 1 / 3). Compound **4** was obtained as colorless oil (12.2 g, 96 %).

^{1}H NMR ($CDCl_3$, 600 MHz, TMS, 298 K): δ 2.32 (s, 3H), 7.03 (d, J = 6.0 Hz, 1H), 7.08 – 7.10 (m, 1H), 7.29 – 7.31 (m, 2H), 7.41 – 7.45 (m, 2H).

Synthesis of compound 5: A 500 mL flask was charged with compound **4** (8.1 g, 27.4 mmol). After addition of dry DCM (270 mL), I_2 (3.9 g, 15 mmol) and (Diacetoxyiodo)benzene (4.8g 15 mmol) was added at 0 ºC. The resulting mixture was stirred at room temperature for 2 hours, and then, washed with water and extracted with DCM. The organic layer was washed with brine and dried over $MgSO_4$. After solvent was evaporated, product was purified by column chromatography (silica gel, DCM / hexane = 1 / 4). Compound **5** was obtained as colorless oil (10.8 g, 94 %).

^{1}H NMR ($CDCl_3$, 400 MHz, TMS, 298 K): δ 2.32 (s, 3H), 7.10 (m, 1H), 7.20 (s, 1H), 7.24 (t, J = 2.0 Hz, 1H), 7.35 – 7.38 (m, 1H), 7.43 (t, J = 8.0 Hz, 1H). ^{13}C NMR ($CDCl_3$, 100 MHz, TMS, 298 K): δ 21.26, 72.32, 112.04, 121.30, 121.84, 126.06, 129.55, 135.14, 138.56, 142.22, 150.68, 169.45.

Synthesis of compound 6: A 500 mL flask was charge with compound **5** (10.4 g, 24.6 mmol). After addition of THF (100 mL) and NaOH solution, the resulting mixture was stirred at 78 ºC for 3 hours, and then, washed with water and extracted with Ethyl acetate three times. After solvent was evaporated, product was purified by column chromatography (silica gel, DCM / hexane = 1 / 1) and reprecipitation (hexane). Compound **6** was obtained as white solid (9.0 g, 96 %).

M. p.: 89.5 ºC . ^{1}H NMR ($CDCl_3$, 400 MHz, TMS, 298 K): δ 4.81 (s, 1H), 6.84 (dd, J = 8.0 & 2.0 Hz, 1H), 6.97 (t, J = 2.0 Hz, 1H), 7.05 (d, J = 8.0 Hz, 1H), 7.18 (s, 1H), 7.29 (t, J = 8.0 Hz, 1H). ^{13}C NMR ($CDCl_3$, 100 MHz, TMS, 298 K): δ. 72.17, 111.70, 115.11, 115.51, 121.26, 129.83, 135.33, 138.65, 142.83, 155.48.

Synthesis of compound M8: A 100 mL two-neck bound-button flask was charged with compound **6** (700 mg, 1.84 mmol) and Cs_2CO_3 (1.2 g, 3.68 mmol). The flask was evacuated and re-filled argon three times. After addition of DMF (5 mL) and 1-bromooctane (710 mg, 3.68 mmol), the resulting mixture was stirred at 100 ºC for 2 days. and then, purified by distillation. The crude product was washed with water and extracted DCM. The combined organic layer was washed with brine and dried over $MgSO_4$. After solvent was evaporated, product was purified by column chromatography (silica gel, DCM / hexane = 1 / 8). Compound **M8** was obtained as colorless oil (710 mg, 78.5 %).

^{1}H NMR ($CDCl_3$, 400 MHz, TMS, 298 K): δ 0.90 (m, 3H), 1.28 – 1.35 (m, 8H), 1.47 (m, 2H), 1.80 (m, 2H), 3.99 (t, J = 8.0 Hz, 2H), 6.90 (dd, J = 8.0 & 2.0 Hz, 1H), 7.02 (t, J = 2.0 Hz, 1H), 7.05 (d, J = 8.0 Hz, 1H), 7.19 (s, 1H), 7.32 (t, J = 8.0 Hz, 1H). ^{13}C NMR ($CDCl_3$, 100 MHz, TMS, 298 K): δ 14.21, 22.76, 26.16, 29.34, 29.45, 31.94, 68.18, 72.05, 111.57, 114.43, 114.69, 120.80, 129.51, 134.98, 138.75, 143.30, 159.15.

Synthesis of compound GMms. GMm (**m** = 4, 6, 8, 6′) were obtained through the same synthetic process with that for **M8**.

GM4 M. p.: 91.7 ºC . ^{1}H NMR ($CDCl_3$, 400 MHz, TMS, 298 K): δ 2.01 (m, 2H), 4.08 (m, 2H), 6.90 (dd, J = 8.0 & 2.0 Hz, 1H), 7.02 (t, J = 2.0 Hz, 1H), 7.05 (d, J = 8.0 Hz, 1H), 7.18 (s, 1H), 7.32 (t, J = 8.0 Hz, 1H). ^{13}C NMR ($CDCl_3$, 100 MHz, TMS, 298 K): δ 26.09, 67.61, 72.12, 111.61, 114.39, 114.69, 121.00, 129.57, 135.04, 138.71, 143.20, 158.96.

GM6 M. p.: 114.9 ºC . ^{1}H NMR ($CDCl_3$, 400 MHz, TMS, 298 K): δ 1.56 (m, 2H), 1.84 (m, 2H), 4.00 (t, J = 6.4 Hz, 2H), 6.90 (dd, J = 8.0 & 2.0 Hz, 1H), 7.02 (t, J = 2.0 Hz, 1H), 7.05 (d, J = 8.0 Hz, 1H), 7.19 (s, 1H), 7.32 (t, J = 8.0 Hz, 1H). ^{13}C NMR ($CDCl_3$, 100 MHz, TMS, 298 K): δ 25.97, 29.28, 67.96, 72.10, 111.59, 114.40, 114.67, 120.89, 129.54, 135.01, 138.73, 143.26, 159.08.

GM8 M. p.: 79.9 ºC . ^{1}H NMR ($CDCl_3$, 400 MHz, TMS, 298 K): δ 1.41 (m, 2H), 1.48 (m, 2H), 1.80 (m, 2H), 3.99 (t, J = 6.4 Hz, 2H), 6.89 (dd, J = 8.0 & 2.0 Hz, 1H), 7.01 (t, J = 2.0 Hz, 1H), 7.04 (d, J = 8.0 Hz, 1H),

7.19 (s, 1H), 7.32 (t, J = 8.0 Hz, 1H). ^{13}C NMR ($CDCl_3$, 100 MHz, TMS, 298 K): δ. 26.09, 29.31, 29.40, 68.10, 72.08, 111.57, 114.41, 114.67, 120.84, 129.53, 134.99, 138.74, 143.28, 159.11.

GM6′ M. p.: 117.1 ºC . ^{1}H NMR ($CDCl_3$, 400 MHz, TMS, 298 K): δ 2.52 – 2.56 (m, 2H), 4.02 (t, J = 6.8 Hz, 2H), 5.68 (m, 1H), 6.89 (dd, J = 8.0 & 2.0 Hz, 1H), 7.02 (t, J = 2.0 Hz, 1H), 7.05 (d, J = 8.0 Hz, 1H), 7.18 (s, 1H), 7.31 (t, J = 8.0 Hz, 1H). ^{13}C NMR ($CDCl_3$, 100 MHz, TMS, 298 K): δ 32.67, 67.71, 72.09, 111.77, 114.49, 114.75, 121.01, 128.60, 129.55, 135.03, 138.72, 158.91.

Synthesis of compound 7: A flask was charge with **M8** (100 mg, 0.2 mmol), and evacuated and re-filled with argon three times. After addition of a solution of LiCl (0.5 mol/L in THF, 0.8 mmol) and dry THF, a solution of isopropylmagnesium chloride (2 mol/L in THF, 0.2 mmol) was added under 0 °C. The resulting mixture was stirred at room temperature for 1 h, and then, quenched with MeOH. The mixture was washed with water and extracted with DCM. The combined organic layer was washed with brine and dried over $MgSO_4$. After the solvent was evaporated, product obtained quantitatively.
^{1}H NMR ($CDCl_3$, 400 MHz, TMS, 298 K): δ 0.89 (m, 3H), 1.26 – 1.35 (m, 8H), 1.47 (m, 2H), 1.80 (m, 2H), 4.00 (t, J = 6.8 Hz, 2H), 6.90 (dd, J = 6.0 & 2.4 Hz, 1H), 7.03 (d, J = 6.0 Hz, 1H), 7.08 – 7.12 (m, 2H), 7.29 – 7.35 (m, 2H). ^{13}C NMR ($CDCl_3$, 100 MHz, TMS, 298 K): δ 14.20, 22.75, 26.16, 29.34, 29.36, 29.46, 31.90, 68.16, 108.72, 114.04, 114.86, 120.97, 125.90, 129.25, 129.42, 136.32, 141.18, 159.12.

2.4.3 Theoretical Calculations

All quantum chemical calculations for all compounds were carried out using the Gaussian 09, Revision E.01 suite of programs[43] with default thresholds and algorism. The geometry optimizations of cyclic bithiophenes **CBT4**, **CBT6**, **CBT8** and acyclic bithiophene **ABT** in the ground state were performed at the B3LYP/6-31+G(d,p) level of theory. The geometry optimizations of trimers of **CBT4**, **CBT6**, and **CBT8** in the ground state were performed at the B3LYP/6-31G(d) level of theory. The initial geometries of trimers **CT**s were construct by referring to the atomic coordinates of each optimized structures of **CBT**s and the dihedral angle of bithiophene moiety in the optimized structure of **ABT**. The stationary point in the lowest single state was optimized without any assumption and characterized by frequency analysis at the same level of theory (the number of imaginary frequencies was 0). The global minimum of **CBT**s and **ABT** were determined by comparing the total energies of several conformers. For the estimation of absorption wavelengths of trimers, the time-dependent density functional theory (TD-DFT) calculations were conducted by using the optimized structures at the B3LYP/6-31G(d) level of theory.

The Cartesian coordinates of cyclic bithiophenes **CBT4**, **CBT6**, and **CBT8** are given in Table 2-2 – 2-4. The optimized structure and Cartesian coordinates of **ABT** are given in Figure 2-8 and Table 2-5, respectively. The Cartesian coordinates of trimers of **CBT4**, **CBT6**, and **CBT8** are given in Table 2-6 – 2-8.

Table 2-2. The Cartesian Coordinates (Å) of Optimized Structure for **CBT4** in the Ground State.

atom	X	Y	Z
C	4.672507	-0.949867	0.264345
H	5.041973	-1.954383	0.433746
C	5.491861	0.121222	0.054231
H	6.572658	0.145982	0.034087
C	3.270228	-0.643438	0.191913
C	3.048896	0.705873	-0.079995
S	4.580328	1.562677	-0.217461
C	2.268838	-1.721223	0.403893
C	0.463285	-3.859054	0.812053
C	1.126606	-1.854331	-0.391858
C	2.498496	-2.675703	1.417279
C	1.610644	-3.731075	1.602048
C	0.212436	-2.894933	-0.172094
H	0.918419	-1.149084	-1.188246
H	3.365746	-2.580308	2.062084
H	-0.206841	-4.694937	0.970821
H	1.80419	-4.467656	2.376729
C	-1.812643	2.291556	0.382836
C	-4.525363	2.231587	1.102278
C	-2.625638	1.211615	-0.007605
C	-2.365356	3.339396	1.12917
C	-3.718118	3.297795	1.486361
C	-3.98041	1.183702	0.343425
H	-2.18252	0.420592	-0.599616
H	-1.737116	4.166605	1.443732
H	-5.576999	2.191773	1.366685
H	-4.146158	4.106571	2.071851
O	-0.898812	-2.866795	-0.971319
O	-4.860003	0.194596	-0.011011
C	-4.452677	-0.835349	-0.91866
H	-3.877467	-0.398226	-1.745848
H	-5.389978	-1.220804	-1.332174
C	-3.6637	-1.953831	-0.23874
H	-4.266508	-2.36589	0.579336
H	-2.763126	-1.530783	0.215325
C	-0.383346	2.304974	-0.023659
C	0.178525	3.295367	-0.794392
H	-0.309476	4.168495	-1.205622
C	0.564362	1.282364	0.307025
H	0.321793	0.440103	0.942235
C	1.822081	1.486377	-0.221262
S	1.838094	2.976915	-1.158995
C	-1.982152	-3.780568	-0.760342
H	-2.062036	-4.042515	0.301211
H	-1.796094	-4.698422	-1.333259
C	-3.254169	-3.072079	-1.216791
H	-4.057717	-3.811378	-1.32128
H	-3.06814	-2.663893	-2.218611

Table 2-3. The Cartesian Coordinates (Å) of Optimized Structure for **CBT6** in the Ground State.

atom	X	Y	Z
C	-4.803654	-1.264818	-0.722128
H	-5.046116	-2.257209	-1.084232
C	-5.748094	-0.321748	-0.430851
H	-6.82312	-0.402032	-0.51603
C	-3.456897	-0.844639	-0.452154
C	-3.4093	0.454019	0.041798
S	-5.025448	1.132683	0.16157
C	-2.312514	-1.765783	-0.671335
C	-0.220602	-3.620404	-1.07696
C	-1.297398	-1.914374	0.278937
C	-2.270416	-2.556524	-1.838035
C	-1.237701	-3.470765	-2.02649
C	-0.250194	-2.824432	0.075723
H	-1.303288	-1.333389	1.194336
H	-3.040084	-2.44354	-2.594765
H	0.56581	-4.347001	-1.24112
H	-1.215337	-4.079686	-2.925909
C	1.159147	2.742231	-0.186842
C	3.725259	3.329902	-1.169748
C	2.013492	1.707662	-0.609223
C	1.601012	4.071382	-0.260186
C	2.878553	4.353629	-0.75178
C	3.29245	1.997618	-1.097277
H	1.661521	0.686211	-0.536295
H	0.93861	4.877551	0.038408

H	4.718385	3.535735	-1.555236
H	3.215596	5.384415	-0.815668
O	0.69284	-2.857855	1.06515
O	4.175563	1.059091	-1.568961
C	4.093331	-0.299944	-1.12394
H	4.518033	-0.888631	-1.942982
C	-0.190653	2.412101	0.326846
C	-0.768835	3.014709	1.421835
H	-0.334524	3.764296	2.069105
C	-1.06079	1.43435	-0.258902
H	-0.81486	0.879467	-1.15621
C	-2.26935	1.298786	0.38556
S	-2.344866	2.390037	1.761208
C	1.8234	-3.727795	0.946851
H	2.267052	-3.629221	-0.053144
H	1.500527	-4.769929	1.077019
C	2.821494	-3.315118	2.02438
H	3.607407	-4.080223	2.081985
H	2.299404	-3.325334	2.98807
H	3.051351	-0.614779	-1.00755
C	3.440063	-1.929183	1.767072
H	2.644518	-1.255271	1.42666
H	3.802385	-1.507694	2.712673
C	4.604511	-1.931272	0.757718
H	4.39493	-2.634029	-0.06272
H	5.50288	-2.319735	1.252643
C	4.890051	-0.536186	0.163276
H	5.955048	-0.413706	-0.063045
H	4.633477	0.23992	0.895183

Table 2-4. The Cartesian Coordinates (Å) of Optimized Structure for **CBT8** in the Ground State.

atom	X	Y	Z
C	-3.892462	-2.650556	-1.293038
H	-3.648531	-3.706753	-1.311891
C	-4.948496	-2.104459	-1.970516
H	-5.671082	-2.606066	-2.599689
C	-3.157826	-1.696245	-0.515325
C	-3.671796	-0.414981	-0.635171
S	-5.064989	-0.39844	-1.701224
C	-2.029276	-2.079965	0.379111
C	0.047566	-2.906372	2.090811
C	-0.81103	-2.520657	-0.147144
C	-2.203038	-2.044438	1.774602
C	-1.172642	-2.461763	2.611851
C	0.233513	-2.919728	0.702398
H	-0.648038	-2.553226	-1.220046
H	-3.146631	-1.705002	2.18896
H	0.830907	-3.225549	2.766796
H	-1.312703	-2.446006	3.689051
C	-0.232308	3.124906	0.544071
C	2.363475	4.235747	0.601128
C	0.661325	2.92484	-0.5195
C	0.191101	3.89404	1.641629
C	1.47513	4.442092	1.660535
C	1.946781	3.46707	-0.492421
H	0.366377	2.356491	-1.394954
H	-0.472734	4.03784	2.488544
H	3.355632	4.674956	0.620216
H	1.792355	5.034936	2.513987
O	1.400015	-3.286211	0.083718
O	2.729618	3.266377	-1.608306
C	4.033417	2.689968	-1.426359
H	4.649813	3.327121	-0.777002
C	-1.572483	2.500313	0.491427
C	-2.73579	3.051184	0.981558
H	-2.866522	4.017107	1.450301
C	-1.813787	1.228107	-0.121434
H	-1.033897	0.618485	-0.559995
C	-3.126744	0.826705	-0.096324
S	-4.113013	2.036448	0.70664
C	2.385269	-3.992768	0.84982
H	1.935952	-4.92832	1.210374
H	2.679492	-3.39876	1.726031
H	4.47382	2.713073	-2.427739
C	3.60997	-4.27107	-0.024878
H	4.042932	-5.222135	0.309979
H	3.27169	-4.430595	-1.056207

C	4.710526	-3.197438	0.035287	C	5.328194	0.535318	-1.067145
H	5.612718	-3.59485	-0.449466	H	5.49563	0.34884	-2.137555
H	4.983697	-3.043228	1.090111	H	6.143465	1.198174	-0.743272
C	4.371084	-1.838949	-0.597272	C	3.983269	1.257449	-0.89205
H	4.264215	-1.963747	-1.684699	H	3.192654	0.718291	-1.426482
H	3.396856	-1.491345	-0.234754	H	3.697154	1.270448	0.167637
C	5.451342	-0.787831	-0.293634	H	6.439949	-1.219181	-0.505395
H	5.440092	-0.57357	0.785092				

Table 2-5. The Cartesian Coordinates (Å) of Optimized Structure for **ABT** in the Ground State.

atom	X	Y	Z	H	1.283279	1.096538	-0.796949
H	-4.396705	2.819196	-0.835507	C	0.922905	0.589208	0.090916
C	-3.350036	2.765638	-0.558777	C	-0.349503	0.78355	0.579192
C	-2.505038	3.839575	-0.597919	C	1.690427	-0.382904	0.814763
C	-2.711059	1.540589	-0.168283	C	0.967325	-0.905635	1.865259
C	-1.361314	1.721837	0.098566	S	-0.617732	-0.227376	1.986559
S	-0.897973	3.398394	-0.133504	C	3.074465	-0.77933	0.470837
C	-3.443351	0.250207	-0.120848	C	5.718143	-1.503682	-0.174219
C	-4.864801	-2.175135	-0.08316	C	3.521073	-2.093425	0.670524
C	-4.699664	0.174733	0.496052	C	3.96525	0.17359	-0.062209
C	-2.903104	-0.898292	-0.729996	C	5.277688	-0.187745	-0.38321
C	-3.60935	-2.10456	-0.707409	C	4.836939	-2.442977	0.351294
C	-5.399034	-1.037162	0.511515	H	2.836874	-2.845092	1.050691
H	-5.118517	1.052036	0.978922	H	3.626956	1.194035	-0.193348
H	-1.940068	-0.826372	-1.219193	H	5.174527	-3.46397	0.505097
H	-6.368897	-1.093155	0.997537	H	6.740567	-1.761078	-0.430008
H	-5.395107	-3.121737	-0.079984	O	6.208489	0.672477	-0.897247
O	-3.163623	-3.266887	-1.273159	C	5.835169	2.024441	-1.132127
C	-1.893632	-3.27003	-1.915506	H	5.017413	2.093405	-1.860624
H	-1.875508	-2.580065	-2.768492	H	6.722754	2.510908	-1.538432
H	-1.745246	-4.289808	-2.272747	H	5.539356	2.525977	-0.202134
H	-1.090453	-3.007367	-1.216402	H	1.294483	-1.636208	2.592557
H	-2.730344	4.856796	-0.888141				

Table 2-6. The Cartesian Coordinates (Å) of Optimized Structure for **CT4** in the Ground State.

atom	X	Y	Z	C	12.064216	0.597229	0.448407
C	11.939904	-0.736677	0.198322	C	10.585056	-1.213977	0.185851
H	12.78529	-1.379948	-0.01753	C	9.677034	-0.188344	0.44186

S	10.522784	1.333541	0.705693	C	4.471531	2.692342	0.400176
C	10.304029	-2.644835	-0.095501	H	5.311718	3.338617	0.628667
C	9.89419	-5.381851	-0.672823	C	4.582479	1.319126	0.392738
C	9.215417	-3.059012	-0.868957	C	3.159705	3.203717	0.170586
C	11.190141	-3.626537	0.393667	C	2.235392	2.176911	-0.028538
C	10.986716	-4.968555	0.093944	S	3.021174	0.606192	0.057533
C	8.989951	-4.417095	-1.130645	C	2.920922	4.669468	0.198144
H	8.514015	-2.339544	-1.274922	C	2.590767	7.473963	0.312074
H	12.028183	-3.334162	1.018161	C	1.784973	5.233409	0.786157
H	9.763291	-6.433041	-0.901732	C	3.895969	5.532889	-0.341579
H	11.68453	-5.714324	0.465653	C	3.729892	6.911138	-0.269541
C	4.900371	-1.703272	1.415912	C	1.601851	6.622367	0.816695
C	2.922949	-3.529127	2.187998	H	1.014617	4.608755	1.223104
C	4.587239	-2.795826	0.589505	H	4.774953	5.118649	-0.824943
C	4.222943	-1.530778	2.627543	H	2.489802	8.551709	0.365851
C	3.237273	-2.447283	3.002845	H	4.495096	7.566886	-0.676587
C	3.597694	-3.709288	0.9714	C	-2.331676	3.687009	-1.731828
H	5.124419	-2.905965	-0.344814	C	-4.133938	5.444347	-2.958843
H	4.469795	-0.690738	3.269093	C	-2.67442	4.897454	-1.105499
H	2.158029	-4.246861	2.467469	C	-2.891224	3.363209	-2.972454
H	2.708879	-2.316446	3.943394	C	-3.789934	4.246713	-3.575582
O	7.851186	-4.68563	-1.838856	C	-3.57708	5.776831	-1.715003
O	3.206127	-4.795613	0.238289	H	-2.229794	5.124513	-0.14398
C	3.832724	-5.065559	-1.017643	H	-2.620541	2.431786	-3.459657
H	3.883415	-4.148643	-1.620811	H	-4.832959	6.137921	-3.415609
H	3.147781	-5.754206	-1.522524	H	-4.226395	3.998268	-4.5393
C	5.217277	-5.693744	-0.859674	O	0.416011	7.034508	1.359454
H	5.122403	-6.612331	-0.267275	O	-3.990487	6.969416	-1.187818
H	5.850723	-5.011979	-0.284274	C	-3.477175	7.403277	0.073318
C	5.981713	-0.770853	0.990542	H	-3.525576	6.584855	0.804779
C	5.790606	0.535824	0.561796	H	-4.176581	8.179153	0.400755
C	7.354846	-1.154299	0.988289	C	-2.057574	7.960059	-0.03149
H	7.685767	-2.126611	1.33205	H	-2.053357	8.779552	-0.760964
C	8.224844	-0.179585	0.551393	H	-1.401297	7.180423	-0.429796
S	7.322395	1.261212	0.107794	C	-1.34546	2.789248	-1.068175
C	7.424188	-6.032909	-2.051153	C	-1.637702	1.5513	-0.510205
H	7.697203	-6.663526	-1.195821	C	0.032045	3.133299	-0.949776
H	7.915074	-6.436011	-2.947519	H	0.439486	4.044752	-1.369282
C	5.90571	-5.99333	-2.202985	C	0.807574	2.196392	-0.299094
H	5.558854	-6.94896	-2.61602	S	-0.199059	0.845654	0.2041
H	5.663994	-5.220748	-2.94474	C	0.033784	8.410922	1.320222
H	12.967567	1.190963	0.485499	H	0.419044	8.892898	0.413016

H	0.451974	8.932443	2.192048	H	-9.6924	-2.77435	-0.125795
C	-1.492469	8.442049	1.316284	H	-10.904676	0.559404	2.286506
H	-1.834058	9.460094	1.542245	H	-13.233893	-3.074666	2.298177
H	-1.841818	7.800827	2.136242	H	-12.86389	-0.743281	3.100354
C	-3.055686	-0.53	-0.241267	O	-7.092981	-4.910186	-1.058975
H	-2.223958	-1.223928	-0.291413	O	-11.815651	-4.349303	0.652172
C	-2.888478	0.828993	-0.38746	C	-11.092229	-4.970977	-0.410696
C	-4.405309	-0.97155	-0.097197	H	-10.919348	-4.249881	-1.221405
C	-5.304364	0.095416	-0.13167	H	-11.7698	-5.742167	-0.792397
S	-4.44589	1.620001	-0.314248	C	-9.775149	-5.593777	0.049959
C	-4.686107	-2.422565	0.053616	H	-9.982674	-6.301352	0.86197
C	-5.081984	-5.208814	0.311832	H	-9.140312	-4.808643	0.471514
C	-5.753183	-3.055973	-0.589329	C	-9.01712	-0.26408	0.513751
C	-3.813441	-3.206195	0.836205	C	-9.133757	0.964547	-0.090192
C	-4.009024	-4.577742	0.946632	C	-7.657247	-0.710399	0.556843
C	-5.972452	-4.431783	-0.436756	H	-7.358519	-1.632865	1.038324
H	-6.44155	-2.495083	-1.2111	C	-6.756233	0.159222	-0.021807
H	-2.991049	-2.732946	1.362871	S	-7.613807	1.568861	-0.646849
H	-5.208919	-6.281022	0.405642	C	-7.507997	-6.263333	-0.86373
H	-3.321161	-5.173007	1.541353	H	-7.27833	-6.593087	0.157411
C	-10.177243	-1.032022	1.029931	H	-6.972902	-6.917573	-1.565828
C	-12.3837	-2.492445	1.957005	C	-9.015898	-6.293542	-1.093596
C	-10.38894	-2.350044	0.587686	H	-9.344829	-7.334551	-1.201816
C	-11.076569	-0.45244	1.93232	H	-9.21551	-5.797738	-2.052781
C	-12.170203	-1.1902	2.392945	H	-10.042275	1.519039	-0.283096
C	-11.495067	-3.077092	1.041805				

Table 2-7. The Cartesian Coordinates (Å) of Optimized Structure for **CT6** in the Ground State.

atom	X	Y	Z	C	9.0628	-4.090212	-1.460158
C	12.162752	-0.776071	0.335513	H	8.787751	-1.969797	-1.436276
H	12.979421	-1.443046	0.082345	H	11.958351	-3.499757	1.053485
C	12.341054	0.532442	0.676652	H	9.603232	-6.187696	-1.332682
C	10.78776	-1.184292	0.280654	H	11.434893	-5.787204	0.27165
C	9.9267	-0.144104	0.608142	C	5.253989	-1.572796	2.005275
S	10.829911	1.31974	0.972691	C	3.443594	-3.293142	3.274899
C	10.41337	-2.55902	-0.133871	C	5.133483	-2.908678	1.583726
C	9.812979	-5.178186	-0.998333	C	4.463458	-1.105697	3.062563
C	9.372272	-2.791084	-1.036969	C	3.562394	-1.970525	3.686557
C	11.156447	-3.658583	0.338914	C	4.233814	-3.771495	2.219078
C	10.854424	-4.944848	-0.095607	H	5.748615	-3.243808	0.757097

H	4.564877	-0.079001	3.398966	H	1.161059	4.344048	1.538374
H	2.75208	-3.978111	3.755371	H	4.777948	5.199124	-0.647724
H	2.950856	-1.610172	4.509445	H	2.289963	8.414041	0.746425
O	8.013876	-4.181109	-2.329477	H	4.309679	7.618377	-0.427034
O	4.065666	-5.096229	1.920788	C	-1.806088	3.404062	-2.310408
C	4.651267	-5.654026	0.744402	C	-3.26359	4.918239	-4.163317
H	4.796431	-6.713446	0.980733	C	-1.894117	4.800282	-2.169552
C	6.270574	-0.699996	1.363345	C	-2.451819	2.773729	-3.38138
C	6.042272	0.561125	0.8274	C	-3.178054	3.537136	-4.297207
C	7.647912	-1.071895	1.308291	C	-2.616662	5.559548	-3.096417
H	8.018336	-2.001161	1.724764	H	-1.394537	5.264146	-1.327359
C	8.477601	-0.126276	0.752104	H	-2.372979	1.698068	-3.500669
S	7.538985	1.26229	0.237358	H	-3.81902	5.52491	-4.871588
C	7.578066	-5.46052	-2.78893	H	-3.676801	3.04928	-5.130436
H	7.462948	-6.147097	-1.937911	O	0.425714	6.721229	1.844943
H	8.328478	-5.888257	-3.469073	O	-2.732386	6.922725	-3.082366
C	6.243482	-5.24235	-3.496217	C	-2.297791	7.676736	-1.950872
H	5.962932	-6.169159	-4.014932	H	-2.03454	8.659856	-2.355274
H	6.395968	-4.480161	-4.269369	C	-0.969166	2.630104	-1.357879
H	5.644714	-5.229063	0.558799	C	-1.363627	1.493435	-0.662708
C	5.129262	-4.805856	-2.528575	C	0.400206	2.959054	-1.127235
H	5.556911	-4.085823	-1.819681	H	0.893801	3.784271	-1.626572
H	4.3546	-4.257188	-3.078486	C	1.064812	2.099101	-0.282131
C	4.460744	-5.968118	-1.770176	S	-0.033907	0.85638	0.288464
H	5.209602	-6.733348	-1.513598	C	0.022403	8.084569	1.972565
H	3.751917	-6.468724	-2.441377	H	0.086269	8.589176	0.997788
C	3.742755	-5.515882	-0.481032	H	0.692795	8.608497	2.668785
H	2.838232	-6.108608	-0.302503	C	-1.415095	8.071261	2.484961
H	3.417555	-4.472334	-0.577989	H	-1.701191	9.095207	2.761406
H	13.268577	1.083397	0.755805	H	-1.43594	7.476697	3.405846
C	4.658575	2.680258	0.645797	H	-1.38265	7.252331	-1.521583
H	5.464343	3.353363	0.91813	C	-2.401113	7.493825	1.454108
C	4.814916	1.311625	0.627909	H	-1.926438	6.626478	0.97857
C	3.33825	3.142451	0.363809	H	-3.288036	7.102705	1.967866
C	2.467403	2.089689	0.100613	C	-2.859719	8.503577	0.384829
S	3.298132	0.547105	0.206384	H	-2.028119	9.172529	0.114498
C	3.004823	4.587178	0.430177	H	-3.627918	9.155766	0.818487
C	2.4734	7.349668	0.654876	C	-3.396713	7.82853	-0.894818
C	1.858092	5.041401	1.087216	H	-4.214348	8.409935	-1.336185
C	3.889689	5.534453	-0.12104	H	-3.810529	6.841052	-0.654277
C	3.6199	6.893764	-0.002227	C	-2.893041	-0.510864	-0.377586
C	1.584329	6.411301	1.192138	H	-2.09923	-1.249659	-0.398586

C	-2.653026	0.833727	-0.553923	C	-10.402769	-4.78211	1.803767
C	-4.269223	-0.869489	-0.249393	H	-10.167498	-5.623665	2.463619
C	-5.100799	0.243884	-0.311296	C	-8.772345	0.084778	0.552235
S	-4.164859	1.713868	-0.517725	C	-8.927001	1.116794	-0.344655
C	-4.671071	-2.293086	-0.120662	C	-7.405607	-0.337217	0.638764
C	-5.303146	-5.038336	0.05546	H	-7.061614	-1.102111	1.324529
C	-5.730216	-2.829491	-0.85855	C	-6.546712	0.357412	-0.181012
C	-3.928242	-3.148556	0.716712	S	-7.438503	1.564435	-1.100907
C	-4.245395	-4.500344	0.793756	C	-7.53604	-5.951289	-1.500978
C	-6.054905	-4.189516	-0.765686	H	-7.644834	-6.295538	-0.462551
H	-6.31681	-2.207153	-1.525068	H	-6.775417	-6.579461	-1.986395
H	-3.112271	-2.746336	1.309197	C	-8.870079	-6.022379	-2.238343
H	-5.524729	-6.097151	0.122399	H	-9.129361	-7.078419	-2.394703
H	-3.663877	-5.153648	1.43901	H	-8.727454	-5.580585	-3.231631
C	-9.87913	-0.509199	1.334462	H	-9.454321	-4.426979	1.386754
C	-11.961893	-1.665941	2.819716	C	-9.999988	-5.295018	-1.488873
C	-9.891052	-1.89196	1.584616	H	-9.599439	-4.349556	-1.102403
C	-10.918735	0.28707	1.835734	H	-10.791892	-5.016559	-2.195481
C	-11.948705	-0.29629	2.574418	C	-10.630745	-6.113924	-0.346182
C	-10.928329	-2.471464	2.322212	H	-9.859837	-6.710359	0.165605
H	-9.084488	-2.496314	1.186448	H	-11.328476	-6.844614	-0.774051
H	-10.902075	1.360356	1.672375	C	-11.355132	-5.234842	0.692741
H	-12.755717	-2.134298	3.39287	H	-12.193013	-5.772307	1.151792
H	-12.748795	0.325074	2.968296	H	-11.781075	-4.350548	0.201345
O	-7.120952	-4.585636	-1.522971	H	-9.846941	1.608148	-0.631301
O	-10.997911	-3.80012	2.654608				

Table 2-8. The Cartesian Coordinates (Å) of Optimized Structure for **CT8** in the Ground State.

atom	X	Y	Z	C	11.529328	-1.887376	-0.302624
C	10.799668	-1.474723	4.18388	H	10.972817	-3.058585	1.40598
H	11.860332	-1.672378	4.072369	H	10.118893	1.158236	1.655688
C	10.150307	-1.480374	5.385533	H	12.014949	-0.447306	-1.849637
C	9.955997	-1.135555	3.076879	H	11.107179	1.468177	-0.60001
C	8.646759	-0.904204	3.467636	C	5.558549	-1.431045	-0.483673
S	8.471551	-1.097171	5.204204	C	4.997103	-2.606419	-2.982299
C	10.477397	-0.969907	1.691947	C	5.663047	-2.81626	-0.666009
C	11.585908	-0.608137	-0.867861	C	5.166095	-0.6335	-1.57106
C	10.989928	-2.059262	0.981506	C	4.887098	-1.22553	-2.801794
C	10.511615	0.308055	1.107171	C	5.39097	-3.404497	-1.902468
C	11.06808	0.477078	-0.155578	H	5.96055	-3.462381	0.153578

H	5.101041	0.443508	-1.455055	C	1.67817	3.604691	2.062342
H	4.770225	-3.052449	-3.945572	C	0.640659	6.028323	3.042614
H	4.584029	-0.602843	-3.639441	C	2.070008	4.822398	1.498613
O	11.957687	-3.028098	-0.927379	C	0.749521	3.604216	3.11781
O	5.488008	-4.773878	-1.955482	C	0.248259	4.808051	3.599544
C	6.166589	-5.370991	-3.066007	C	1.543517	6.033614	1.97317
H	5.656598	-5.137226	-4.01151	H	2.78274	4.8533	0.679993
C	5.972957	-0.857705	0.820893	H	0.44557	2.66211	3.562672
C	5.301694	0.086449	1.586177	H	0.235432	6.951625	3.439048
C	7.197003	-1.271501	1.426349	H	-0.457703	4.806712	4.425931
H	7.85901	-1.995251	0.967098	C	-2.594743	3.071473	-1.176619
C	7.4833	-0.668475	2.626043	C	-3.965765	5.205482	-2.40369
S	6.204271	0.449197	3.052787	C	-2.008913	3.79436	-2.223996
C	12.829009	-2.895908	-2.054666	C	-3.883171	3.428027	-0.746397
H	13.737401	-2.366523	-1.733699	C	-4.553893	4.483407	-1.362364
H	12.351029	-2.292984	-2.839656	C	-2.68116	4.855096	-2.833882
H	6.056745	-6.4466	-2.894355	H	-1.016015	3.543214	-2.5829
C	13.163664	-4.285893	-2.601058	H	-4.344264	2.893212	0.077655
H	14.171711	-4.237118	-3.033226	H	-4.504368	6.020326	-2.877256
H	13.221327	-4.984501	-1.756885	H	-5.550535	4.755005	-1.024375
C	12.202153	-4.8029	-3.684426	O	1.958127	7.162358	1.317452
H	12.635789	-5.705766	-4.136739	O	-2.028708	5.464417	-3.878339
H	12.163118	-4.055963	-4.492271	C	-2.012709	6.894892	-3.937297
C	10.76999	-5.117893	-3.226472	H	-3.031753	7.297118	-4.029459
H	10.787966	-5.982892	-2.546999	C	-1.783644	2.030019	-0.497897
H	10.373835	-4.280807	-2.639679	C	-2.162562	0.732851	-0.178026
C	9.847928	-5.40693	-4.421584	C	-0.445443	2.316214	-0.096551
H	9.756021	-4.490432	-5.023452	H	0.016876	3.282307	-0.257308
C	8.440486	-5.913493	-4.067799	C	0.208393	1.278944	0.523537
H	8.513977	-6.907794	-3.603878	S	-0.844683	-0.117768	0.618545
H	7.882099	-6.057106	-5.004616	C	1.768408	8.426415	1.96049
C	7.646098	-4.986241	-3.136329	H	2.309722	8.416293	2.91717
H	8.056945	-5.027012	-2.120492	H	0.703875	8.58856	2.18096
H	7.737216	-3.944414	-3.470921	H	-1.490556	7.114016	-4.874251
H	10.328999	-6.149116	-5.075003	C	2.282487	9.541061	1.046191
H	10.561048	-1.672628	6.367678	H	2.645792	10.354195	1.688147
C	3.649492	2.000087	1.805602	H	3.15543	9.164027	0.498656
H	4.350429	2.693931	2.257831	C	1.23259	10.122039	0.084059
C	4.011551	0.731756	1.403078	H	1.645636	11.027657	-0.381835
C	2.275666	2.319544	1.605722	H	0.372043	10.4616	0.680907
C	1.575396	1.275938	1.017605	C	0.732412	9.180265	-1.02182
S	2.621636	-0.10328	0.735555	H	1.553559	8.978287	-1.725518

H	0.459469	8.210395	-0.589667
C	-0.467825	9.779106	-1.772054
H	-1.312571	9.863231	-1.072078
C	-0.927394	9.0025	-3.016366
H	-0.144777	9.04866	-3.787528
H	-1.801044	9.519242	-3.440393
C	-1.281337	7.53144	-2.753345
H	-0.370604	6.950828	-2.564186
H	-1.901796	7.446101	-1.851448
H	-0.22503	10.80771	-2.075811
C	-3.942965	-1.004155	0.324254
H	-3.534549	-1.300201	1.284863
C	-3.386995	-0.004455	-0.445877
C	-5.082552	-1.635841	-0.25318
C	-5.414643	-1.092865	-1.484233
S	-4.301855	0.185979	-1.93014
C	-5.76551	-2.799208	0.378644
C	-6.92664	-5.042629	1.614443
C	-6.477433	-2.659782	1.573338
C	-5.646503	-4.072181	-0.205227
C	-6.217879	-5.176015	0.417594
C	-7.073074	-3.773179	2.185536
H	-6.587656	-1.688361	2.045937
H	-5.091083	-4.186456	-1.130613
H	-7.359824	-5.92021	2.079194
H	-6.111393	-6.162102	-0.026939
C	-10.283039	-1.928159	-2.624409
C	-13.028149	-2.190144	-2.029199
C	-10.871147	-1.181926	-1.593351
C	-11.091019	-2.811611	-3.358402
C	-12.447463	-2.934387	-3.058215
C	-12.227425	-1.308633	-1.294205
H	-10.2869	-0.471727	-1.017758
H	-10.649523	-3.420018	-4.142447
H	-14.088279	-2.279946	-1.812544
H	-13.063695	-3.622026	-3.631831
O	-7.789778	-3.516876	3.324673
O	-12.72648	-0.481449	-0.314072
C	-13.425128	-1.081025	0.7833
H	-14.288757	-1.660954	0.42703
C	-8.836083	-1.778719	-2.888706
C	-8.238201	-1.815145	-4.127296
C	-7.880315	-1.527041	-1.853309
H	-8.140349	-1.47199	-0.803354
C	-6.591037	-1.370038	-2.296396
S	-6.529163	-1.543347	-4.043808
C	-8.097737	-4.614292	4.189365
H	-7.155141	-5.069965	4.524487
H	-8.665549	-5.382921	3.646371
H	-13.813299	-0.228487	1.350158
C	-8.919922	-4.110724	5.377484
H	-8.695178	-4.762845	6.231676
H	-8.561804	-3.109561	5.648642
C	-10.442316	-4.115635	5.158426
H	-10.936877	-3.948953	6.125627
H	-10.739653	-5.128066	4.844295
C	-10.987504	-3.097522	4.145049
H	-10.856323	-2.081714	4.546652
H	-10.397856	-3.13663	3.221691
C	-12.471319	-3.353471	3.836164
H	-12.559199	-4.313165	3.305351
C	-13.178946	-2.26233	3.017366
H	-13.233633	-1.337994	3.610758
H	-14.21986	-2.577938	2.852753
C	-12.522556	-1.946063	1.665386
H	-11.577818	-1.410821	1.818571
H	-12.276057	-2.875633	1.134979
H	-13.017233	-3.481964	4.782132
H	-8.717052	-1.939773	-5.089381

2.5 References

[1] Butler, G. B. *Acc. Chem. Res.* **1982**, 15, 370.

[2] Butler, G. B. *J. Polym. Sci. part A: Polym. Chem.* **2000**, 38, 3451.

[3] Ochiai, B., Ootani, Y.; Endo, T. *J. Am. Chem. Soc.* **2008**, 130, 10832.

[4] Edizer, S., Veronesi, B., Karahan, O., Aviyente, V., Degirmenci, I., Galbiati, A.; Pasini, D. *Macromolecules* **2009**, 42, 1860.

[5] Zhu, L., Lin, N. T., Xie, Z. Y., Lee, S. L., Huang, S. L., Y, J. H., Lee, Y. D., Chen, C.-h., Chen, C. H.; Luh, T. Y. *Macromolecules* **2013**, 46, 656.

[6] Narumi, A., Sakai, R., Ishido, S., Sone, M., Satoh, T., Kaga, H., Nakade, H.; Kakuchi, T. *Macromolecules* **2007**, 40, 9272.

[7] Sakai, R., Satoh, T., Kakuchi, R., Kaga, H.; Kakuchi, T. *Macromolecules* **2004**, 37,.

[8] Terashima, T., Kawabe, M., Miyabara, Y. Yoda, H.; Sawamoto, M. *Nat. Commun.* **2013**, 4, 2321.

[9] Hibi, Y., Tokuoka, S., Terashima, T., Ouchi, M.; Sawamoto, M. *Polym. Chem.* **2011**, 2, 341.

[10] Hibi, Y., Ouchi, M.; Sawamoto, M. *Angew. Chem. Int. Ed.* **2011**, 50, 7434.

[11] Perepichka, I. G.; Perepichka, D. F. *Handbook of Thiophene-Based Materials: Applications in Organic Electronics and Photonics* (John Wiley & Sons, Ltd., **2009**).

[12] Roncali, J. *Chem. Rev.* **2009**, 92, 711.

[13] McCullough, R. D. *Adv. Mater.* **1998**, 10, 93.

[14] Mishra, A., Ma, C. Q.; Bäuerle, P. *Chem. Rev.* **2009**, 109, 1141.

[15] Yokoyama, A., Miyakoshi, R.; Yokozawa, T. *Macromolecules* **2004**, 37, 1169.

[16] Sheina, E. E., Liu, J. S., Iovu, M. C., Laird, W.; McCullough, R. D. *Macromolecules* **2004**, 37, 3526.

[17] Bryan, Z. J.; McNeil, A. J. *Macromolecules* **2013**, 46, 8395.

[18] Yokozawa, T.; Yokoyama, A. *Chem. Rev.* **2009**, 109, 5595.

[19] Yokozawa, T.; Ohta, Y. *Chem. Rev.* **2016**, 4, 1950.

[20] Kiriy, A., Senkovskyy, V.; Sommer, M. *Macromol. Rapid Commun.* **2011**, 32, 1503.

[21] Ahn, T. K., Kim, K. S., Kim, D. Y., Noh, S. B., Aratani, N., Ikeda, C., Osuka, A.; Kim, D. *J. Am. Chem. Soc.* **2006**, 128, 1700.

[22] Mishchenko, A., Vonlanthen, D. Meded, V., Burkle, M., Li, C., Pobelov, I. V., Bagrets, A., Viljas, J. K., Pauly, F., Evers, F., Mayor, M.; Wandlowski, T. *Nano Lett.* **2010**, 10, 156.

[23] Ko, S., Hoke, E. T., Pandey, L., Hong, S., Mondal, R., Risko, C., Yi, Y., Noriega, R., McGehee, M. D., Brédas, J.-L. Salleo, A.; Bao, Z. *J. Am. Chem. Soc.* **2012**, 134, 5222.

[24] Schattenmann, F. J.; Schrock, R. R. Solube, *Macromolecules* **1996**, 29, 8990.

[25] Anders, U., Nuyken, O., Buchmeiser, M. R.; Wurst, K. *Angew. Chem. Int. Ed.* **2002**, 41, 4044.

[26] Kang, E.-H., Lee, I. S.; Choi, T.-L. *J. Am. Chem. Soc.* **2011**, 133, 11904.

[27] Ohshimizu, K., Takahashi, A., Rho, Y., Higashihara, T., Ree, M.; Ueda, M. *Macromolecules* **2011**, 44, 719.

[28] Lamps, J.-P.; Catala, J.-M. *Macromolecules* **2011**, 44, 7962.

[29] Randl, S., Connon, S. J.; Blechert, S. *Chem. Commun.* **2011**, 1796.

[30] Palermo, E. F.; McNeil, A. J. *Macromolecules* **2012**, 45, 5948.

[31] Bronstein, H. A.; Luscombe, C. K. *J. Am. Chem. Soc.* **2009**, 131, 12894.

[32] Vernet, R. D.; Boekelheide, V. *Proc. Nat. Acad. Sci. USA* **1974**, 71, 2961.

[33] Using a strap that has a capacity of guest recognition, a sensing scheme has been established based on twisting a polythiophene backbone, see Marsella, M. J.; Swager, T. M. *J. Am. Chem. Soc.* **1993**, 115, 12214.

[34] Pan, C. J., Zhao, C. H., Takeuchi, M.; Sugiyasu, K. *Chem. Asian. J.* **2015**, 10, 1820.

[35] Sugiyasu, K., Honsho, Y., Harrison, R. M., Sato, A., Yasuda, T., Seki, S.; Takeuchi, M. *J. Am. Chem. Soc.* **2010**, 132, 14754.

[36] Ouchi, Y., Sugiyasu, K., Ogi, S., Sato, A.; Takeuchi, M. *Chem. Asian. J.* **2012**, 7, 75.

[37] Shomura, R., Sugiyasu, K., Yasuda, T., Sato, A.; Takeuchi, M. *Macromolecules* **2012**, 45, 3759.

[38] Pan, C. J., Sugiyasu, K., Aimi, J., Sato, A.; Takeuchi, M. *Angew. Chem. Int. Ed.* **2014**, 53, 8870.

[39] Wu, S., Sun, Y., Huang, L., Wang, J., Zhou, Y., Geng Y.; Wang, F. *Macromolecules* **2010**, 43, 4438.

[40] Zhang, Y., Tajima, K., Hirota, K.; Hashimoto, K. *J. Am. Chem. Soc.* **2008**, 130, 7812.

[41] Yokoyama, A., Kato, R., Miyakoshi, T.; Yokozawa, T. *Macromolecules* **2008**, 41, 7271.

[42] Hollinger, J., Jahnke, A. A., Coombs, N.; Seferos, D. S. *J. Am. Chem. Soc.* **2010**, 132, 8546.

[43] Frisch, M. J., Trucks, G. W., Schlegel, H. B., Scuseria, G. E., Robb, M. A., Cheeseman, J. R., Scalmani, G., Barone, V., Mennucci, B., Petersson, G. A., Nakatsuji, H., Caricato, M., Li, X., Hratchian, H. P., Izmaylov, A. F., Bloino, J., Zheng, G., Sonnenberg, J. L., Hada, M., Ehara, M., Toyota, K., Fukuda, R., Hasegawa, J., Ishida, M., Nakajima, T., Honda, Y., Kitao, O., Nakai, H., Vreven, T., Montgomery, Jr., J. A., Peralta, J. E., Ogliaro, F., Bearpark, M., Heyd, J. J., Brothers, E., Kudin, K. N., Staroverov, V. N., Keith, T., Kobayashi, R., Normand, J., Raghavachari, K., Rendell, A.; Burant, J. C., Iyengar, S. S., Tomasi, J., Cossi, M., Rega, N., Millam, J. M., Klene, M., Knox, J. E., Cross, J. B., Bakken, V., Adamo, C., Jaramillo, J., Gomperts, R., Stratmann, R. E., Yazyev, O., Austin, A. J., Cammi, R., Pomelli, C., Ochterski, J. W., Martin, R. L., Morokuma, K., Zakrzewski, V. G., Voth, G. A., Salvador, P., Dannenberg, J. J., Dapprich, S., Daniels, A. D., Farkas, O., Foresman, J. B., Ortiz, J. V., Cioslowski, J.,; Fox, D. J., Gaussian 09, Revision E.01, Gaussian, Inc., Wallingford CT, **2013**.

Chapter 3. Stabilization of Charge Carriers in Picket-Fence Polythiophenes Using Dielectric Side Chains

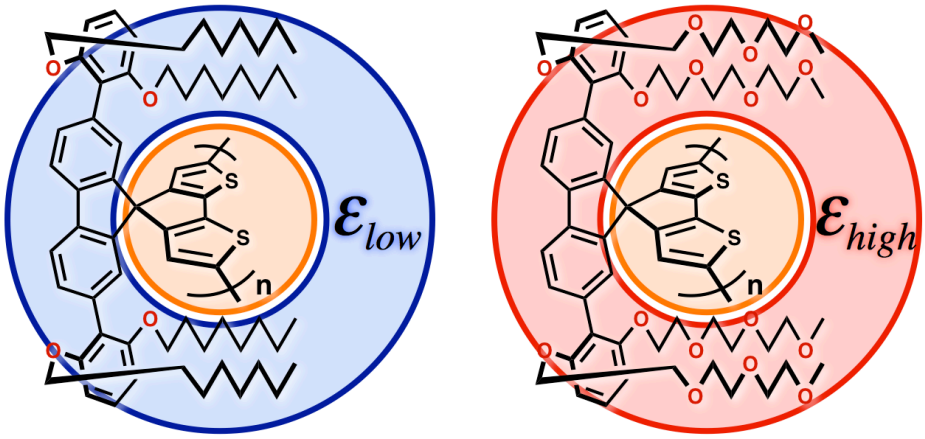

ABSTRACT

Insulated molecular wires (IMWs) are π-conjugated polymers that are molecularly sheathed with an insulating layer and are structurally analogous to electric power cords at the nanoscale. Herein, we propose a new molecular design concept of IMWs, in which the sheaths can be customized, thereby enabling the modulation of the electronic properties of the interior π-conjugated systems. We found that the charge carriers generated in these IMWs can be stabilized by using sheaths with a high dielectric constant owing to the charge screening effect. We expect that IMWs designed in this way will be useful in a variety of applications, where the nature of charge carriers plays an important role.

3.1 Introduction

The generation of charge carriers in π-conjugated polymers (CPs) upon 'doping' is the origin of intriguing properties such as electric conduction,[1,2] electrochromism,[3] and magnetism.[4] A variety of charge carriers may be considered depending on how charges are delocalized over the molecular orbital as a function of both intrachain conjugation and interchain interactions. In addition to conventional polaron and bipolaron charge carriers,[5,6] σ-dimers,[7,8] π-dimers,[9-12] and polaron pairs[13-17] have been proposed. Each charge carrier exhibits unique electronic and magnetic properties, although it is difficult to control the generation of a particular type of charge carrier, especially in the solid state, because of complex redox equilibria among them.

In this context, molecularly sheathed CPs, which are often referred to as insulated molecular wires (IMWs),[18-37] have attracted increasing attention, because molecular design allows the isolation of charge carriers in the 1D electric conduction pathway. We have previously synthesized the polythiophene-based IMWs (**P$_{STB}$**,[32] **P$_{1EDOT}$**,[33] and **P$_{PF}$**[34]) shown in Scheme 3-1a and, with these unique materials in hand, have succeeded in exploring charge carrier mobility[32] and charge carrier transformation[33] within a single polythiophene wire. Importantly, it was found that generation and transformation of charge carriers clearly occurred in the IMWs because of the absence of interchain interactions. Such precise control over charge carrier generation should provide deep insights into the conduction mechanism and reveal the unexplored potential of CPs, thus paving the way for new applications.

However, in our previous study on **P$_{PF}$**,[34] we found that the doped state of insulated polythiophenes (prepared using iodine vapor) was readily de-doped to the neutral state within several minutes, while that of unsheathed polythiophene was retained for several days. Associated with this observation is the study of a poly(3-hexylthiophene) (P3HT) film by Österbacka *et al.*,[38] in which it was found that polarons were two-dimensionally delocalized over several polymer chains though π–π interchain interactions. In other words, charge carriers generated in insulated polythiophenes are less stable than those formed in P3HT films because of the lack of interchain delocalization. To address this tradeoff and to extend the use of 'doped' IMWs to various applications, we sought to stabilize the charge carriers in IMWs by molecular design by focusing on the dielectric properties of the insulating sheaths. The dielectric constant (or relative permittivity) expresses the force between two point charges in materials as:

$$F = q^2/4\pi\varepsilon_0\varepsilon_r r_0$$

where q, ε_0, ε_r, and r_0 are the elementary charge, the permittivity of free space, the dielectric constant of the material, and the separation between two point charges, respectively. As such, the Coulomb attraction

force (F) between positive and negative charges is inversely proportional to ε_r; therefore, we hypothesize that the nature of the charge carriers in IMWs can be modulated by changing the dielectric sheaths.

With this idea in mind, we modified the previously reported "picket-fence" polythiophene ($\mathbf{P_{PF}}$)[34] and designed a new insulated polymer (**P1**), a polythiophene that is fenced by orthogonally equipped rigid "pickets" (Scheme 3-1a). The main framework of the monomer, 7-spiro(9-fluorenyl)-cyclopentadithiophene (SFT), was reported by Bäuerle *et al.*[39] in 2001 as a building block of oligothiophenes for electrogenerated chemiluminescence applications, but its polymerization was not attempted. Later, Ng and co-workers[40] electrochemically synthesized a poly(SFT) film to fabricate a heterojunction diode. However, as is often problematic with such insoluble polymeric materials, thorough characterization of the polymer was not performed. Among IMWs with a similar fluorene-based structure, Aso, Ie, *et al.* have reported the insulated oligothiophenes **R-*n*T-R** for use in single molecule conductance measurements.[25,26] In this study, we introduce a fluorene "picket" with 2,6-dialkoxy phenyl groups that wrap around the polythoiphene backbone (Scheme 3-1b). Compared to the previous IMWs, our new molecular design is unique in that the sheaths can be customized, thereby modulating the electronic properties of π-conjugated systems in the interior (see below). We note that there are several reports on conjugated polymers encapsulated by electronically or photophysically active sheaths;[41-44] however, for 'insulation' purpose, sheaths of IMWs have been regarded as inert protecting components, and little attention has been directed to design the sheaths. To prove the concept of this study, we functionalized the picket with octyl and triethylene glycol chains, which have dielectric constants of 1.9 and 7.6,[45] respectively.

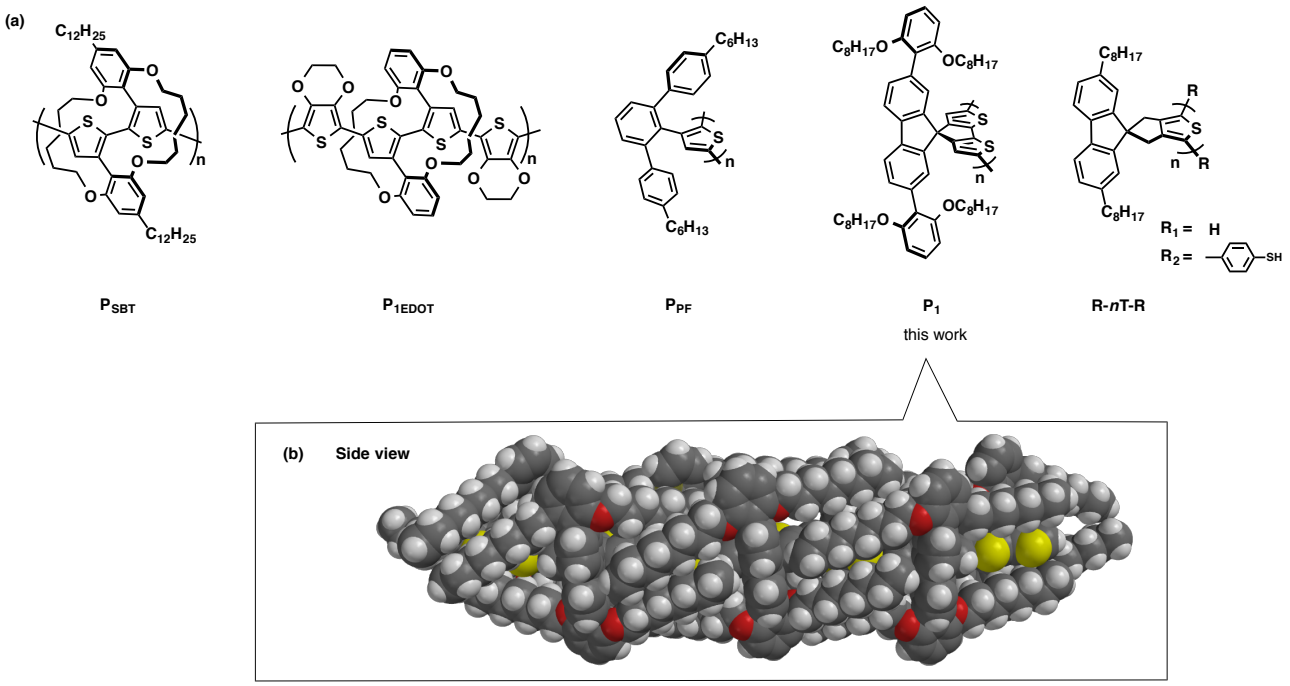

Scheme 3-1. (a) Insulated polythiophenes reported in our previous study ($\mathbf{P_{STB}}$, $\mathbf{P_{1EDOT}}$ **and** $\mathbf{P_{PF}}$) and the one used in this study (**P1**). Insulated oligothiophenes reported by Aso, Ie, *et al.* (**R-*n*T-R**). (b) Computer-generated model of **P1** showing that the polythiophene backbone is completely "insulated" by the picket fence structure.

Herein, we report the synthesis of the new IMWs and their structure-property relationships. Similar to our previously reported insulated polythiophenes, **P1** was found to have completely isolated and well-developed conjugation. We show that the doped state of **P1** film can be stabilized by replacing the octyl chains with triethylene glycol (TEG) chains (namely, **P1-TEG**; see below). This molecular design concept is important, not only for knowing the nature of the charge carriers generated in 1D molecular wires, but also for extending the use of doped IMWs to various applications.

3.2 Results and discussions

3.2.1 Synthesis of monomers, oligomers, and polymers

The monomers were synthesized from 2,3-dibromothiophene in 7 steps (Scheme 3-2). The key step was the protection of the α-positions of 3-bromo-2,2'-bithiophene (**1**) by trimethylsilyl (TMS) groups (step ii),

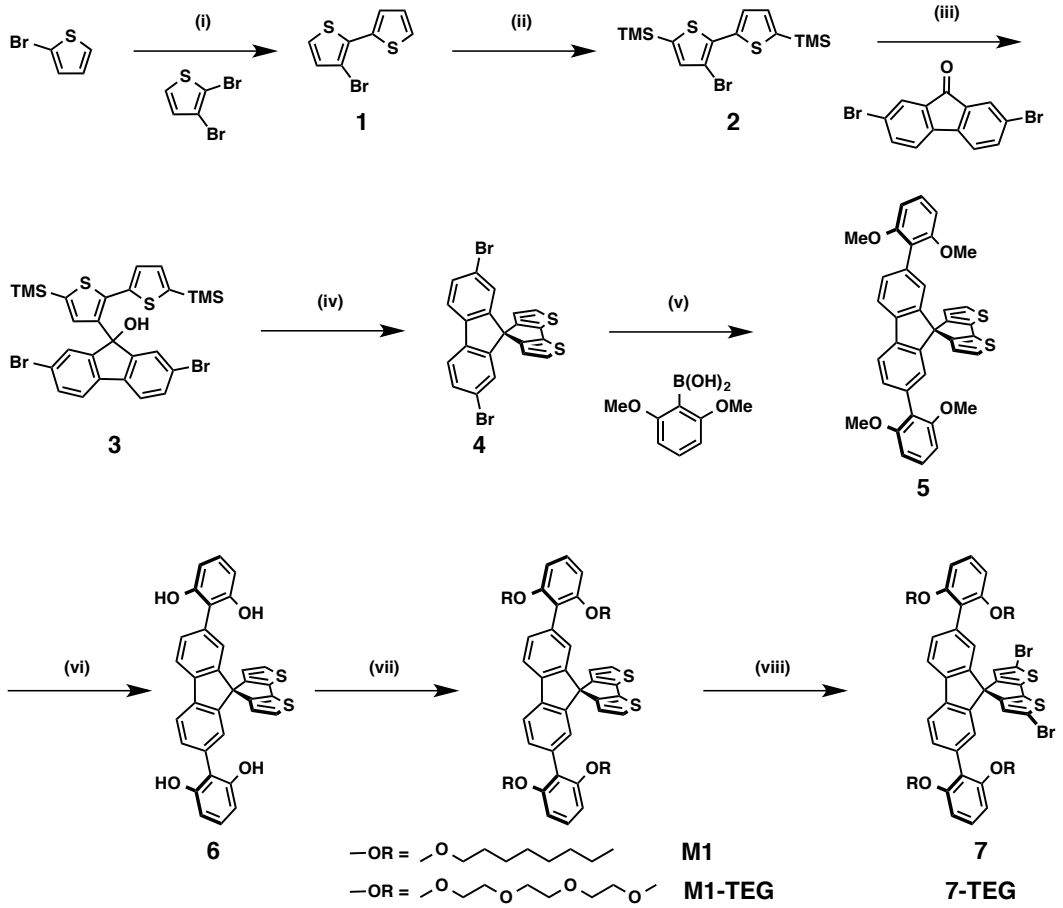

Scheme 3-2. Synthesis of the monomers $\mathbf{M1_1}$ and $\mathbf{M1_1}$**-TEG**: (i) Mg, Et_2O, 0 °C, and then, $Pd(dppf)Cl_2$, 2,3-dibromothiophene; (ii) LDA, THF, -78 °C, and then, TMSCl; (iii) *n*-BuLi, Et_2O, -78 °C, and then, 2,7-dibromo-9-fluorenone; (iv) acetic acid, sulfuric acid, hexane, 65 °C; (v) 2,6-dimethoxyphenylboronic acid, s-phos, $Pd_2(dba)_3$, K_3PO_4, toluene, 80 °C; (vi) BBr_3, DCM; (vii) 1-bromooctane, $CsCO_3$, DMSO, 80 °C; (viii) tri(ethylene glycol) monomethyl ether tosylate, $CsCO_3$, DMSO, 80 °C.

which improved the yields of the subsequent reactions significantly. Otherwise, 3-lithio-2,2'-bithiophene (without TMS groups) was readily transformed into 5-lithio-2,2'-bithiophene in step iii by lithium exchange, which shuffles the reactive position (Figure 3-3). In addition, dimerization and trimerization in step iv via the reactive α-positions was unavoidable in the absence of TMS protecting groups (Figure 3-3).[46] By circumventing these undesired reactions, the SFT framework (**4**) was efficiently synthesized. 2,6-Dimethoxy phenyl groups were introduced through Suzuki–Miyaura coupling under Buchwald conditions in good yield.[47] The X-ray crystallographic structure of **5** shows the orthogonal arrangement of the bithiophene and fluorene frameworks (Scheme 3-4), which should effectively suppress interchain π–π interactions. In addition, given the free volume around the rigid framework of **5**, it is reasonable to assert that the side chains engulf the polymer backbone in the solid state as illustrated in Scheme 3-2. Demethylation using

tribromoborane followed by Williamson ether synthesis afforded the SFT-based monomers **M1$_1$** and **M1$_1$-TEG** with octyl and triethylene glycol chains, respectively. Both monomers were unambiguously characterized by ^{1}H-NMR, ^{13}C-NMR, and MALDI-TOF-MS spectroscopic methods and by elemental analysis.

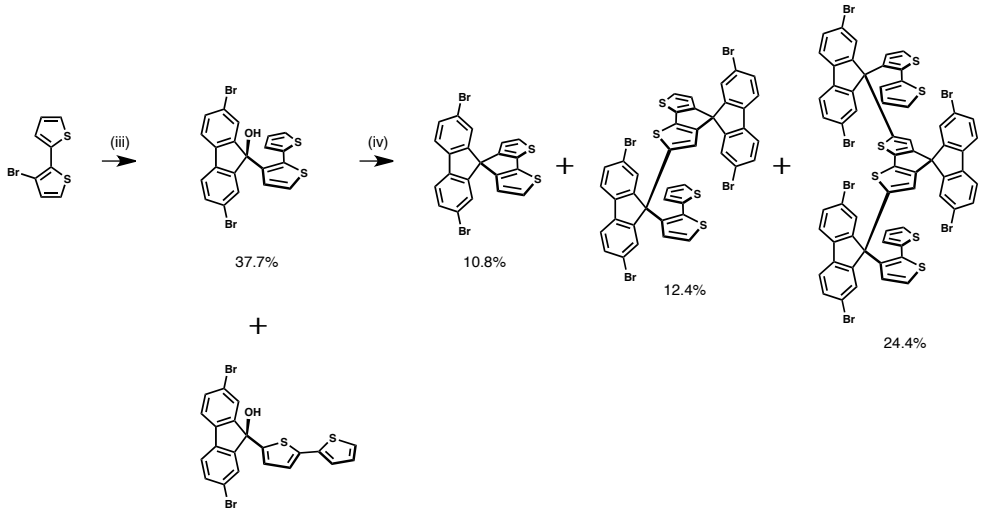

Scheme. 3-3. Without the protecting TMS groups, undesired side reactions were unavoidable: (iii) *n*-BuLi, Et_2O, -78°C, and then, 2,7-dibromo-9-fluorenone, Et_2O, RT; (iv) acetic acid, sulfuric acid, hexane, 65°C.

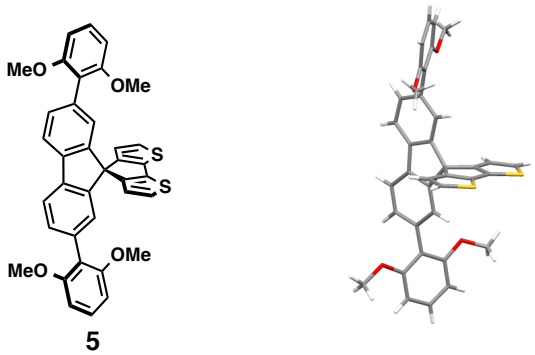

Scheme. 3-4. X-ray crystallographic structure of **5**.

Structures of oligomers and polymers used in this study are shown in Scheme 3-5. To perform oligomer studies *in solution*, we presumed that flexible side chains would spread out and have negligible impact on the electronic characteristics of polythiophene backbone. We synthesized **M1$_2$**–**M1$_5$** oligomers because synthesis and purification of these compounds were relatively easier than **M1$_1$-TEG** analogues.

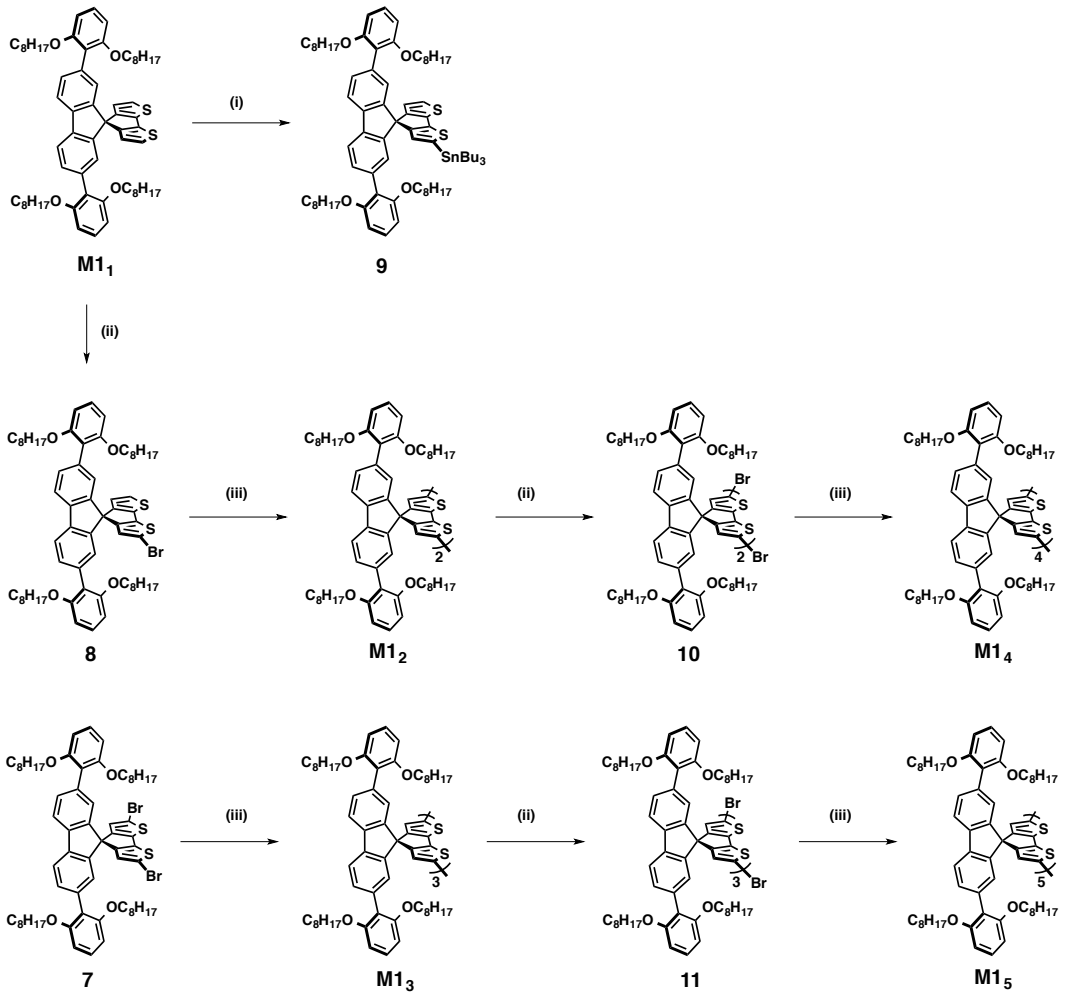

Scheme 3-5. Synthetic scheme toward oligmers: (i) *n*-BuLi, THF, -78 ºC, and then, tributyltin chloride, RT; (ii) NBS, THF, RT; (iii) $Pd(PPh_3)_4$, compound **9**, toluene, reflux.

Oligothiophenes up to the pentamer (*i.e.*, **M1$_2$**–**M1$_5$**) were synthesized in a stepwise manner through Stille coupling; therefore, the end groups of these oligomers are protons (Scheme 3-5). Polymerization was performed under Yamamoto reductive coupling conditions using a $Ni(COD)_2$ and bipyridine system in a toluene and dimethylformamide (DMF) mixture (Scheme 3-6) to yield **P1** and **P1-TEG**.[48-50] The number average molecular weight (M_n), degree of polymerization (DP), and polydispersity index (PDI) determined by size-exclusion chromatography (polystyrene standard) were 21.4K, 22, and 2.75 for **P1** and 15.1K, 14,

and 1.8 for **P1-TEG**, respectively. Note, however, that the M_n of **P1-TEG** could be underestimated due to the polar side chains that may extend the retention time.

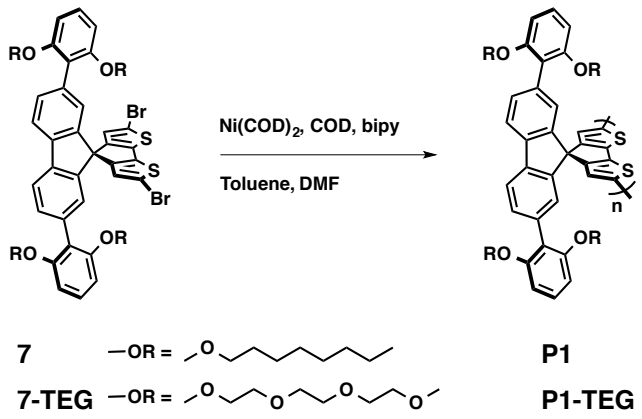

Scheme 3-6. Polymerization scheme toward **P1** and **P1-TEG**.

3.2.2 Characterization of IMWs

Absorption spectra of $\mathbf{M1_1}$–$\mathbf{M1_5}$ measured in dichloromethane (DCM) solution are shown in Figure 3-1a. The absorption band around 305 nm is assigned to the fluorene picket; those appearing at longer wavelengths are attributed to the conjugated cyclopentadithiophene frameworks. As the number of repeat units increases, the longer wavelength band maximum shifts bathochromically. Figure 3-1b shows the linear fit of the electronic transition energy determined from the absorption maximum *vs.* the inverse ring number (1/n') as:

$$E\ (\text{eV}) = 3.76/\text{n}' + 1.93 \quad (1)$$

where n' is the number of thiophenes in the oligomers and not the monomer units (*i.e.*, n' = 2n). The coefficient of the plot (3.76) is comparable to that of unsubstituted oligothiophenes (3.73)[51] and those of other IMWs (3.68 for $\mathbf{P_{STB}}$[32] and 3.85 for **R-*n*T-R**[25]).

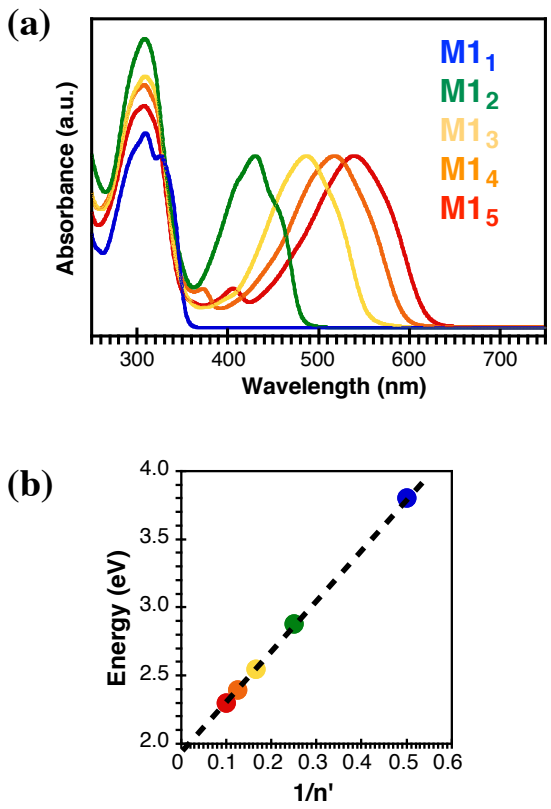

Figure 3-1. (a) Absorption spectra of $\mathbf{M1_1}$ (blue), $\mathbf{M1_2}$ (green), $\mathbf{M1_3}$ (yellow), $\mathbf{M1_4}$ (orange), and $\mathbf{M1_5}$ (red). (b) Plot of transition energy determined from the absorption maxima as a function of the inverse of the number of thiophenes in the oligomers (n').

TD-DFT calculations using the DFT(M06-2X)/6-31G(d,p) method corroborated this result. The first electric-dipole-allowed excitation is assigned to the HOMO-LUMO transition with a large oscillator strength (*f*). In the n = 6 hexamer, *f* was calculated to be 4.293. These molecular orbitals are assigned to the oligo(cyclopentadithiophene) backbone shown in Figure 3-2. They are essentially delocalized over the backbone. In the series of the oligomers, the HOMO-LUMO transition energy was proportional to the inverse ring number, as described by eq. 2 (Figure 3-4).

$$E\ (\text{eV}) = 4.18/\text{n}' + 2.09 \quad (2)$$

This relationship is in agreement with the experimental results taking the approximate nature of the calculations into account. These oligomer studies clearly demonstrate that **P1** has well-developed conjugation in spite of the bulky picket fence side chains.

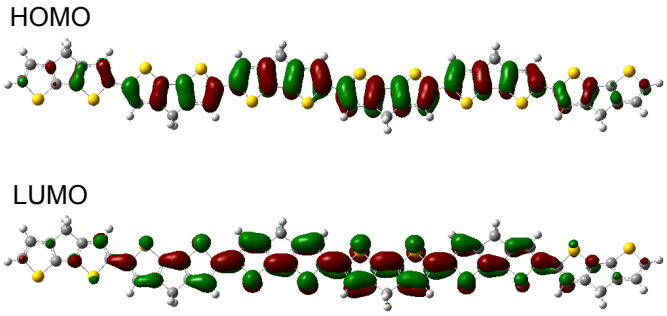

Figure 3-2. HOMO and LUMO of a model of the (cyclopentadithiophene)$_6$ calculated using the DFT(M06-2X)/6-31G(d,p) level. To isolate the fragment, the connecting C-C bonds were replaced with the C-H bonds of 1.085 Å. The HOMO and LUMO of **M1$_6$** are shown in Figure 3-3.

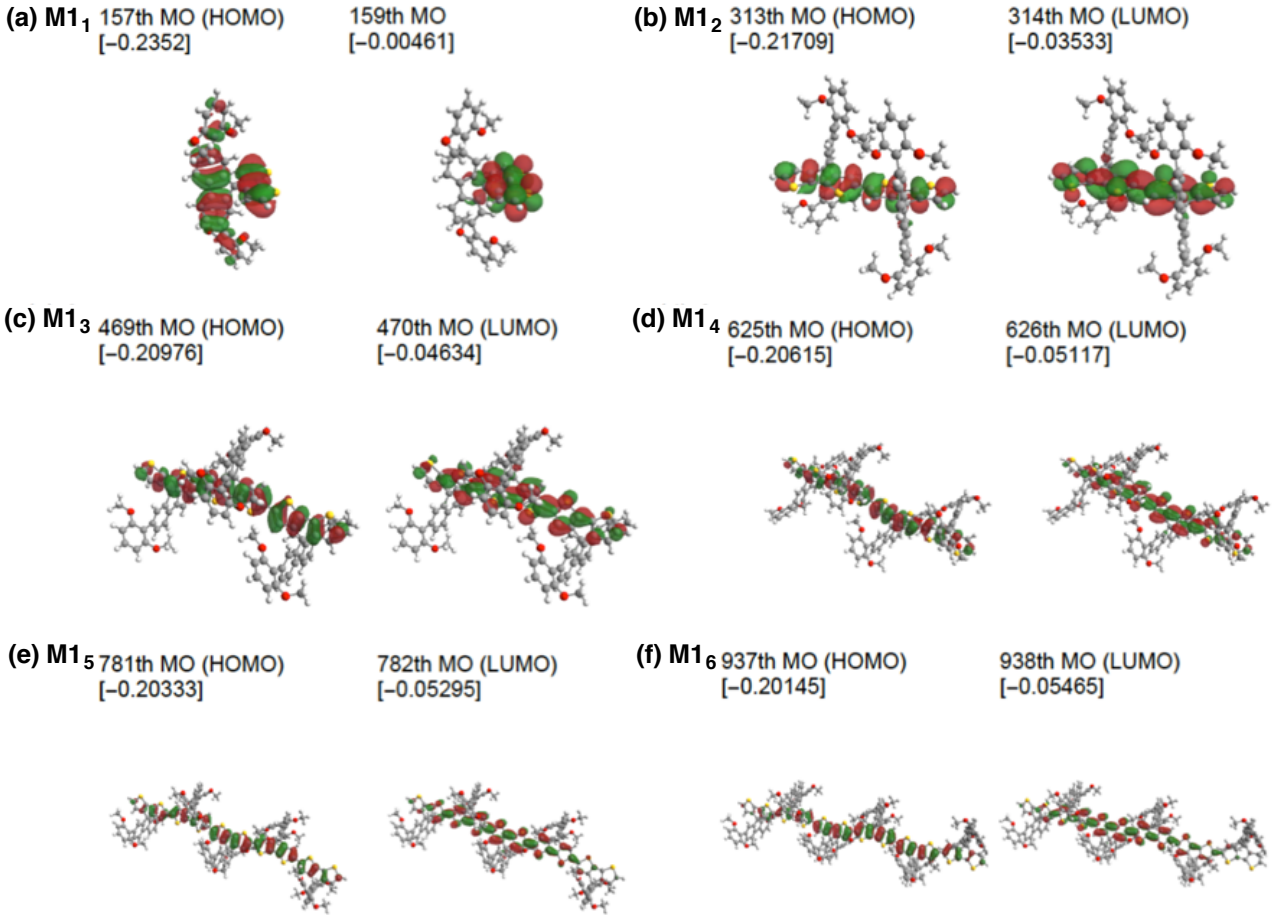

Figure 3-3. The HOMO and LUMO of **M1$_1$**-**M1$_6$**.

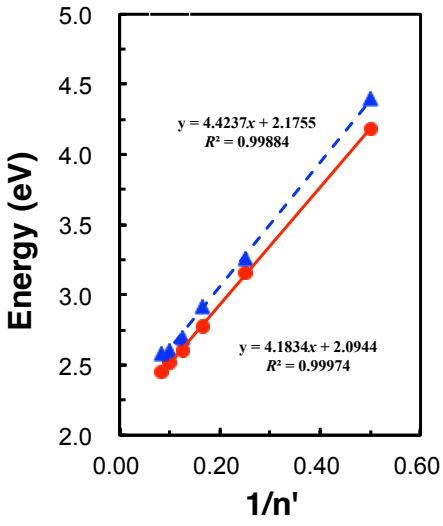

Figure 3-4. Size (*n*') dependence of the $S_0 \rightarrow S_1$ excitation energies (ΔE) of **M1$_1$-M1$_6$** (circle) and the corresponding isolated oligothiophenes (triangle). The solid and dashed lines indicate the results of the linear fitting. The geometries of all the compounds were optimized using the DFT(M06-2X)/6-31G(d,p) method.

To examine the redox behavior, cyclic voltammetry (CV) was carried out in DCM containing tetrabutylammounium hexafluorophosphate ($TBAPF_6$) as the supporting electrolyte. Figure 3-5 shows the CVs of **M1$_3$**, **M1$_5$** and **P1**. Aso, Ie, *et al.* reported the CV of sexithiophene **R-*n*T-R** (**Scheme 3-1a**), which has a π-electronic conjugation comparable to that of **M1$_3$**. Oxidation of **R-*n*T-R** (R = H, n = 6) occurred at 0.21 V and 0.49 V (*vs*. Fc/Fc^+),[25] whereas that of **M1$_3$** was observed at 0.09 V and 0.36 V. This result suggests that the cyclopentadithiophene conjugation produces a slightly higher HOMO that α-oligothiophene conjugation. The two oxidation steps are attributable to the formation of a polaron and bipolaron, repectively. In the longer oligomer **M1$_5$**, a four step oxidation process was clearly observed, and the polymer **P1** showed a broad featureless CV. These results indicated multiple charges can be injected into a poly(cyclopentadithiophene) chain.[13]

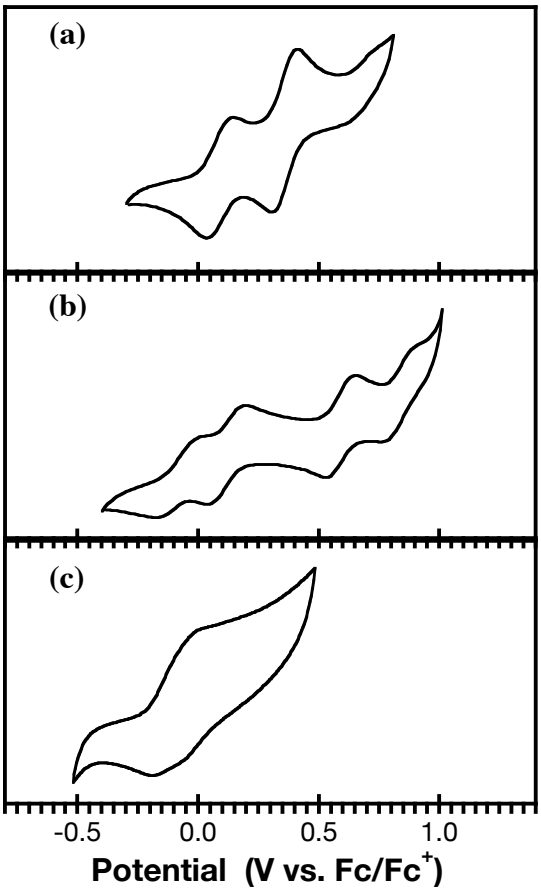

Figure 3-5. Cyclic voltammograms of (a) $\mathbf{M1_3}$, (b) $\mathbf{M1_5}$, and (c) **P1** in DCM with 100 mM $TBAPF_6$.

Absorption spectra of **P1** and **P1-TEG** in solution and as films are compared in Figure 3-6. The polymers showed identical spectra in solution and as films, which indicated that the poly(cyclopentadithiophene) backbone was completely isolated and that interchain π–π interaction was effectively prevented.[32-34] We did not observe a significant difference between **P1** and **P1-TEG**, and thus conclude that the side chains have a negligible impact on electronic structure in the neutral (undoped) state. In fact, these polymers did not show significant solvatochromic behavior in absorption spectra in common organic solvents such as DMF (ε_r = 48.9), tetrahydrofuran (7.5), chloroform (4.8), and benzene (2.3) (Figure 3-7).[52]

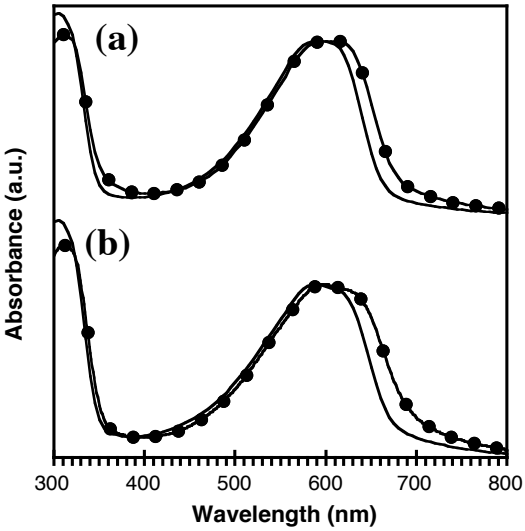

Figure 3-6. Absorption spectra of (a) **P1** and (b) **P1-TEG** in DCM solution (lines with dots) and in the film state (solid lines).

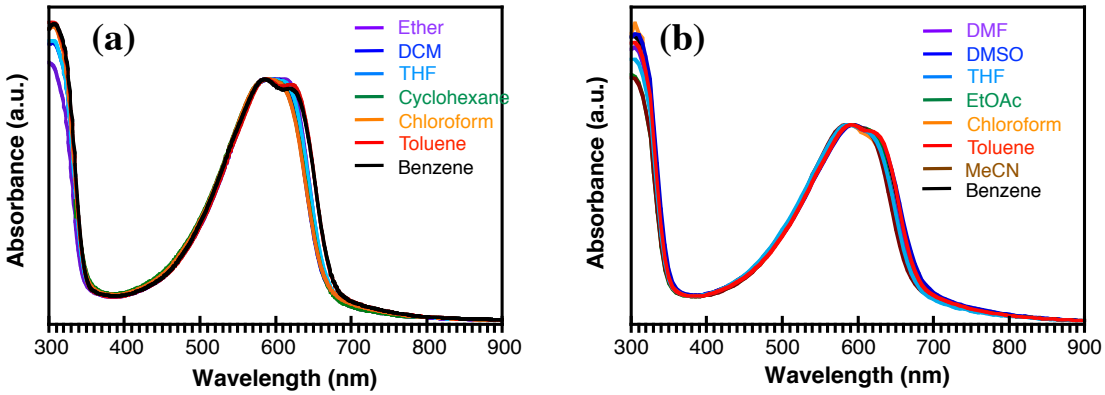

Figure 3-7. UV-Vis absorption spectra of (a) **P1** and (b) **P1-TEG** on various organic solvents: diethyl ether (Ether), dichloromethane (DCM), tetrahydrofuran (THF), cyclohexane, chloroform, toluene, benzene, acetonitrile (MeCN), ethyl acetate (EtOAc), dimethylformamide (DMF), dimethylsulfoxide (DMSO).

2.2.3 Doping experiment

Doping-induced absorption spectral changes were first investigated for **P1** in solution. Chemical oxidation of **P1** using antimony pentachloride ($SbCl_5$) in dichloromethane (DCM) resulted in the bleaching of the neutral band (2.06 eV) and the concomitant appearance of absorption bands in the near infrared (NIR) region. Hereafter, the stoichiometry of $SbCl_5$ against **P1** is shown with respect to the number of thiophene

(not monomer **M1**$_1$) units, and the doping level is calculated as [$SbCl_5$]/[thiophene unit], assuming that each $SbCl_5$ added stoichiometrically generates one positive charge.

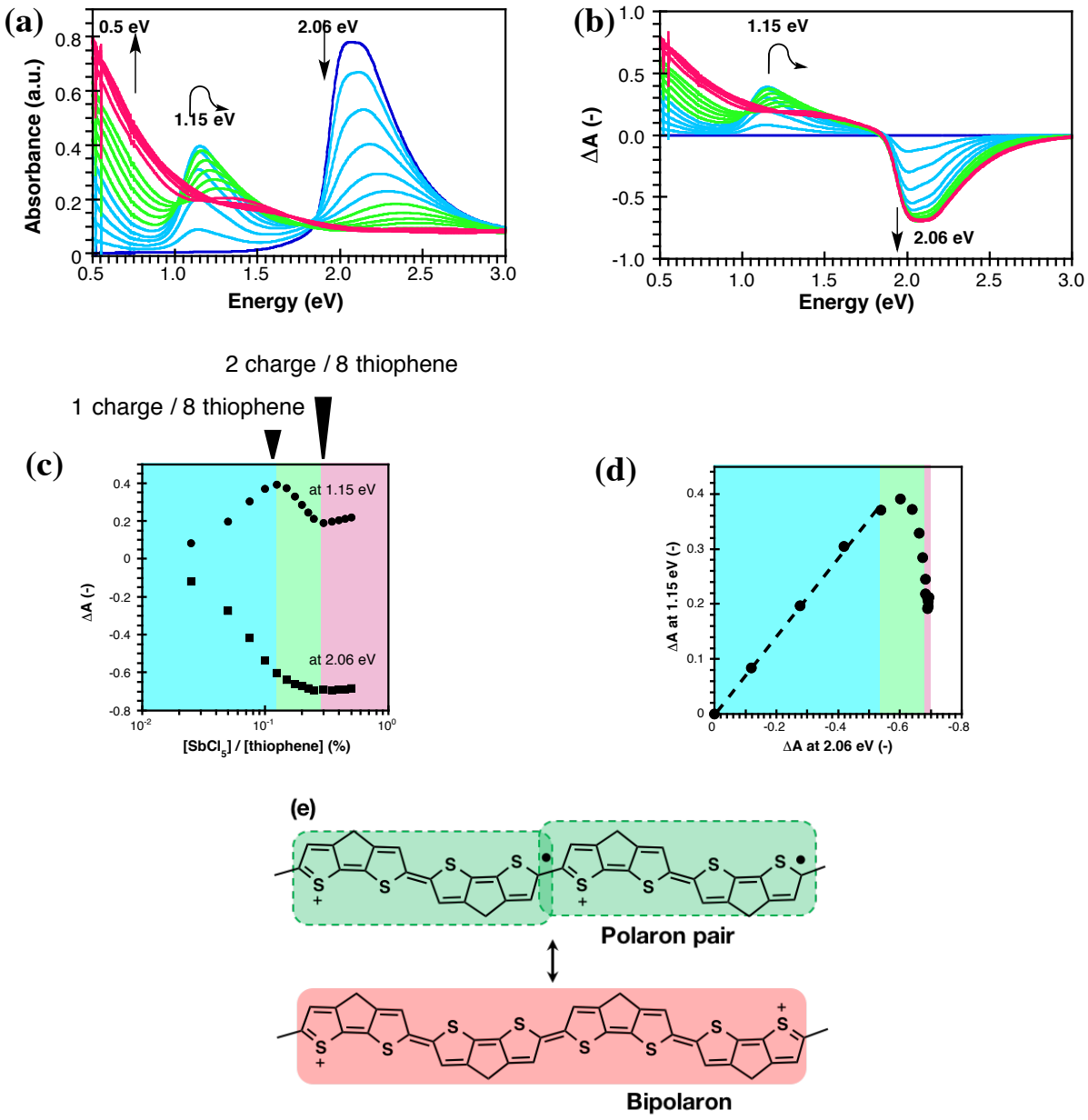

Figure 3-8. (a) Absorption spectra and (b) difference in absorption spectra (ΔA) of **P1** upon oxidation with $SbCl_5$ in DCM solution. (c) Plots of absorbance difference (ΔA) at 1.15 eV (circles) and 2.06 eV (squares) as a function of doping level. (d) Plot of difference in absorbance (ΔA) at 1.15 eV as a function of that at 2.06 eV. (e) Polaron pair *vs.* bipolaron rivalry occurs when two charges are injected onto 8 thiophene units (*ca.* 25 % doping level).

As shown in Figures 3-8a-c, the spectral changes of **P1** upon doping can be divided into three stages as indicated by the blue, green, and red regimes.[33] In the early stage of doping (blue), the bleaching of the neutral band (2.06 eV) correlated linearly with the increase in absorbance at 1.15 eV with accompanying isosbestic points (Figure 3-8d), indicating polaron formation.[53] Further doping caused a deviation of the isosbestic points and a hypsochromic shift of the polaron band (1.15 → 1.25 eV). Here, interchain interaction of the polarons (i.e., π-dimer formation) can be ruled out owing to the sheaths. Therefore, the hypsochromic shift observed in the second stage indicates the interaction of the two polarons in one polymer chain: namely, the formation of a polaron pair.[13,33] The boundary between the first and second stages appeared at a doping level of 12.5%, which suggests that the polaron is delocalized over 8 thiophene units. Eventually, the two absorption bands in the NIR region changed into one broad band when the doping level reached 25% (Figure 3-8c). This spectral change indicates the transformation of the polaron pair to a bipolaron. These results are in good agreement with previous experimental studies[13,33] and theoretical calculations.[14-16]

Next, we investigated the doping process *in the film states* for both **P1** and **P1-TEG**. Drop-cast films were prepared on the inside wall of a septum-capped cuvette, into which iodine vapor was slowly introduced via a syringe. Doping-induced absorption spectral changes of **P1** and **P1-TEG** are shown in Figure 3-9. Comparison between Figure 3-9 and 3-8a allowed us to roughly estimate that the maximum doping level achieved with I_2 vapor was 20%, which is slightly below the point of bipolaron formation. Overall, the doping-induced absorption spectral changes in the film state were similar to those observed in solution, suggesting that the interchain delocalization of charge carriers was prevented owing to the picket fence structure.

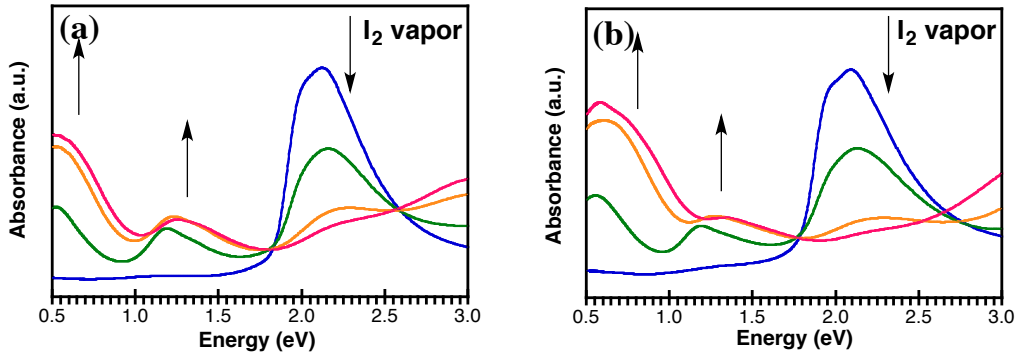

Figure 3-9. Absorption spectral changes of thin films of (a) **P1** and (b) **P1-TEG** upon doping with iodine vapor.

To investigate the stability of the doped states, films of **P1** and **P1-TEG** doped with I_2 vapor were left at ambient conditions, and the de-doping process was monitored by absorption spectroscopy. As shown in Figure 3-10a, the **P1** film was spontaneously de-doped, and the neutral state was recovered. This behavior is consistent with that reported for $\mathbf{P_{PF}}$,[34] suggesting that the doped state of the IMW cannot be retained because interchain delocalization of the charge carriers does not occur. In contrast, the polaron absorption band was observed even after 10 h for the **P1-TEG** film (see Figures 3-10b and c). We assert that a highly doped state can be stabilized by the polar sheaths owing to the charge screening in such a high dielectric media.

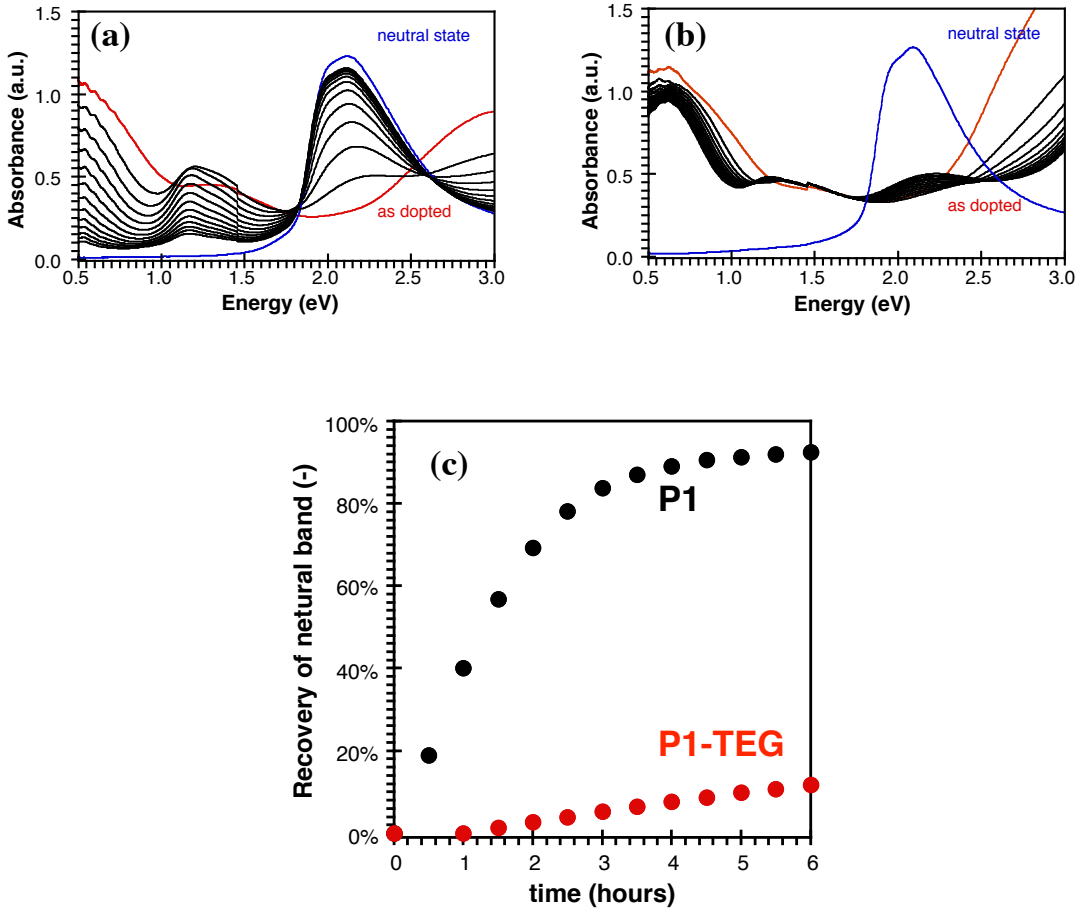

Figure 3-10. Absorption spectral changes of doped (a) **P1** and (b) **P1-TEG** observed during the de-doping process (0 ~ 6 hours). (c) Plots of the recovery of absorbance at 2.1 eV (*i.e.*, neutral band) of **P1** (black) and **P1-TEG** (red) from the as-doped state over time.

To further corroborate the stabilization of charge carriers in **P1-TEG**, we performed flash-photolysis time-resolved microwave conductivity (FP-TRMC) measurements.[54,55] This method allows the decay process of the photogenerated mobile charge carriers to be observed. Upon photoexcitation with a λ = 355 nm laser pulse (in the presence of an electron acceptor, see Experimental Section), the films of **P1** and **P1-TEG** exhibited transient conductivity; *i.e.*, $\phi\sum\mu$, where ϕ and $\sum\mu$ represent the yield of charge carrier generation and the sum of charge carrier mobilities (μ_e + μ_h), respectively. As shown in Figure 3-11, the decay of $\phi\sum\mu$ in **P1-TEG** was slower than that in **P1**, indicating that photogenerated charge carriers have a longer lifetime in **P1-TEG** than in **P1**.

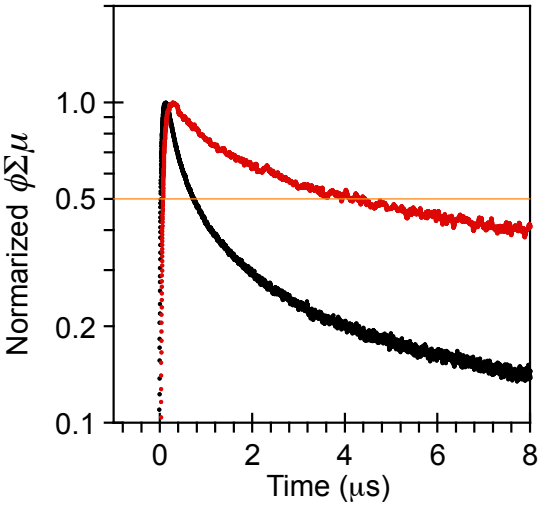

Figure 3-11. Normalized TRMC transients of **P1** (black) and **P1-TEG** (red).

Charge carrier mobility was estimated based on maximum conductivity ($\phi\sum\mu_{max}$) and transient absorption spectroscopy (TAS) measurements. The FP-TRMC/TAS method did not reveal a significant difference in charge carrier mobility between **P1** and **P1-TEG**, with similar μ_h values of *ca.* 0.1 cm^2 V^{-1} s^{-1} for each. We note that Breselge *et al.*[56] synthesized poly(*p*-phenylenevinylene) substituted with triethylene glycol side chains and that Hummelen *et al.*[57] attached triethylene glycol side chains to a fulleropyrrolidine. Both found that the electronic properties of the organic semiconductors, including bulk charge mobility, were unaffected by the triethylene glycol chains. Our result is consistent with these reports, although we measured local intrachain charge carrier transport in this study using the FP-TRMC/TAS method.

The Langevin expression,[58-61] $k_{rec} = q(\mu_e + \mu_h)/\varepsilon_0\varepsilon_r$, describes the non-geminate bimolecular recombination rate constant as a function of charge carrier mobility and dielectric constant. Given that $\mu_e << \mu_h$ can be assumed under our measurement conditions and that the μ_h values of **P1** and **P1-TEG** are

similar, the difference in k_{rec} between **P1** and **P1-TEG** should be governed solely by the difference in ε_r. As shown in Figure 3-11, the half-lives of the charge carriers in **P1** and **P1-TEG** were 0.71 and 4.2 μs, respectively. The difference in the half-lives is reasonably consistent with the difference in the ε_r values of the side chains (1.9 and 7.6 for octyl and TEG side chains, respectively). Thus, we conclude that the sheaths with higher dielectric constants can suppress charge recombination in IMWs owing to charge screening.

2.4 Conclusions

In conclusion, we have designed and synthesized new picket fence polythiophenes based on a 7-spiro(9-fluorenyl)-cyclopentadithiophene (SFT) framework. The spiro linkage was effective in constructing the picket fence structure and preventing interchain interaction. Despite the bulky side chains, well-developed conjugation was achieved as demonstrated by the oligomer studies. The dielectric sheaths can be altered in this new molecular design, thereby allowing the properties of the charge carriers generated in IMWs to be modulated. We found that a highly doped state of insulated polythiophene can be stabilized using sheaths with a high dielectric constant even in the absence of interchain delocalization. We believe that this new molecular design concept can be extended to IMWs in various applications, in which the nature of the charge carriers plays an important role, and particularly when bistability of redox switching is required (*e.g.*, electrochromic and magnetic applications). Synthesis of block and random copolymers using dissimilar sheaths as well as incorporation of other functional groups in sheaths[41-44] could lead to unprecedented IMW-based materials.

2.5 Experimental Section

2.5.1 General

Air and water sensitive synthetic manipulations were performed under an argon atmosphere using standard Schlenk techniques. All chemicals were purchased from Aldrich, TCI, Kanto Chemical, or Wako and used as received without further purification. Column chromatography was performed on silica gel (KANTO Chemical silica gel 60N). ^{1}H NMR and ^{13}C NMR spectra were recorded on a JEOL ECS-400 spectrometer with tetramethylsilane (0 ppm for ^{1}H) or residual $CHCl_3$ (77 ppm for ^{13}C) as an internal standard. MALDI-TOF mass spectra were obtained with SHIMADZU AXIMA-CFR Plus station. UV-Vis absorption spectra were obtained on a JASCO V-670 spectrophotometer. Melting points were determined with a Yanako NP-500P micro melting point apparatus. Elemental analysis (C, H, N) was performed on a Perkin-Elmer 2400 CHN Elemental Analyzer. Gel permeation chromatography was performed using a TOSHO GPC system (HLC-8320GPC EcoSEC) equipped with two TSK gel Super-Multipore HZ-M

columns and a UV detector (254 nm), using THF as an eluent. Electrochemical measurements were conducted with an Eco Chemie AUTOLAB PGSTAT12 potentiostat, using a quasi-internal Ag/Ag^+ reference electrode (Ag wire submersed in MeCN solution of 0.01 M $AgNO_3$ and 0.1 M *n*-Bu_3NPF_6).

2.5.2 Synthesis of monomers, oligomers and polymers

a) Synthesis of monomers and polymers

Synthesis of compound 1: A 500 mL two-neck round-bottom flask was charged with magnesium turnings (3.4 g, 141 mmol) and a small piece of iodine. The flask was evacuated and refilled with argon three times. After addition of diethyl ether (200 mL), 2-bromothiophene (21.1 g, 129 mmol) were slowly added at 0 °C. The mixture was stirred at room temperature for 3 hours, resulting in a Grignard solution. In another 1 L three-neck round-bottom flask, $Pd(dppf)Cl_2$ (898 mg, 1.2 mmol) were placed, and the flask was evacuated and refilled with argon three times. After addition of diethyl ether (300 mL) and 2,3-dibromothiophene (29.7 g, 123 mmol), the Grignard solution was slowly transferred to this flask. The mixture was stirred at room temperature overnight. Then, methanol was slowly added to quench the reaction, and the mixture was washed with water and extracted with diethyl ether. The combined organic layer was washed with brine and dried over $MgSO_4$. After solvent was evaporated, product was purified by column chromatography (silica gel, hexane). Compound **1** was obtained as colorless oil (27 g, 90 %).

^{1}H NMR (CDCl3, 400 MHz, TMS, 298 K): δ 7.03 (d, J = 5.4 Hz, 1H), 7.01–7.02 (m, 1H), 7.19 (d, J = 5.4 Hz, 1H), 7.36 (dd, J = 1.2 & 3.6 Hz, 1H), 7.43 (dd, J = 1.2 & 3.6 Hz, 1H). ^{13}C NMR ($CDCl_3$, 100 MHz, TMS, 298 K): δ 108.01, 124.51, 126.24, 126.90, 127.37, 131.95, 132.39, 134.45. Elemental analysis: Anal. Calcd for C_8H_5BrS: C, 39.19; H, 2.06. Found: C, 38.98; H, 2.06.

Synthesis of compund 2: A 100 mL two-neck round-bottom flask was evacuated and refilled with argon three times. After addition of diisopropylamine (2.60 g, 26 mmol) and THF (30 mL), *n*-BuLi in hexane (2.6 M, 9.5 mL, 24.8 mmol) was added slowly at -78 ºC. The mixture was stirred for 15 minutes. Then, compound **1** (2.76 g, 11.28 mmol) in THF (20 mL) was added to reaction mixture at -78 ºC. After the mixture was stirred for 20 minutes, trimethylsilyl chloride (4.29 g, 39.5 mmol) was added at -78 ºC. The mixture was stirred at room temperature for 1 hour, and then washed with water and extracted with DCM three times. The combined organic layer was washed with brine and dried over $MgSO_4$. After the solvent was evaporated, product was purified by column chromatography (silica gel, DCM / hexane = 1 / 4). Compound **2** was obtained as colorless oil (4.2 g, 95 %).

^{1}H NMR (CDCl3, 400 MHz, TMS, 298 K): δ 0.35 (s, 9H), 0.37 (s, 9H), 7.13 (s, 1H), 7.22 (d, J = 3.8 Hz, 1H), 7.53 (d, J = 3.8 Hz, 1H) ^{13}C NMR (CDCl3, 100 MHz, TMS, 298 K): δ -0.27, 0.30, 108.84, 127.74,

134.32, 137.11, 138.26, 139.69, 139.77, 141.54. Elemental analysis: Anal. Calcd for $C_{14}H_{21}BrS_2Si_2$: C, 43.17; H, 5.43. Found: C, 43.24; H, 5.58.

Synthesis of compound 3: A 200 mL two-neck round-bottom flask was charged with compound **2** (3.37 g, 8.7 mmol), and evacuated and refilled with argon three times. After addition of diethyl ether (50 mL), *n*-BuLi in hexane (2.6 M, 3.4 mL, 8.7 mmol) was added slowly at -78 ºC. The mixture was stirred at room temperature for 1 hour. Then, 2,7-dibromo-9-fluorenone (3.0 g, 8.7 mmol) was added into mixture at -78 ºC, and the resulting solution was stirred at room temperature overnight. The mixture was washed with water and extracted with EtOAc three times. The combined organic layer was washed with brine and dried over $MgSO_4$. After the solvent was evaporated, product was purified by column chromatography (silica gel, DCM / hexane = 1 / 3). Compound **3** was obtained as white solid (4.9 g, 88 %).
M. p.:74.0 ºC. ^{1}H NMR (CDCl3, 400 MHz, TMS, 298 K): δ 0.22 (s, 9H), 0.39 (s, 9H), 2.44 (s, 1H), 6.03 (d, J = 3.4 Hz, 1H), 6.63 (d, J = 3.4 Hz, 1H), 7.21 (d, J = 8.0 Hz, 2H), 7.37 (dd, J = 8.0 & 1.6 Hz, 2H), 7.42 (d, J = 1.2 Hz, 2H), 7.73 (s, 1H) ^{13}C NMR ($CDCl_3$, 100 MHz, TMS, 298 K): δ -0.12, 0.07, 81.95, 121.26, 122.24, 128.41, 129.73, 132.30, 133.04, 134.32, 135.93, 137.70, 138.35, 140.58, 140.64, 142.63, 150.92. MALDI-TOF mass (Matrix: DCTB): Found m/z = 647.82, calculated ($C_{27}H_{28}Br_2OS_2Si_2$) 647.95. Elemental analysis: Anal. Calcd for $C_{27}H_{28}Br_2OS_2Si_2$: C, 50.00; H, 4.35. Found: C, 49.68; H, 4.43.

Synthesis of compound 4: A 500 mL two-neck round-bottom flask was charged with compound **3** (571 mg, 0.9 mmol). After addition of hexane (300 mL), CH_3COOH (25 mL) was added slowly at 60 ºC, and the resulting mixture was stirred for 10 minutes. Then, H_2SO_4 (2.5 mL) was added into flask dropwise. The mixture was stirred at 60 ºC for 2 hours, and poured into $NaHCO_3$ solution. After the organic solvent was evaporated, the mixture of $NaHCO_3$ layer and concentrated organic layer was washed with water and extracted with EtOAc three times. The combined organic layer was washed with brine and dried over $MgSO_4$. After the solvent was evaporated, product was purified by column chromatography (silica gel, DCM / hexane = 1 / 4). The compound **4** was obtained as white solid (400 mg, 87 %).
M.p.: 260 ºC. ^{1}H NMR (CDCl3, 400 MHz, TMS, 298 K): δ 6.41 (d, J = 4.8 Hz, 2H), 6.96 (d, J = 2.0 Hz, 2H), 7.12 (d, J = 4.8 Hz, 2H), 7.48 – 7.50 (m, 2H), 7.63 (d, J = 8.4 Hz, 2H). ^{13}C NMR ($CDCl_3$, 100 MHz, TMS, 298 K): δ 61.32, 121.42, 121.62, 121.91, 126.21, 126.97, 131.38, 139.00, 139.62, 147.13, 152.97. MALDI-TOF mass (Matrix: DCTB): Found m/z = 485.92, calculated ($C_{21}H_{10}Br_2S_2$) 485.86. Elemental analysis: Anal. Calcd for $C_{21}H_{10}Br_2S_2$: C, 51.87; H, 2.07. Found: C, 51.83; H, 1.98.

Synthesis of compound 5: A 100 mL two-neck round-bottom flask was charged with compound **4** (2.31 g, 4.7 mmol), 2,6-dimethylphenylboronic acid (3.46 g, 19 mmol), K_3PO_4 (6.05 g, 28.5 mmol), $Pd_2(dba)_3$(174 mg, 0.19 mmol) and s-phos(156 mg, 0.38 mmol). The flask was evacuated and refilled argon three times.

After addition of anhydrous toluene (13 mL), the mixture was stirred at 100 ºC overnight, then cooled to room temperature, and washed with water and extracted with DCM three times. The combined organic layer was washed with brine and dried over $MgSO_4$. After the solvent was evaporated, the product was purified by reprecipitation (DCM / hexane). Compound **5** was obtained as brown solid (2.46 g, 80 %).

M. p.: > 300 °C. ^{1}H NMR (CDCl3, 400 MHz, TMS, 298 K): δ 3.60 (s, 12H), 6.54 – 6.56 (m, 6H), 6.83 (d, J = 1.6 Hz, 2H), 7.03 (d, J = 4.8 Hz, 2H), 7.17 (t, J = 8.0 Hz, 2H), 7.39 (dd, J = 8.0 & 1.6 Hz, 2H), 7.82 (d, J = 8.0 Hz, 2H). ^{13}C NMR ($CDCl_3$, 100 MHz, TMS, 298 K): δ 55.90, 62.06, 104.54, 119.28, 119.53, 122.19, 124.79, 126.75, 128.53, 130.52, 132.97, 138.21, 140.50, 144.36, 155.31, 157.57. MALDI-TOF mass (Matrix: DCTB): Found m/z = 600.09, calculated ($C_{37}H_{28}O_4S_2$) 600.14. Elemental analysis: Anal. Calcd for $C_{37}H_{28}O_4S_2$•1.2CH_2Cl_2: C, 65.30; H, 4.36. Found: C, 65.29; H, 3.96.

Synthesis of compound 6: A 2 L three-neck round-bottom flask was charged with compound **5** (3.6 g, 6.0 mmol), and evacuated and refilled argon three times. After addition of DCM (1.2 L), BBr_3 (6.0 g, 24.2 mmol) was added slowly at 0 ºC. The mixture was stirred at room temperature overnight. Then, methanol was added slowly to quench the reaction, and the mixture was washed with water and extracted with DCM three times. The combined organic layer was washed with brine and dried over $MgSO_4$. After the solvent was evaporated, product was purified by column chromatography (silica gel, EtOAc / hexane = 1 / 1). Compound **6** was obtained as white solid (2.9 g, 90 %).

M. p.: > 300 ºC. ^{1}H NMR (DMSO, 400 MHz, TMS, 298 K): δ 6.29 (d, J = 8.4 Hz, 4H), 6.51 (d, J = 4.4 Hz, 2H), 6.69 (d, J = 1.6 Hz, 2H), 6.83 (t, J = 8.4 Hz, 2H), 7.34 (d, J = 4.4 Hz, 2H), 7.38 (dd, J = 8.4 & 1.6 Hz, 2H), 7.90 (d, J = 8.4 Hz, 2H), 9.06 (s, 4H). ^{13}C NMR (DMSO, 100 MHz, TMS, 298 K): δ 61.98, 107.13, 115.82, 119.60, 122.12, 126.16, 127.26, 128.53, 131.41, 134.53, 137.88, 139.70, 143.98, 155.49, 155.86. MALDI-TOF mass (Matrix: DCTB): Found m/z = 544.15, calculated ($C_{33}H_{20}O_4S_2$) 544.08. Elemental analysis: Anal. Calcd for $C_{33}H_{20}O_4S_2$•1.1H_2O: C, 70.22; H, 3.96. Found: C, 70.39; H, 4.21.

Synthesis of compound M1$_1$: A 100 mL round-bottom flask was charged with compound **6** (830 mg, 1.5 mmol) and Cs_2CO_3 (5.0 g, 15.0 mmol). The flask was evacuated and refilled with argon three times. After addition of DMSO (16 mL), the mixture was stirred at 80 ºC for 1 hour. Then, 1-bromooctane (2.3 g, 12.0 mmol) was added, the mixture was stirred at 80 ºC for 60 hours. After cooling to room temperature, the solvent was distilled under reduced pressure. The resulting solid was washed with water and extracted with DCM three times. The combined organic layer was washed with brine and dried over $MgSO_4$. After the solvent was evaporated, product was purified by column chromatography (DCM / hexane = 1 / 2). Compound **M1$_1$** was obtained as white solid (1.25 g, 83 %).

M. p.: 96.8 ºC. ^{1}H NMR ($CDCl_3$, 400 MHz, TMS, 298 K): δ 0.88 (t, J = 6.8 Hz, 12H), 1.21 – 1.29 (m, 20H), 1.43 – 1.46 (m, 8H), 3.76 (t, J = 6.8 Hz, 8H), 6.50 – 6.53 (m, 6H), 6.89 (d, J = 1.6 Hz, 2H), 6.98 (d, J = 4.8

Hz, 2H), 7.12 (t, *J* = 8.0 Hz, 2H), 7.41 (dd, *J* = 8.0 & 1.6 Hz, 2H), 7.79 (d, *J* = 8.0 Hz, 2H). ^{13}C NMR ($CDCl_3$, 100 MHz, TMS, 298 K): δ 14.23, 22.78, 25.85, 28.90, 29.23, 29.36, 31.92, 62.04, 68.73, 105.56, 118.70, 120.17, 122.08, 124.77, 126.58, 128.30, 131.03, 133.10, 138.06, 140.19, 143.89, 155.55, 157.15. MALDI-TOF mass (Matrix: DCTB): Found m/z = 992.15, calculated ($C_{65}H_{84}O_4S_2$) 992.58. Elemental analysis: Anal. Calcd for $C_{65}H_{84}O_4S_2$: C, 78.58; H, 8.52. Found: C, 78.56; H, 8.60.

Synthesis of compound M1$_1$-TEG: A 100 mL round-bottom flask was charged with compound **6** (700 mg, 1.3 mmol) and Cs_2CO_3 (4.2 g, 12.9 mmol). The flask was evacuated and refilled with argon three times. After addition of DMF (11 mL), the mixture was stirred at 80 °C for 1 hour. Then, tri(ethylene glycol) monomethyl ether tosylate (3.3 g, 10.3 mmol) was added, and the mixture was stirred at 80 ºC for 60 hours. After cooling to room temperature, the solvent was distilled under reduced pressure. The resulting solid was washed with water and extracted with DCM three times. The combined organic layer was washed with brine and dried over $MgSO_4$. After the solvent was evaporated, product was purified by column chromatography (DCM / hexane = 1 / 2). Compound **M1$_1$-TEG** was obtained as colorless oil (1.2 g, 83 %).
^{1}H NMR ($CDCl_3$, 400 MHz, TMS, 298 K): δ 3.34 (s, 12H), 3.48 – 3.60 (m, 40H), 3.94 (t, *J* = 6.8 Hz, 8H), 6.53 – 6.58 (m, 6H), 6.86 (d, *J* = 1.6 Hz, 2H), 7.06 (d, *J* = 4.8 Hz, 2H), 7.13 (t, *J* = 8.0 Hz, 2H), 7.45 (dd, *J* = 8.0 & 1.6 Hz, 2H), 7.77 (d, *J* = 8.0 Hz, 2H). ^{13}C NMR ($CDCl_3$, 100 MHz, TMS, 298 K): δ 59.11, 68.41, 69.36, 70.61, 70.73, 70.84, 71.99, 106.38, 118.85, 120.36, 122.04, 125.28, 126.49, 128.55, 131.21, 133.06, 138.23, 140.16, 143.95, 155.43, 156.78. MALDI-TOF mass (Matrix: DCTB): Found m/z = 1128.63, calculated ($C_{61}H_{76}O_{16}S_2$) 1128.46. Elemental analysis: Anal. Calcd for $C_{61}H_{76}O_{16}S_2 \bullet 1.1H_2O$: C, 63.75; H, 6.86. Found: C, 63.99; H, 7.12.

Synthesis of compound 7: A 100 mL brown round-bottom flask was charged with compound **M1$_1$** (1.1 g, 1.1 mmol). After addition of DCM (40 mL), NBS (380 mg, 2.1 mmol) was added. The mixture was stirred at room temperature for 2 hours, and then washed with water and extracted with DCM three times. The combined organic layer was washed with brine and dried over $MgSO_4$. After the solvent was evaporated, product was purified by column chromatography (DCM / hexane = 1 / 3.5). Compound **7** was obtained as white solid (1.1 g, 85 %).
M. p.: 89.4 ºC. ^{1}H NMR ($CDCl_3$, 400 MHz, TMS, 298 K): δ 0.88 (t, *J* = 6.8 Hz, 12H), 1.24 – 1.31 (m, 20H), 1.49 – 1.52 (m, 8H), 3.81 (t, *J* = 6.8 Hz, 8H), 6.54 – 6.57 (m, 6H), 6.92 (s, 2H), 7.15 (t, *J* = 8.0 Hz, 2H), 7.45 (dd, *J* = 8.0 & 1.6 Hz, 2H), 7.78 (d, *J* = 8.0 Hz, 2H). ^{13}C NMR ($CDCl_3$, 100 MHz, TMS, 298 K): δ 14.24, 22.78, 25.85, 28.82, 29.11, 29.40, 29.80, 31.91, 62.99, 68.63, 105.47, 111.44, 118.93, 119.72, 124.98, 126.51, 128.51, 131.53, 133.38, 137.81, 140.12, 142.34, 153.48, 157.11. MALDI-TOF mass (Matrix: DCTB): Found m/z = 1149.68, calculated ($C_{65}H_{82}Br_2O_4S_2$) 1150.40. Elemental analysis: Anal. Calcd for $C_{65}H_{82}Br_2O_4S_2$: C, 67.81; H, 7.18. Found: C, 68.00; H, 7.52.

Synthesis of compound 7-TEG: A 100 mL brown round-bottom flask was charged with compound **M1$_1$-TEG** (1.0 g, 0.9 mmol). After addition of DCM (40 mL), NBS (305 mg, 1.7 mmol) was added. The mixture was stirred at room temperature for 2 hours, and then washed with water and extracted with DCM three times. The combined organic layer was washed with brine and dried over $MgSO_4$. After the solvent was evaporated, product was purified by column chromatography (EtOAc / MeOH = 30 / 1). Compound **7-TEG** was obtained as colorless oil (1.1 g, 95 %).

^{1}H NMR ($CDCl_3$, 400 MHz, TMS, 298 K): δ 3.34 (s, 12H), 3.49 – 3.60 (m, 40H), 3.97 (t, J = 6.8 Hz, 8H), 6.58 – 6.60 (m, 6H), 6.88 (s, 2H), 7.15 (t, J = 8.0 Hz, 2H), 7.48 (dd, J = 8.0 & 1.6 Hz, 2H), 7.75 (d, J = 8.0 Hz, 2H). ^{13}C NMR ($CDCl_3$, 100 MHz, TMS, 298 K): δ 59.12, 68.40, 69.37, 70.61, 70.75, 70.92, 72.00, 106.37, 111.68, 119.06, 120.00, 124.90, 126.38, 128.71, 131.71, 133.30, 137.97, 140.10, 142.41, 153.40, 156.76. MALDI-TOF mass (Matrix: DCTB): Found m/z =1285.41, calculated ($C_{61}H_{74}Br_2O_{16}S_2$) 1286.28. Elemental analysis: Anal. Calcd for $C_{61}H_{74}Br_2O_{16}S_2$: C, 56.92; H, 5.79. Found: C, 56.64; H, 6.16.

Synthesis of P1: A 30 mL bottle was charged with compound **7** (200 mg, 0.17 mmol), $Ni(COD)_2$ (78.2 mg, 0.28 mmol), and bipyridine (44.4 mg, 0.28 mmol). The bottle was evacuated and refilled with argon three times. After addition of toluene (3.6 mL), COD (30.8 mg, 0.28 mmol) and DMF (0.6 mL), the mixture was stirred at 80 ºC for 3 days, and then cooled to room temperature. 5 M HCl was added to quench the reaction, the mixture was diluted with $CHCl_3$ and washed with EDTA solution, $NaHCO_3$ solution, then extracted with $CHCl_3$ three times. The combined organic layer was washed with brine and dried over $MgSO_4$. After the solvent was evaporated, product was purified by reprecipitation and centrifugation ($CHCl_3$ / MeOH, 1 hour, 600 rpm). **P1** was obtained as purple solid (159 mg, 92.2 %).

^{1}H NMR ($CDCl_3$, 400 MHz, TMS, 298 K): δ 0.74 – 0.77 (m, 12H), 0.96 – 1.14 (m, 20H), 1.26 (broad, 8H), 3.57 (broad, 8H), 6.39 (broad, 6H), 6.80 (broad, 2H), 7.04 (broad, 2H), 7.31 – 7.33 (broad, 2H), 7.65 – 7.67 (broad, 2H).

Synthesis of P1-TEG: P1-TEG was obtained through the same synthetic process with that for **P1**.

^{1}H NMR ($CDCl_3$, 400 MHz, TMS, 298 K): δ 3.22 (broad, 12H), 3.25 – 3.53 (m, 40H), 3.79 (broad, 8H), 6.47 – 6.54 (broad, 6H), 6.79 (broad, 2H), 7.05 (broad, 2H), 7.39 – 7.40 (broad, 2H), 7.66 – 7.67 (broad, 2H).

b) Synthesis of Oligmers

Synthesis of compound 9: A 30 mL flask was charged with compound **M1$_1$** (500 mg, 0.5 mmol) and evacuated and refilled with argon three times. After addition of THF (5.5 mL), *n*-BuLi was added slowly at -78 ºC. The mixture was stirred at room temperature for 1 hour. Then, tributyltin chloride was added at -78 ºC, the resulting mixture was stirred at room temperature overnight. MeOH was added slowly to quench the

reaction. The mixture was wash with water and extracted with DCM three times. The combined organic layer was washed with brine and dried over $MgSO_4$. After the solvent was evaporated, product was purified by column chromatography (silica gel treated with triethylamine, hexane). The compound **9** was obtained as white solid (520 mg, 80.5 %).

^{1}H NMR ($CDCl_3$, 400 MHz, TMS, 298 K): δ 0.83 (t, J = 7.6 Hz, 9H), 0.90 (t, J = 8.0 Hz, 12H), 1.00 – 1.29 (m, 52H), 1.45 – 1.51 (m, 14H), 3.78 (m, 8H), 6.49 (d, J = 4.8 Hz, 1H), 6.53 – 6.55 (m, 5H), 6.93 (d, J = 1.6 Hz, 2H), 6.95 (d, J = 4.8 Hz, 1H), 7.13 (t, J = 8.0 Hz, 2H), 7.43 (dd, J = 8.0 & 1.6 Hz, 2H), 7.81 (d, J = 8.0 Hz, 2H). ^{13}C NMR ($CDCl_3$, 100 MHz, TMS, 298 K): δ 10.90, 13.67, 14.25, 22.81, 25.90, 27.35, 28.90, 29.02, 29.12, 29.23, 29.41, 31.95, 61.65, 68.72, 105.68, 118.60, 120.38, 122.00, 124.25, 126.76, 128.26, 129.91, 130.90, 132.99, 137.09, 138.14, 140.19, 144.01, 144.48, 155.65, 157.04, 157.19. Elemental analysis: Anal. Calcd for $C_{77}H_{110}O_4S_2Sn$: C, 72.11; H, 8.64. Found: C, 72.12; H, 8.92.

Synthesis of compound 8: A 50 mL brown round-bottom flask was charged with compound **M1$_1$** (233 mg, 0.24 mmol). After addition of DCM (6 mL), NBS (40 mg, 0.22 mmol) was added. The mixture was stirred at room temperature for 2 hours, and then washed with water, extracted with DCM three times. The combined organic layer was washed with brine and dried over $MgSO_4$. After the solvent was evaporated, product was purified by column chromatography (DCM / hexane = 1 / 3). Compound **8** was obtained as white solid (182 mg, 72.3 %).

^{1}H NMR ($CDCl_3$, 400 MHz, TMS, 298 K): δ 0.88 (t, J = 6.8 Hz, 12H), 1.22 – 1.30 (m, 20H), 1.45 – 1.51 (m, 8H), 3.78 (t, J = 6.8 Hz, 8H), 6.51 – 6.55 (m, 6H), 6.90 (d, J = 1.6 Hz, 2H), 7.00 (d, J = 4.4 Hz, 1H), 7.13 (t, J = 8.0 Hz, 2H), 7.42 (dd, J = 8.0 & 1.6 Hz, 2H), 7.78 (d, J = 8.0 Hz, 2H). ^{13}C NMR ($CDCl_3$, 100 MHz, TMS, 298 K): δ 14.25, 22.79, 25.84, 28.83, 29.17, 29.39, 31.92, 62.48, 68.64, 105.44, 118.21, 119.83, 122.08, 125.00, 125.34, 126.54, 128.41, 131.28, 133.20, 140.15, 143.09, 154.26, 154.66, 157.10. MALDI-TOF mass (Matrix: DCTB): Found m/z = 1070.03, calculated ($C_{65}H_{83}BrO_4S_2$) 1070.49.

Synthesis of compound M1$_2$: A 30 mL flask was charged with compound **9** (180 mg, 0.14 mmol), compound **8** (156 mg, 0.14 mmol) and $Pd(PPh_3)_4$ (13 mg, 0.01 mmol). The flask was evacuated and refilled with argon three times. After addition of toluene (1.5 mL), the mixture was stirred at 120 ºC for 40 hours, and then cooled to room temperature. The mixture was washed with water and extracted with DCM three times. The combined organic layer was washed with brine and dried over $MgSO_4$. After the solvent was evaporated, product was purified by column chromatography (DCM / hexane = 1 / 3). The compound **M1$_2$** was obtained as yellow solid (150 mg, 54 %).

^{1}H NMR ($CDCl_3$, 400 MHz, TMS, 298 K): δ 0.84 (t, J = 7.2 Hz, 24H), 1.12 – 1.25 (m, 80H), 1.37 – 1.40 (m, 16H), 3.69 (t, J = 6.8 Hz, 16H), 6.47 – 6.49 (m, 12H), 6.87 (d, J = 1.6 Hz, 4H), 6.95 (d, J = 4.8 Hz, 2H), 7.10 (t, J = 8.0 Hz, 4H), 7.39 (dd, J = 8.0 & 1.6 Hz, 4H), 7.75 (d, J = 8.0 Hz, 4H). ^{13}C NMR ($CDCl_3$, 100 MHz,

TMS, 298 K): δ 14.23, 22.77, 25.80, 28.81, 29.09, 29.34, 31.87, 62.25, 68.60, 105.31, 117.94, 118.66, 119.99, 121.97, 124.99, 126.66, 128.21, 131.06, 133.12, 136.36, 137.99, 138.44, 140.09, 143.61, 155.28, 156.01, 157.31. MALDI-TOF mass (Matrix: DCTB): Found m/z = 1983.48, calculated ($C_{130}H_{166}O_8S_4$) 1983.15. Elemental analysis: Anal. Calcd for $C_{130}H_{166}O_8S_4$: C, 78.66; H, 8.43. Found: C, 78.73; H, 8.76.

Synthesis of compound 10: A 50 mL brown round-bottom flask was charged with compound **M1$_2$** (48.4 mg, 0.024 mmol). After addition of THF (5 mL), NBS (8.2 mg, 0.046 mmol) was added at 0 ºC. The mixture was stirred at room temperature for 2 hours, and then washed with water and extracted with DCM three times. The combined organic layer was washed with brine and dried over $MgSO_4$. After the solvent was evaporated, product was purified by column chromatography (acetone / hexane = 1 / 25). Compound **10** was obtained as yellow solid (40 mg, 77 %).

^{1}H NMR ($CDCl_3$, 400 MHz, TMS, 298 K): δ 0.84 (t, J = 7.2 Hz, 24H), 1.11 – 1.29 (m, 80H), 1.39 – 1.43 (m, 16H), 3.71 (t, J = 6.8 Hz, 16H), 6.48 – 6.50 (m, 14H), 6.87 (s, 4H), 7.11 (t, J = 8.0 Hz, 4H), 7.40 (dd, J = 8.0 & 1.6 Hz, 4H), 7.75 (d, J = 8.0 Hz, 4H). ^{13}C NMR ($CDCl_3$, 100 MHz, TMS, 298 K): δ 14.22, 22.76, 25.80, 28.76, 29.03, 29.37, 29.80, 31.87, 32.02, 62.73, 68.56, 105.30, 111.12, 118.08, 118.78, 119.73, 124.90, 126.59, 128.33, 131.34, 133.29, 138.11, 138.72, 140.06, 142.78, 154.08, 155.22, 157.11. MALDI-TOF mass (Matrix: DCTB): Found m/z = 2138.70, calculated ($C_{130}H_{166}Br_2O_8S_4$) 2138.97.

Synthesis of compound M1$_4$: A two necked flask was charged with compound **9** (52.7 mg, 0.04 mmol), compound **10** (39 mg, 0.019 mmol) and $Pd(PPh_3)_4$ (4.3 mg, 0.0037 mmol). The flask was evacuated and refilled with argon three times. After addition of toluene (1 mL), the mixture was stirred at 120 °C for 40 hours, then cooled to room temperature, and washed with water and extracted with DCM three times. The combined organic layer was washed with brine and dried over $MgSO_4$. After the solvent was evaporated, product was purified by column chromatography (acetone / hexane = 1 / 25). The compound **M1$_4$** was obtained as red solid (20 mg, 28 %).

^{1}H NMR ($CDCl_3$, 400 MHz, TMS, 298 K): δ 0.78 (t, J = 7.2 Hz, 24H), 0.83 (t, J = 6.8 Hz, 24H), 0.97 – 1.39 (m, 192H), 3.58 (t, J = 6.8 Hz, 16H), 3.68 (t, J = 6.8 Hz, 16H), 6.40 – 6.48 (m, 24H), 6.84 (s, 2H), 6.85 (s, 2H), 6.94 (d, J = 4.8 Hz, 2H), 7.03 – 7.10 (m, 8H), 7.33 – 7.39 (m, 8H), 7.69 (d, J = 8.0 Hz, 4H), 7.73 (d, J = 8.0 Hz, 4H). MALDI-TOF mass (Matrix: DCTB): Found m/z = 3964.11, calculated ($C_{260}H_{330}O_{16}S_8$) 3964.28.

Synthesis of compound M1$_3$: A 30 mL flask was charged with compound **9** (258 mg, 0.2 mmol), compound **7** (110 mg, 0.1 mmol) and $Pd(PPh_3)_4$ (11 mg, 0.01 mmol). The flask was evacuated and refilled with argon three times. After addition of toluene (1.5 mL), the mixture was stirred at 125 ºC for 40 hours, then cooled to room temperature, and washed with water and extracted with DCM three times. The combined organic layer was washed with brine and dried over $MgSO_4$. After the solvent was evaporated, product was purified by

column chromatography (DCM / hexane = 1 / 2). The compound **M1$_3$** was obtained as red solid (142 mg, 50 %).

^{1}H NMR ($CDCl_3$, 400 MHz, TMS, 298 K): δ 0.80 (t, J = 7.2 Hz, 12H), 0.83 (t, J = 7.2 Hz, 24H), 0.98 – 1.39 (m, 144H), 3.60 (t, J = 6.8 Hz, 8H), 3.68 (t, J = 6.8 Hz, 16H), 6.41 – 6.48 (m, 18H), 6.85 (s, 6H), 6.94 (d, J = 4.8 Hz, 2H), 7.05 – 7.11 (m, 6H), 7.35 – 7.39 (m, 6H), 7.71 (d, J = 8.0 Hz, 2H), 7.74 (d, J = 8.0 Hz, 4H). MALDI-TOF mass (Matrix: DCTB): Found m/z = 2973.15, calculated ($C_{195}H_{246}O_{12}S_6$) 2973.71. Elemental analysis: Anal. Calcd for $C_{195}H_{248}O_{12}S_6$: C, 78.69; H, 8.40. Found: C, 78.72; H, 8.75.

Synthesis of compound 11: A 50 mL brown round-bottom flask was charged with compound **M1$_3$** (56 mg, 0.019 mmol). After addition of THF (8 mL), NBS (6.4 mg, 0.036 mmol) was added at 0 ºC. The mixture was stirred at room temperature for 2 hours, and then washed with water and extracted with DCM three times. The combined organic layer was washed with brine and dried over $MgSO_4$. After the solvent was evaporated, product was purified by column chromatography (acetone / hexane = 1 / 20). Compound **11** was obtained as yellow solid (42 mg, 71 %).

^{1}H NMR ($CDCl_3$, 400 MHz, TMS, 298 K): δ 0.80 – 0.91 (m, 36H), 0.99 – 1.44 (m, 144H), 3.60 (t, J = 6.8 Hz, 8H), 3.70 – 3.73 (m, 16H), 6.42 – 6.50 (m, 18H), 6.85 (s, 2H), 6.88 (s, 4H), 7.08 – 7.13 (m, 6H), 7.39 – 7.41 (m, 6H), 7.71 – 7.50 (m, 6H). ^{13}C NMR ($CDCl_3$, 100 MHz, TMS, 298 K): δ 14.23, 22.76, 25.74, 25.82, 28.66, 28.78, 28.88, 29.04, 29.33, 29.38, 31.69, 31.82, 31.87, 32.03, 68.45, 68.55, 105.09, 105.25, 118.61, 118.76, 119.72, 126.61, 126.70, 128.14, 128.31, 131.33, 133.25, 140.00, 140.05, 142.80, 157.11. MALDI-TOF mass (Matrix: DCTB): Found m/z = 3128.69, calculated ($C_{195}H_{246}Br_2O_{12}S_6$) 3129.53.

Synthesis of compound M1$_5$: A two necked flask was charged with compound **9** (36.0 mg, 0.028 mmol), compound **11** (40.0 mg, 0.013 mmol) and $Pd(PPh_3)_4$ (3.0 mg, 0.0025 mmol). The flask was evacuated and refilled with argon three times. After addition of toluene (1 mL), the mixture was stirred at 120 ºC for 40 hours, then cooled to room temperature, and washed with water and extracted with DCM three times. The combined organic layer was washed with brine and dried over $MgSO_4$. After the solvent was evaporated, product was purified by column chromatography (acetone / hexane = 1 / 13). The compound **M1$_5$** was obtained as purple solid (10 mg, 19 %).

^{1}H NMR ($CDCl_3$, 400 MHz, TMS, 298 K): δ 0.74 – 0.84 (m, 60H), 0.96 – 1.37 (m, 240H), 3.58 – 3.59 (m, 24H), 3.68 (t, J = 6.8 Hz, 16H), 6.38 – 6.47 (m, 30H), 6.82 (s, 2H), 6.83 (s, 4H), 6.84 (s, 4H), 6.94 (d, J = 4.8 Hz, 2H), 7.03 – 7.08 (m, 10H), 7.33 – 7.38 (m, 10H), 7.66 – 7.69 (m, 6H), 7.73 (d, J = 8.0 Hz, 4H). MALDI-TOF mass (Matrix: DCTB): Found m/z = 4954.17, calculated ($C_{325}H_{412}O_{20}S_{10}$) 4954.84.

2.5.3 Electronic-Structure Calculation

The electronic structure calculations were implemented using the Gaussian09 program.[62] The density functional theory (DFT) method was applied in geometry optimization where the M06-2X functional[63] and the 6-31G(d,p) basis set were used. The normal mode analysis was carried out only for the small-sized molecules like $\mathbf{M1_1}$ and $\mathbf{M1_2}$. No imaginary frequency modes were observed in these molecules. Although the same analysis was not carried out to the larger molecules, it seems reasonable to expect that they would also be energy minima on the potential energy surface.

To investigate UV/Vis absorption, the spin-singlet excited states were calculated by the time-dependent density functional theory (TD-DFT) method where all the valence orbitals were included in the active space. The low-lying 20 excited states were calculated at the ground-state optimized geometry. The calculated excited states are summarized in Tables 3-1 – 3-6 for $\mathbf{M1_1}$-$\mathbf{M1_6}$ where the low-lying six excited states are shown. In the all the molecules, the $S_0 \rightarrow S_1$ state is assigned to the HOMO-LUMO transition. These frontier orbitals are shown in Figure 3-3. Figure 3-4 shows the size (n') dependence of the $S_0 \rightarrow S_1$ excitation energies of $\mathbf{M1_1}$-$\mathbf{M1_6}$ and the isolated oligothiophene included therein. The structures of the isolated oligothipohenes were also optimized by using the DFT method.

Table 3-1. Spin-singlet excited states of $\mathbf{M1_1}$ at the optimized ground-state geometry and their assignment where ΔE, λ, and f are excitation energy from the ground state, excitation wavelength, and oscillator strength, respectively.

Solution	ΔE (ev)	λ (nm)	f	Configuration			
				occ. MO		unocc. MO	coeff.
1	4.185	296.3	0.204	157	→	159	0.602
				156	→	159	-0.334
				157	→	158	0.111
2	4.244	292.2	0.899	157	→	158	0.617
				156	→	158	0.263
				157	→	159	-0.109
3	4.653	266.5	0.255	156	→	158	0.557
				157	→	158	-0.209
				156	→	161	-0.187
				157	→	161	-0.186
				152	→	158	0.163
4	4.875	254.3	0.095	157	→	161	0.498
				156	→	158	0.273
				156	→	161	0.190
				152	→	158	-0.164
				157	→	158	-0.161
				157	→	160	0.136
				148	→	158	-0.110
5	4.912	252.4	0.031	156	→	159	0.597
				157	→	159	0.332
				152	→	159	-0.111
6	4.996	248.2	0.007	155	→	158	0.505
				154	→	160	0.258
				156	→	160	0.196
				155	→	162	0.156
				157	→	160	0.147
				153	→	165	-0.140
				151	→	158	-0.110

Table 3-2. Spin-singlet excited states of $\mathbf{M1_2}$ at the optimized ground-state geometry and their assignment where ΔE, λ, and f are excitation energy from the ground state, excitation wavelength, and oscillator strength, respectively.

Solution	ΔE (ev)	λ (nm)	f	Configuration			
				occ. MO		unocc. MO	coeff.
1	3.152	393.4	0.977	313	→	314	0.688
				310	→	317	0.111
2	4.078	304.0	0.156	313	→	315	0.461
				313	→	317	0.298
				311	→	315	0.257
				310	→	314	0.201
				312	→	314	-0.192
				311	→	314	0.142
3	4.097	302.6	0.035	313	→	317	0.383
				313	→	315	-0.366
				312	→	314	-0.246
				310	→	314	0.242
				311	→	315	-0.188
				311	→	314	0.118
4	4.196	295.5	0.475	313	→	316	0.472
				312	→	316	0.467
5	4.324	286.8	0.012	312	→	314	0.582
				313	→	317	0.321
				312	→	317	-0.151
6	4.381	283.0	0.676	311	→	315	0.550
				313	→	315	-0.297
				311	→	314	0.156
				310	→	315	-0.153
				313	→	316	0.130

Table 3-3. Spin-singlet excited states of $\mathbf{M1_3}$ at the optimized ground-state geometry and their assignment where ΔE, λ, and f are excitation energy from the ground state, excitation wavelength, and oscillator strength, respectively.

Solution	ΔE (ev)	λ (nm)	f	Configuration			
				occ. MO		unocc. MO	coeff.
1	2.777	446.5	1.743	469	→	470	0.673
				468	→	471	-0.141
2	3.498	354.5	0.060	469	→	471	0.493
				468	→	470	-0.398
				467	→	470	-0.179
				469	→	472	-0.140
				468	→	475	-0.107
3	3.967	312.6	0.074	469	→	473	0.636
				466	→	473	0.193
4	3.992	310.6	0.002	468	→	470	0.476
				469	→	471	0.401
				469	→	473	-0.133
				467	→	470	0.128
5	4.045	306.5	0.079	469	→	475	0.360
				468	→	471	-0.329
				466	→	470	-0.278
				467	→	470	-0.243
				463	→	470	-0.186
				469	→	472	0.123
				462	→	470	0.104
				467	→	471	-0.100
6	4.070	304.6	0.145	469	→	472	0.511
				468	→	472	-0.308
				467	→	472	-0.199
				465	→	472	-0.170
				469	→	471	0.141

Table 3-4. Spin-singlet excited states of $\mathbf{M1_4}$ at the optimized ground-state geometry and their assignment where ΔE, λ, and f are excitation energy from the ground state, excitation wavelength, and oscillator strength, respectively.

Solution	ΔE (ev)	λ (nm)	f	Configuration			
				occ. MO		unocc. MO	coeff.
1	2.607	475.7	2.568	625	→	626	0.653
				624	→	627	-0.211
2	3.153	393.3	0.002	625	→	627	0.485
				624	→	626	-0.454
				624	→	631	0.120
3	3.655	339.3	0.258	624	→	627	0.396
				625	→	631	0.371
				619	→	626	0.247
				625	→	632	-0.188
				623	→	626	-0.165
				624	→	633	0.121
				622	→	626	-0.121
4	3.754	330.3	0.000	624	→	626	0.476
				625	→	627	0.436
				624	→	631	0.139
				619	→	627	0.131
5	3.945	314.3	0.052	625	→	629	0.620
				624	→	629	0.186
				621	→	629	0.179
6	3.953	313.7	0.066	625	→	628	0.612
				624	→	628	-0.203
				620	→	628	-0.165
				622	→	628	-0.112

Table 3-5. Spin-singlet excited states of $\mathbf{M1_5}$ at the optimized ground-state geometry and their assignment where ΔE, λ, and f are excitation energy from the ground state, excitation wavelength, and oscillator strength, respectively.

Solution	ΔE (ev)	λ (nm)	f	Configuration			
				occ. MO		unocc. MO	coeff.
1	2.521	491.9	3.415	781	→	782	0.620
				780	→	783	-0.245
				779	→	784	-0.113
2	2.929	423.3	0.024	781	→	783	0.472
				780	→	782	-0.447
				780	→	784	0.160
3	3.349	370.2	0.258	781	→	784	0.400
				780	→	783	0.385
				779	→	782	-0.320
				777	→	782	-0.133
				780	→	790	0.121
4	3.627	341.9	0.002	780	→	782	0.460
				781	→	783	0.413
				780	→	784	0.200
				779	→	783	-0.146
5	3.746	331.0	0.084	781	→	790	0.364
				780	→	784	0.329
				779	→	783	0.322
				773	→	782	-0.211
				780	→	791	0.130
				778	→	782	-0.126
6	3.927	315.7	0.035	781	→	785	0.520
				781	→	784	0.252
				779	→	785	-0.197
				779	→	782	0.195
				781	→	786	-0.142
				777	→	785	-0.112

Table 3-6. Spin-singlet excited states of $\mathbf{M1_6}$ at the optimized ground-state geometry and their assignment where ΔE, λ, and f are excitation energy from the ground state, excitation wavelength, and oscillator strength, respectively.

Solution	ΔE (ev)	λ (nm)	f	Configuration			
				occ. MO		unocc. MO	coeff.
1	2.449	506.3	4.293	937	→	938	0.592
				936	→	939	-0.269
				935	→	940	0.151
2	2.773	447.2	0.005	937	→	939	0.460
				936	→	938	-0.436
				936	→	940	0.174
				935	→	939	-0.128
3	3.126	396.6	0.314	937	→	940	0.398
				936	→	939	0.365
				935	→	938	0.344
				936	→	943	0.111
4	3.469	357.5	0.007	936	→	940	0.357
				935	→	939	-0.300
				937	→	943	0.290
				937	→	944	-0.182
				934	→	938	0.166
				931	→	938	-0.126
				928	→	938	0.124
				936	→	948	0.107
				936	→	938	0.101
5	3.544	349.9	0.001	936	→	938	0.433
				937	→	939	0.405
				935	→	939	0.229
				936	→	940	0.162
				937	→	938	-0.109
6	3.783	327.7	0.006	935	→	938	0.452
				937	→	940	-0.395
				936	→	943	-0.185
				936	→	944	0.114
				935	→	948	0.109

2.5.4 FP-TRMC/TAS measurements.

a) Flash-photolysis time-resolved microwave conductivity (FP-TRMC).

The charge carrier transport property along the single polymer chain was evaluated by FP-TRMC technique at room temperature under air. FP-TRMC can monitor kinetic trances of transient changes of power of microwaves from a resonant cavity after generation of photo charge with a time constant of ~ 10 ns, resulting in dynamic observation of charge carrier species. Due to the limitation of π-π stacking in IMWs, the generated charge in **P1** and **P1-TEG** can transport only along the polymer backbone. As a result, charge carrier transport property along the single polymer chain can be evaluated. Figure 3-12 shows the observed kinetic trances of the transient conductivity and optical absorption of **P1** and **P1-TEG** upon irradiation by UV light. Uniform thin films were prepared on a quartz plate by spin-coating of $CHCl_3$ solution of polythiophene derivatives (**P1** or **P1-TEG**) and *N,N'*-Bis(2,5-di-*tert*-butylphenyl)-3,4,9,10-perylenedicarboximide (PDI) (ratio of thiophene rings/PDI = 5/1). Transient charge carriers were photo-generated upon excitation to laser pulses of third harmonic generation (λ = 355 nm) from a Spectra Physics model INDI-HG Nd:YAG laser with a pulse duration of 5–8 ns. The photon density of a 355 nm pulse was 4.5×10^{15} photons cm^{-2} $pulse^{-1}$. The probing microwave frequency and power were set at 9.1 GHz and 3 mW, respectively. Photoconductivity transients, demodulated through a GaAs crystal-diode with Schottky-barriers (rise time < 1 ns), were monitored by a Tektronix model TDS3032B digital oscilloscope. The observed conductivities were normalized, given by a photocarrier generation yield (φ) multiplied by sum of the charge carrier mobilities ($\Sigma\mu$), according to the equation, $\varphi\Sigma\mu = (A/eI_0F_{light})(\Delta P_r/P_r)$, where, e, A, I_0, F_{light}, P_r, and ΔP_r are unit charge of a single electron, sensitivity factor (S cm^{-1}), incident photon density of the excitation laser (photon cm^{-2}), correction (or filling) factor (cm^{-1}), and reflected microwave power and its change, respectively.

b) Transient absorption spectroscopy (TAS).

Transient absorption spectroscopy (TAS) measurements were carried out at room temperature under air. The identical spin-coated films used for FP-TRMC measurements were used for TAS measurements. The film was photoexcited using the third harmonic generation (λ = 355 nm) from the identical Spectra Physics laser, where the photon density of a 355 nm pulse was $4.4–4.6 \times 10^{15}$ photons cm^{-2} $pulse^{-1}$. A white light continuum from a Xe lamp was used as a probe light source for transient absorption spectroscopy. The monochromated probe light was guided into a Hamamatsu model C7700 wide-dynamic-range streak camera system, which collected a two-dimensional image of the spectral and temporal profiles of light intensity.

c) Evaluation of hole mobility along polythiophene chains.[64)]

Based on the transient absorption band at around 710 nm in the TAS measurements, the maximum charge carrier generation efficiency of PDI radical anions ($\varphi_{710\ nm,max}$) was evaluated by using the value of ε = 71200 M^{-1} cm^{-1}.[65] This efficiency was equal to the hole generation efficiency on polythiophene chains. The observed TRMC signals most likely originate from hole transport on polythiophene chains because PDI molecules were dispersed due to their bulky substituents. Thus, hole mobility was evaluated by $\mu_h = 3 \times (\varphi\Sigma\mu)_{max}/\varphi_{710\ nm,max}$, where the triplication means a hypothesis of random orientation of the polymer chains in the films.

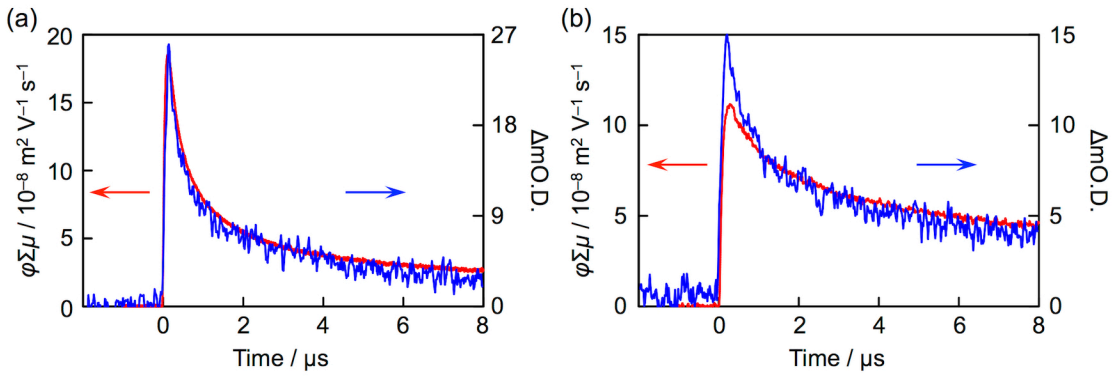

Figure 3-12. Kinetic traces of conductivity transient (red) and optical absorption at 710 nm (red) for (a) **P1**/PDI and (b) **P1-TEG**/PDI films. The slight difference between conductivity and absorption transients in (b) is considered to result from partial electron trapping in oxyethylene chains.

2.6 Reference:

[1] Shirakawa, H.; Louis, E. J.; MacDiarmid, A. G.; Chiang, C. K.; Heeger, A. J. *J. Chem. Soc. Chem. Commun.* **1977**, 16, 578.

[2] Roncali, J. *Chem. Rev.* **1992**, 92, 711.

[3] Beaujuge, P. M.; Reynolds, J. R. *Chem. Rev.* **2010**, 110 , 268.

[4] Bujak, P.; Kulszewicz-Bajer, I.; Zagorska, M.; Maurel, V.; Wielgus I.; Pron, A. *Chem. Soc. Rev.* **2013**, 42, 8895.

[5] Brédas, J.-L.; Street, G. B. *Acc. Chem. Res.* **1985**, 18, 309.

[6] Furukawa, Y *Synth. Met.* **1995**, 69, 629.

[7] Smie, A.; Heinze, J. *Angew. Chem. Int. Ed.* **1997**, 36, 363.

[8] Merz, A.; Kronberger, J.; Dunsch, L.; Neudeck, A.; Petr, A.; Parkanyi, L. *Angew. Chem. Int. Ed.* **1999**, 38, 1442.

[9] Hill, M. G.; Mann, K. R.; Miller L. L.; Penneau, J.-F. *J. Am. Chem. Soc.* **1992**, 114, 2728.

[10] Hill, M. G.; Penneau, J.-F.; Zinger, B.; Mann, K. R.; Miller, L. L. *Chem. Mater.* **1992**, 4, 1106.

[11] Bäuerle, P.; Segelbacher, U.; Gaudi, K.-U.; Huttenlocher, D.; Mehring, M. *Angew. Chem. Int. Ed.* **1993**, 32, 76.

[12] Sakai, T.; Satou, T.; Kaikawa, T.; Takimiya, K.; Ostubo, T.; Aso, Y. *J. Am. Chem. Soc.* **2005**, 127, 8082.

[13] Van Haare, J. A. E. H.; Havinga, E. E.; van Dongen, J. L. J.; Janssen, R. A. J.; Cornil, J. Bredas, J.-L. *Chem. Eur. J.* **1998**, 4, 1509.

[14] Salzner, U. *J. Phys. Chem. A* **2008**, 112, 5458.

[15] Zade, S. S.; Bendikov, M. *J. Phys. Chem. C* **2007**, 111, 10662.

[16] Geskin, V. M.; Brédas, J.-L. *ChemPhysChem* **2003**, 4, 498.

[17] Nishinaga, T.; Tateno, M.; Fujii, M.; Fujita, W.; Takase, M.; Iyoda, M. *Org. Lett.* **2010**, 12, 5374.

[18] Frampton, M. J.; Anderson, H. L. *Angew. Chem. Int. Ed.* **2007**, 46, 1028.

[19] Pan, C.; Zhao, C.; Takeuchi, M.; Sugiyasu, K. *Chem. Asian J.* **2015**, 10, 1820.

[20] Terao, J. *Polym. Chem.* **2011**, 2, 2444.

[21] Lee, D.; Swager, T. M. *Synlett* **2004**, 149.

[22] Cardin, D. J. *Adv. Mater.* **2002**, 14, 553.

[23] Ie, Y.; Han, A.; Otsubo, T.; Aso, Y. *Chem. Commun.* **2009**, 3020.

[24] González, S. R.; Ie, Y.; Aso, Y.; Navarrete, J. T. L.; Casado, J. *J. Am. Chem. Soc.* **2011**, 133, 16350.

[25] Ie, Y.; Endou, M.; Lee, S. K.; Yamada, R.; Tada, H.; Aso, Y. *Angew. Chem. Int. Ed.* **2011**, 50, 11980.

[26] Ie, Y.; Okamoto, Y.; Tone, S.; Aso, Y. *Chem. Eur. J.* **2015**, 21, 16688.

[27] Yamada, R.; Kumazawa, H.; Noutoshi, T.; Tanaka, S.; Tada, H. *Nano Lett.* **2008**, 8, 1237.

[28] Lee, S. K.; Yamada, R.; Tanaka, S.; Chang, G. S.; Asai, Y.; Tada, H. *ACS Nano* **2012**, 6, 5078.

[29] Tanaka, S.; Yamashita, Y. *Synth. Met.* **1999**, 101, 532.

[30] Wakamiya, A.; Yamazaki, D.; Nishinaga, T.; Kitagawa, T.; Komatsu, K. *J. Org. Chem.* **2003**, 68, 8305.

[31] Malenfant, P. R. L.; Fréchet, J. M. J. *Macromolecules* **2000**, 33, 3634.

[32] Sugiyasu, K.; Honsho, Y.; Harrison, R. M.; Sato, A.; Yasuda, T.; Seki S.; Takeuchi, M. *J. Am. Chem. Soc.* **2010**, 132, 14754.

[33] Shomura, R.; Sugiyasu, K.; Yasuda, T.; Sato, A.; Takeuchi, M. *Macromolecules* **2012**, 45, 3759.

[34] Pan, C.; Sugiyasu, K.; Aimi, J.; Sato, A.; M. Takeuchi, *Angew. Chem. Int. Ed.* **2014**, 53, 8870.

[35] Ouchi, Y.; Sugiyasu, K.; Ogi, S.; Sato, A.; Takeuchi, M. *Chem. Asian J.* **2012**, 7, 75.

[36] Kiguchi, M.; Ohto, T.; Fujii, S.; Sugiyasu, K.; Nakajima, S.; Takeuchi, M.; Nakamura, H. *J. Am. Chem. Soc.* **2014**, 136, 7327.

[37] Sahoo, D.; Sugiyasu, K.; Tian, Y.; Takeuchi, M.; Scheblykin, I. G. *Chem. Mater.* **2014**, 26, 4867.

[38] Österbacka, R.; An, C. P.; Jiang, X. M.; Vardeny, Z. V. *Science* **2000**, 287, 839.

[39] Mitschke, U.; Bäuerle, P. *J. Chem. Soc., Perkin Trans. 1* **2001**, 740.

[40] Ong, T.-T.; Ng, S.-C.; Chan, H. S. O.; Vardhanan, R. V.; Kumura, K.; Mazaki, Y.; Kobayashi, K. *J. Mater. Chem.* **2003**, 13, 2185.

[41] Buey, J.; Swager, T. M. *Angew. Chem. Int. Ed.* **2000**, 39, 608.

[42] McNeil, A.; Müller, P.; Whitten, J. E.; Swager, T. M. *J. Am. Chem. Soc.* **2006**, 128, 12426.

[43] Sforazzini, G.; Kahnt, A.; Wykes, M.; Sprafke, J. K.; Brovevlli, S.; Montarnal, D.; Meinardi, F.; Cacialli, F.; Beljonne, D.; Albinsson, B.; Anderson, H. L. *J. Phys. Chem. C* **2014**, 118, 4553.

[44] Becker, K.; Lagoudakis, P. G.; Gaefke, G.; Höger, S.; Lupton, J. M. *Angew. Chem. Int. Ed.* **2007**, 46, 3450.

[45] Wallace, W. J.; Shephard, C. S.; Underwood, C. *J. Chem. Eng. Data* **1968**, 13, 11.

[46] A similar synthetic approach was also reported recently, see Ting, H.-C.; Tsai, C.-H.; Chen, J.-H.; Chen, L.-Y.; Chou, S.-H.; Wong, K.-T.; Huang, T.-W. Wu, C.-C. *Org. Lett.* **2012**, 14, 6338.

[47] Walker, S. D.; Barder, T. E.; Martinelli, J. R.; Buchwald, S. L. *Angew. Chem. Int. Ed.* **2004**, 43, 1871.

[48] Asawapirom, U.; Scherf, U. *Macromol. Rapid Commun.* **2001**, 22, 746.

[49] Zhang, Z.-B.; Fujiki, M.; Tang, H.-Z.; Motonaga, M.; Torimitsu, K. *Macromolecules* **2002**, 35, 1988.

[50] Chen, Z.; Swager, T. M. *Macromolecules* **2008**, 41, 6880.

[51] Bidan, G.; De Nicola, A.; Enée, V.; Guillerez, S. *Chem. Mater.* **1998**, 10, 1052.

[52] Although the π-conjugated system is "insulated", the side chains are flexible in solution, and solvent molecules should be able to get into the sheaths.

[53] Takeda, N.; Miller, J. R. *J. Phys. Chem. B* **2012**, 116, 14715.

[54] Saeki, A.; Koizumi, Y.; Aida, T.; Seki, S. *Acc. Chem. Res.* **2012**, 45, 1193.

[55] Seki, S.; Saeki, A.; Sakurai, T.; Sakamaki, D. *Phys. Chem. Chem. Phys.* **2014**, 16, 11093.

[56] Breselge, M.; Van Severen, I.; Lutsen, L.; Adriaensens, P.; Manca, J.; Vanderzande, D.; Cleij, T. *Thin Solid Films* **2006**, 511-512, 328.

[57] Jahani, F.; Torabi, S.; Chiechi, R. C.; Koster L. J. A.; Hummelen, J. C. *Chem. Commun.* **2014**, 50, 10645.

[58] Koster, L. J. A.; Mihailetchi, V. D.; Blom, P. W. M. *App. Phys. Lett.* **2006**, 88, 052104.

[59] Groves, C.; Greenham, N. C. *Phys. Rev. B* **2008**, 78, 155205.

[60] Cho, N.; Schlenker, C. W.; Knesting, K. M.; Koelsch, P.; Yip, H.-L.; Ginger, D. S.; Jen, A. K.-Y. *Adv. Energy Mater.* **2014**, 4, 1301857.

[61] Oga, H.; Saeki, A.; Ogomi, Y.; Hayase, S.; Seki, S. *J. Am. Chem. Soc.* **2014**, 136, 13818.

[62] Frisch, M. J., Trucks, G. W., Schlegel, H. B., Scuseria, G. E., Robb, M. A., Cheeseman, J. R., Scalmani, G., Barone, V., Mennucci, B., Petersson, G. A., Nakatsuji, H., Caricato, M., Li, X., Hratchian, H. P., Izmaylov, A. F., Bloino, J., Zheng, G., Sonnenberg, J. L., Hada, M., Ehara, M., Toyota, K., Fukuda, R., Hasegawa, J., Ishida, M., Nakajima, T., Honda, Y., Kitao, O., Nakai, H., Vreven, T., Montgomery, Jr., J. A., Peralta, J. E., Ogliaro, F., Bearpark, M., Heyd, J. J., Brothers, E., Kudin, K. N., Staroverov, V. N.,

Keith, T., Kobayashi, R., Normand, J., Raghavachari, K., Rendell, A.; Burant, J. C., Iyengar, S. S., Tomasi, J., Cossi, M., Rega, N., Millam, J. M., Klene, M., Knox, J. E., Cross, J. B., Bakken, V., Adamo, C., Jaramillo, J., Gomperts, R., Stratmann, R. E., Yazyev, O., Austin, A. J., Cammi, R., Pomelli, C., Ochterski, J. W., Martin, R. L., Morokuma, K., Zakrzewski, V. G., Voth, G. A., Salvador, P., Dannenberg, J. J., Dapprich, S., Daniels, A. D., Farkas, O., Foresman, J. B., Ortiz, J. V., Cioslowski, J.,; Fox, D. J., Gaussian 09, Revision E.01, Gaussian, Inc., Wallingford CT, **2013**.

[63] Zhao, Y.; Truhlar, D. J. *Theor. Chem. Acc.*, **2008**, 120, 215.

[64] Saeki, A.; Ohsaki, S.; Seki, S.; Tagawa, S. *J. Phys. Chem. C*, **2008,** 112*,* 16643.

[65] Gosztola, D.; Niemczyk, M. P.; Svec, W.; Lukas, A. S.; Wasielewski, M. R. *J*. *Phys*. *Chem*. *A*, **2000,** 104*,* 6545.

Chapter 4. The impact of head-to-head defect on the charge carrier mobility along the polythiophene chain.

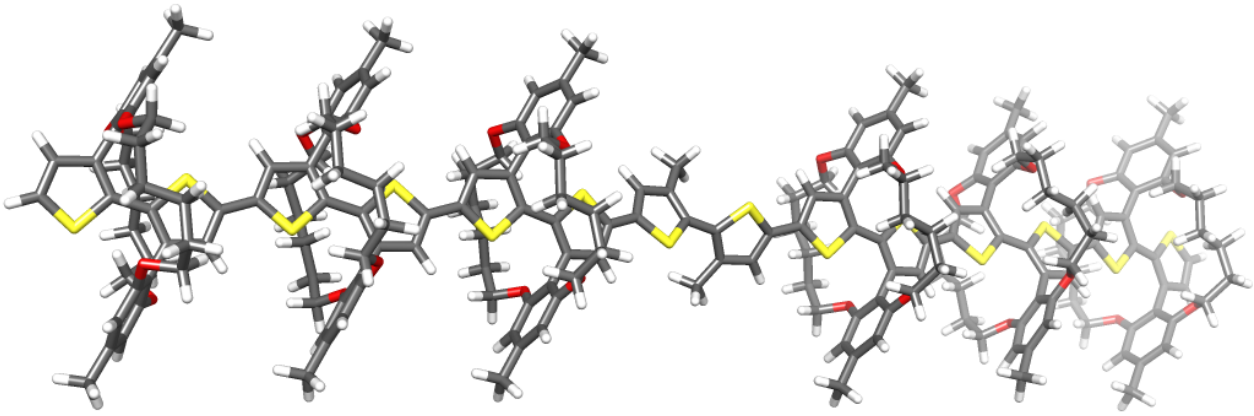

ABSTRACT

The performance of various electronics is highly relied on the charge carrier mobility. Increasing regioregularity of conjugated polymers is the strategy for molecular design as it can enhance the crystallinity of the materials, thereby improving the charge carrier mobility. However, it has recently been reported that some poorly ordered films of conjugated polymers also exhibited high charge carrier mobility. To investigate the effect of regioregularity on charge carrier mobility, we designed and synthesized new thiophene-based polymers in which the structural defect was intentionally introduced to examine the effect of regioregularity on the intra-wire charge carrier transport. We found that the defect copolymer backbone was isolated and interchain π–π interaction was effectively prevented. Even 1% structural defect deteriorates the electronic property of polythiophene, which lead to the decrease of the effective conjugation length. Block copolymers were obtained despite using the polycondensation reaction.

4.1 Introduction

Polythiophenes, which are one of the most studied conjugated polymers (CPs), have attracted increasing attention due to its versatile chemical synthetic and processability from solution at low temperature. These advantages make the polythiophenes as good polymeric materials which can be applied in printed and flexible organic electrics, such as organic field effect transistor (OFET), organic light emitting diode (OLED), organic solar cell and so on.[1-4] The performance of those electrics is highly relied on the charge carrier mobility of polymeric materials. In the past decades, researchers have been mainly focused on increasing the regioregularity of CPs as it can enhance the crystallinity of the materials, thereby improving the charge carrier mobility. Indeed, the charge carrier mobility experienced great increasing from 10^{-3} to 0.6 $cm^2V^{-1}s^{-1}$ based on this strategy.[5-7] Nevertheless, it has recently been reported that some poorly ordered films of CPs, for example $\mathbf{P_{IDT\text{-}BT}}$ (Scheme 4-1a) and $\mathbf{P_{DPP\text{-}T}}$ (Scheme 4-1b), also exhibited high charge carrier mobility.[8-9] These unexpected results challenged the tradition understanding of relationship between crystallinity and charge carrier mobility. The given explanation for those phenomena is that the conduction primarily occurs along the conjugated polymer bankbones even in the disorder film.[10-11]

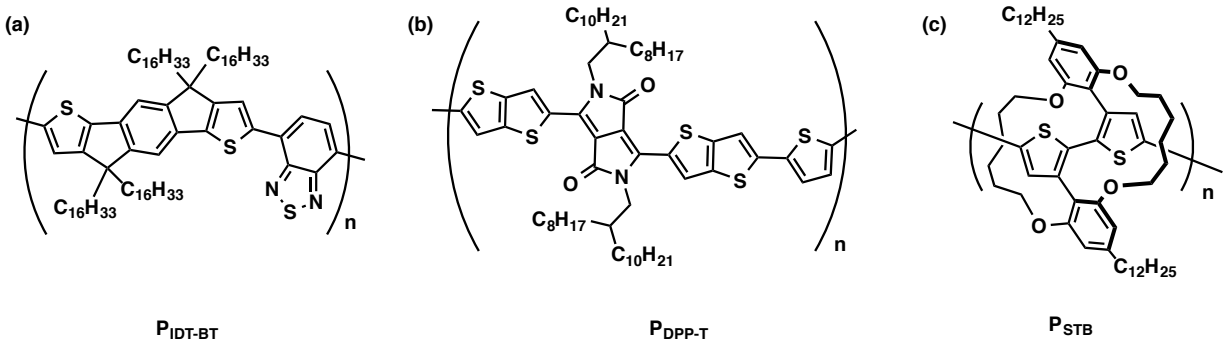

$\mathbf{P_{IDT\text{-}BT}}$ $\mathbf{P_{DPP\text{-}T}}$ $\mathbf{P_{STB}}$

Scheme 4-1. Chemical structure of (a) $\mathbf{P_{IDT\text{-}BT}}$ [8], (b) $\mathbf{P_{DPP\text{-}T}}$ [9], and (c) $\mathbf{P_{STB}}$ [12].

According to the widely accepted mechanism of charge carrier conduction, there are two conceivable carrier transport pathways in the polymeric materials: namely, *intrawire* and *interwire* charge transport.[13] The difficulty of understanding the mechanism exists in analyzing the charge carrier mobility of two transport pathway independently. Recently, our group developed a single polythiophene chain which can be molecularly sheathed by molecular design so that the interwire chain interaction between polymer chains are effectively limited.[12-16] This molecular design concept allows us to isolate and investigate the electronic properties of a single polythiophene (Scheme 4-1c. $\mathbf{P_{STB}}$). With this molecular design in hand, defect segment can be randomly introduced into the single polythiophene chain. Thus, in this chapter, we designed

and synthesized new thiophene-based polymers (Scheme 4-2) in which the structural defect was intentionally introduced to examine the effect of regioregularity on the intra-wire charge carrier carrier transport.

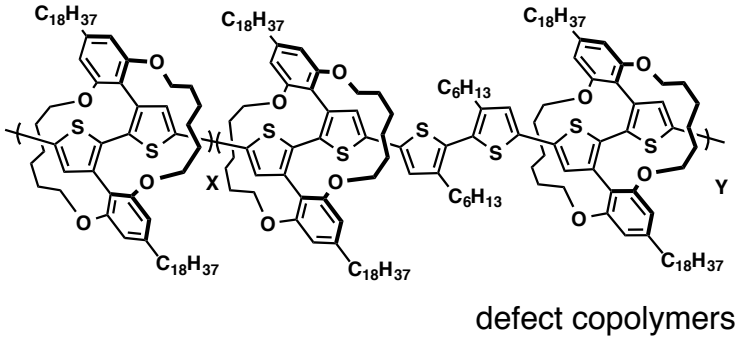

Scheme 4-2. Chemical structure of defect copolymers

Reichmanis and co-workers reported that differences in regioregularity of side chain attachment in poly(3-hexylthiophene) (P3HT) as small as ca. 4% are sufficient to induce dramatic changes in the electronic and morphological properties of the material.[17] Sirringhaus and co-works also reported that the difference in high regioreguarity (96%) and low regioregularity about (81%) in P3HT makes the FET mobility of which differ by more than a factor of 100.[6] Thus, small amount of structural defect ca. 1% is necessary for the investigation of relationship between structural defect and intrawire charge carrier mobility. Therefore, the degree of polymerization of the synthesized polymer should be at least 100. However, the insulated polythiophene wires would encounter the solubility issues which hinder the application and extension of single polythiophene wires. To this end, we first synthesized defect-free self-sheathed polythiophenes with different side chains. (Scheme 4-3) Based on the molecular weight of $\mathbf{P_{STB}}$, two branched alkyl side chains: $-CH_2CH(C_2H_5)C_4H_9$ and $-C_2H_4CH(CH_3)C_3H_6CH(CH_3)CH_3$, and one linear alky side chain: $-C_{18}H_{37}$ were decided to use.

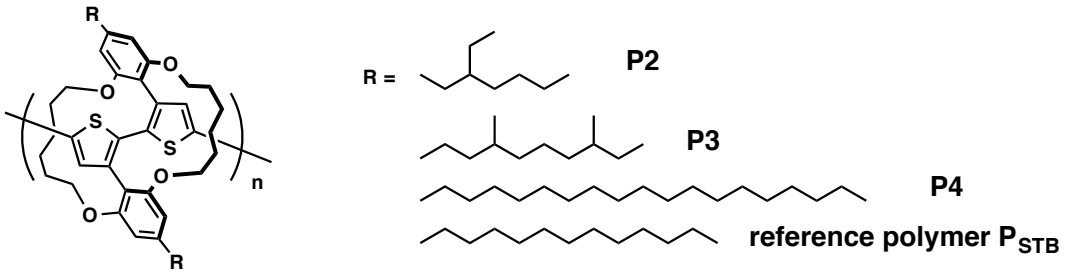

Scheme 4-3. Chemical structure of self-threading polythiophenes: **P2**, **P3**, **P4** and $\mathbf{P_{STB}}$ (reported previously [12]).

4.2 Results and Discussion

4.2.1 Monomers

The synthetic scheme of monomers ($\mathbf{M_{STB}}$, Scheme 4-4) is the same as previous report.[12] Although the frame structure of monomers is same, but the steric hindrance, which caused by the long linear alkyl side chain, led to the modified conditions and reaction yield. The linear side chain $-C_{18}H_{37}$ was introduced on the phenyl group in the first step. The Suzuki–Miyaura coupling reaction is one of the key step for synthesis of monomer with long linear side chain. In order to obtain high reaction yield, very high concertation in s-phos and $Pd_2(dba)_3$ reaction system was used. Otherwise, low reaction yield will be obtained. Another key step still is the double ring closing olefin metathesis reaction. But due to the steric hindrance, which caused by the long linear alkyl side chain, the yield of metathesis reaction is not high.

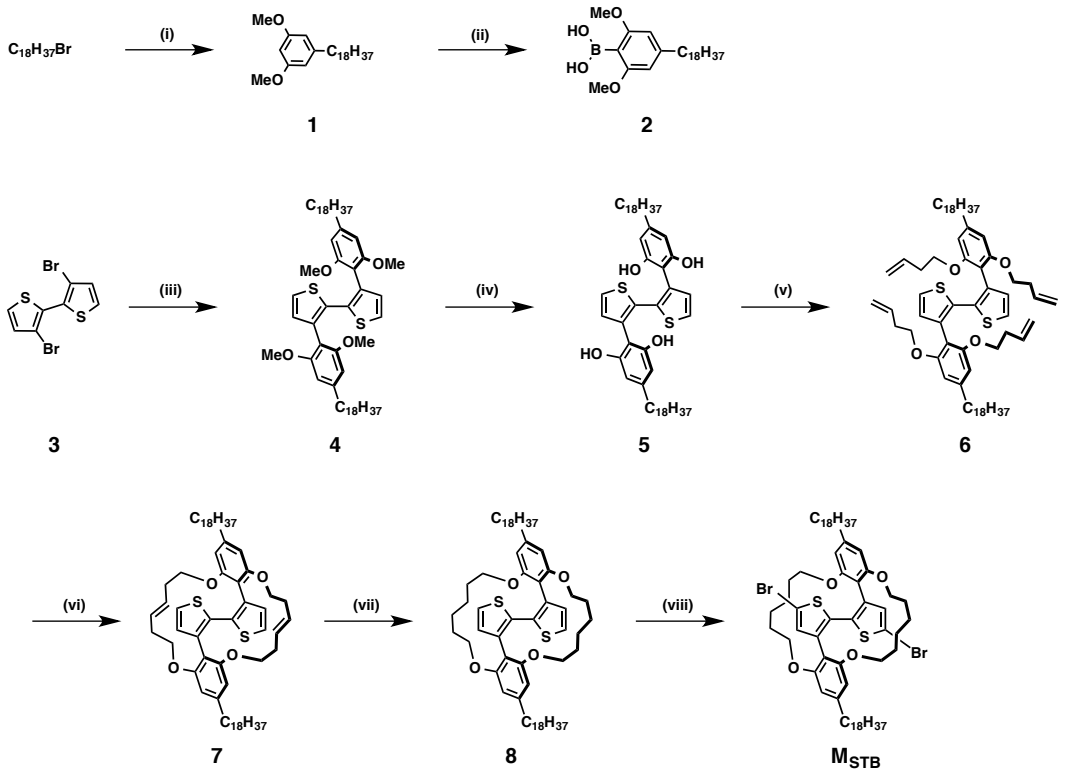

Scheme 4-4. Synthetic scheme towards Monomer $\mathbf{M_{STB}}$: (i) Mg, Et_2O, 0 °C, and then, $Pd(dppf)Cl_2$, 3,5-dimethoxyphenylboronic acid; (ii) *n*-BuLi, Et_2O, -78 °C, and then,$B(OMe)_3$; (iii) compound 2, s-phos, $Pd_2(dba)_3$, K_3PO_4, toluene, 80 °C; (iv) BBr_3, DCM; (v) PPh_3, DIAD, THF, 3-butene-1-ol, sonication; (vi) Wilkinson catalyst, THF, tert-Butanol, (vii) NBS, THF.

4.2.2 Homopolymers

With different monomers, polymerization was performed under Yamamoto reductive coupling conditions using a $Ni(COD)_2$ and bipridine system in a toluene and dimethylformamide (DMF) mixture to yield **P2**, **P3** and **P4**. (Scheme 4-5) The number average molecular weight (M_n) of the polymers determined to be 6k, 8k and 50k (Table 4-1) for **P2**, **P3**, **P4**, respectively by size-exclusion chromatography (polystyrene standard). This results indicated that introduction of long linear alkyl sides chain rather than branched side chains endow insulated polythiophene wires with higher solubility, thus achieving high molecular weight.

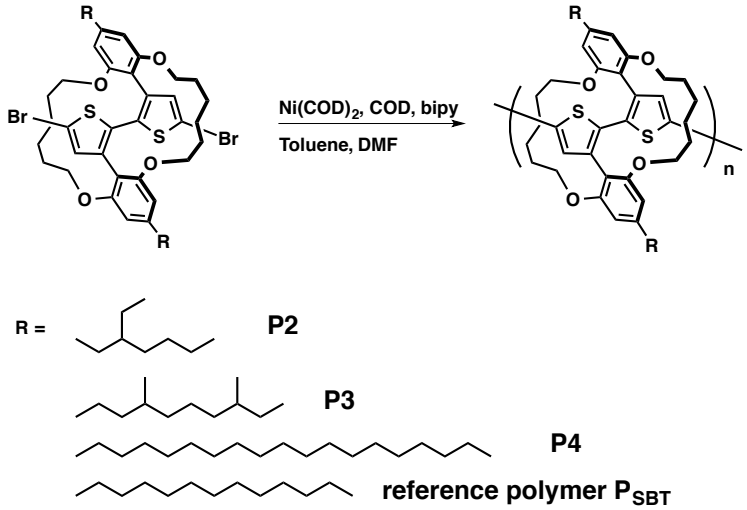

Scheme 4-5. Polymerization scheme towards **P2**, **P3**, and **P4**.

Table 4-1. Number average molecular weight (M_n) of the homopolymers (**P2**, **P3**, and **P4**)

Homopolymers	M_n
P2	6 k
P3	8 k
P4	50 k
$\mathbf{P_{STB}}$	12 k

The partially resolved vibronic structure in the UV/vis absorption of **P4** observed at room temperature undergoes major transformations when lowering the temperature. Figure 4-1 shows the changes in absorption spectrum of **P4** in 2-methyltetrahydrofuran (2Me-THF) solution with decreasing temperature. Upon decreasing the temperature, the vibronic peaks sharpen and become more intense. At low temperatures, the spectra show no significance peak shifting or separating. This results indicates that the homopolymer **P4** contains planar backbone and good conjugation system.

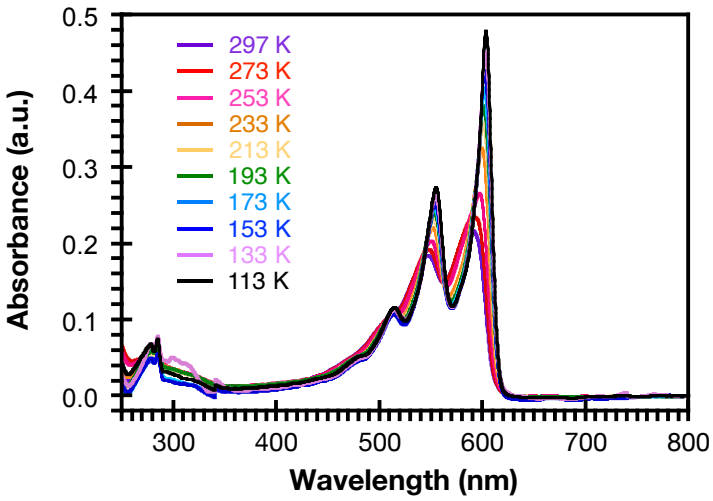

Figure 4-1. Absorption spectra of homopolymer **P4** at various temperature (113 K – 297 K).

The morphology of **P4** (M_n = 50k Da) was investigated by AFM measurement using mica substrates. We prepared the specimen by spin-coating a highly diluted solution ($2\times10^{-7}\ mol/L$), in which aggregation of individual polymer chain was prevented. From the AFM image and a section analysis (Figure 4-2), several single long **P4** polymer chain were observed. As shown in Figure 4-2, **P4** showed a rigid and straight structure. The height of polymer chains was determined to be about 2 nm. The long length of polymer chains observed by AFM is not consistent with the molecular weight estimated by SEC. We assert that longer polymers, which tend to adsorb on the substrate during the spin-coating, were selectively observed by AFM. We also note that spin-coating may affect the backbone conformation by centrifugal stretching.

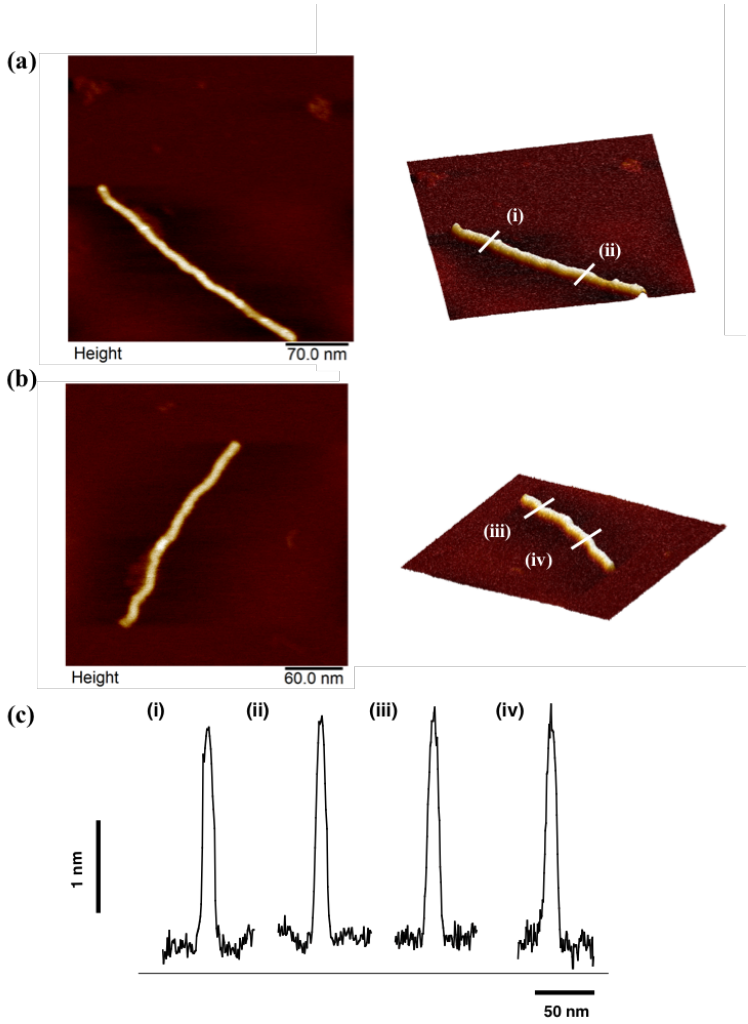

Figure 4-2. Typical AFM images of (a, b) **P4** single molecular wires. (c) Height profiles of **P4** obtained along the white lines in the AFM images

4.2.3 Block copolymers

In view of the planar backbone and high molecular weight of **P4**, it can be a promising platform to investigate intra-wire charge carrier transport. We designed a new thiophene-based random copolymer in which structural defect can be intentionally incorporated. (Scheme 4-2) Here, 3,3'-dihexyl-2,2'-bithiophene (defect bithiophene monomer, $\mathbf{M_{DB}}$) is selected as the defect segment because it is known that the head-to-head connection is the structural defect in regioregular poly(3-hexylthiophene). However, block copolymers were obtained through Yamamoto reductive coupling copolymerization of $\mathbf{M_{STB}}$ and $\mathbf{M_{DB}}$.

Copolymerization of $\mathbf{M_{STB}}$ and $\mathbf{M_{DB}}$ were performed under common conditions. (Scheme 4-6) Namely, a solution (dimethylformamide : toluene = 1 : 8) of a mixture of $\mathbf{M_{STB}}$ and $\mathbf{M_{DB}}$ (9 : 1 and 8 : 2 ratios) was stirred in the presence of cyclooctadiene (COD), $Ni(COD)_2$, and bipyridine at 90 °C for 48 hours. The

obtained polymers are hereafter referred to as **P-STB$_9$DB$_1$** and **P-STB$_8$DB$_2$**, in which the subscripts indicate the feed ratio of the unsheathed monomer **M$_{DB}$**. Similarly, we also synthesized homopolymers, **P4** and **P$_{DB}$**.

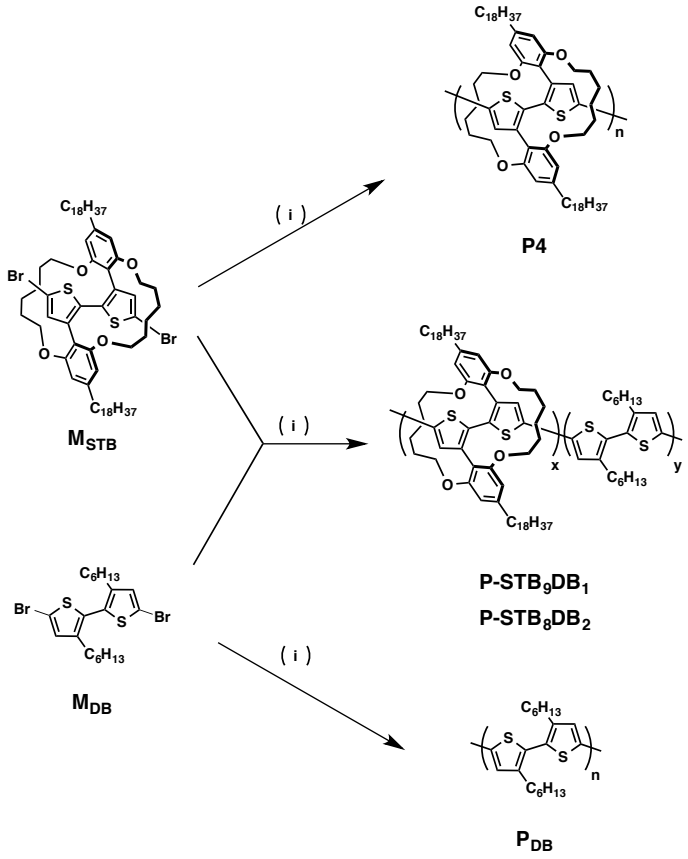

Scheme 4-6. Synthesis scheme towards block copolymers (**P-SBT$_9$DB$_1$** and **P-SBT$_8$DB$_2$**) and homopolymers **P4** and **P$_{DB}$**. (i) COD, Ni(COD)$_2$, bipyridine, DMF and toluene.

^{1}H-NMR spectra of the polymers are shown in Figure 4-3. Peaks that are characteristic to **P4** (6.43 ppm) and **P$_{DB}$** (7.04 ppm) are independently observed in **P-STB$_9$DB$_1$** and **P-STB$_8$DB$_2$**. This result indicates that random copolymers were not formed, and that the segments of **P-STB$_9$DB$_1$** and **P-STB$_8$DB$_2$** are electronically independent. Compositions of **P$_{DB}$** segments in **P-STB$_9$DB$_1$** and **P-STB$_8$DB$_2$** were determined to be 7.4 and 17.3%, respectively, thus were slightly smaller than the feed ratio. This result would imply that monomer **M$_{DB}$** is less reactive than **M$_{STB}$**. Size exclusion chromatography (SEC) profiles of the obtained polymers showed unimodal peaks (Figure 4-4), suggesting that the **P-STB$_9$DB$_1$** and **P-STB$_8$DB$_2$** segments are connected in one polymer chain. These results briefly indicate the formation of polymer chains consisting of **P-STB$_9$DB$_1$** and **P-STB$_8$DB$_2$** blocks. Number-average molecular weight (M_n) and polydispersity index (PDI) of the polymers were determined to be 54 ~ 73 K and 1.7 ~ 2.3 using polystyrene standard (Table 4-2).

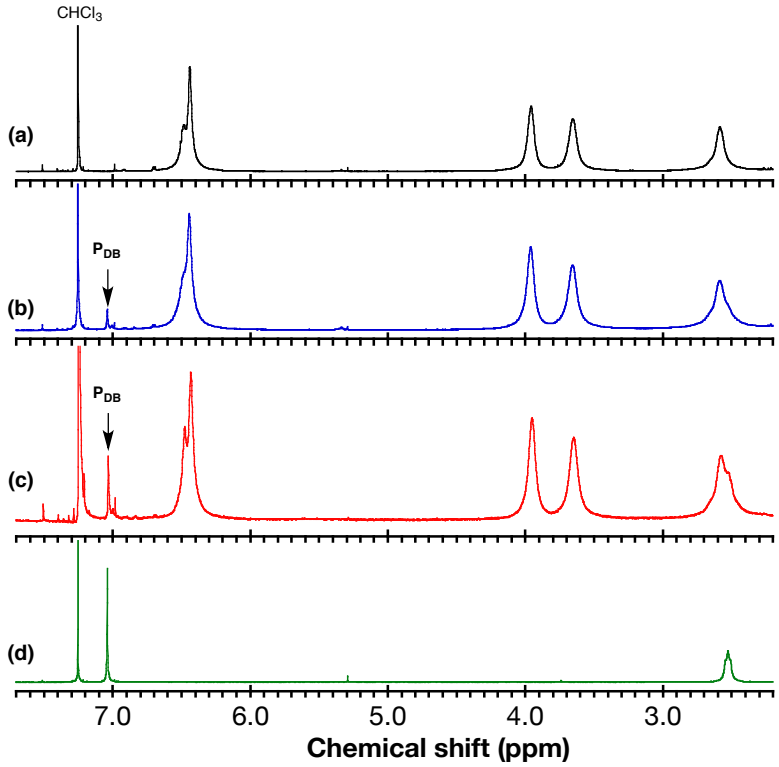

Figure 4-3. Partial ^{1}H-NMR spectra of (a) **P4**, black, (b) **P-STB$_9$DB$_1$**, blue, (c) **P-STB$_8$DB$_2$**, red, and (d) **P$_{DB}$**, green: $CDCl_3$, 298 K

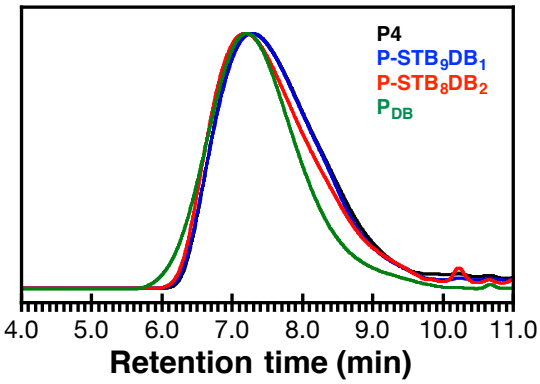

Figure 4-4. GPC profiles of (black) **P4**, (blue) **P-STB$_9$DB$_1$**, (red) **P-STB$_8$DB$_2$**, and (green) **P$_{DB}$**

Table 4-2. Number-average molecular weight (*M*n) and polydispersity index (PDI) of the block copolymers and homopolymers

Polymers	M_n	PDI
P4	50 k	1.7
P-STB$_9$DB$_1$	55 k	2.2
P-STB$_8$DB$_2$	59 k	2.3
P$_{DB}$	73 k	2.3

Figure 4-5 compares absorption spectra of **P4**, **P-STB$_9$DB$_1$**, **P-STB$_8$DB$_2$**, and **P$_{DB}$**. Well-separated absorption maxima, which can be attributed to those of **P4** and **P$_{DB}$** segments, are observed for **P-STB$_9$DB$_1$** and **P-STB$_8$DB$_2$**. This result is consistent with those reported by Scherf group.[18] If the monomer **M$_{DB}$** was randomly incorporated into the **P4** backbone, then the effective conjugation of **P4** segment should be significantly reduced; for example, in the case of **P-STB$_8$DB$_2$**, **P4** backbone could be stochastically segmented into as small as tetramer or pentamer[12]. Nonetheless, the π–π* transition of **P4** backbone at 500 - 600 nm was scarcely affected by **M$_{DB}$**, thus corroborating the block copolymer structure. Importantly, the spectra could be deconvoluted into those of **P4** and **P$_{DB}$**, (Figure 4-6) which reasonably reflected the compositions of each block determined by ^{1}H-NMR spectra.

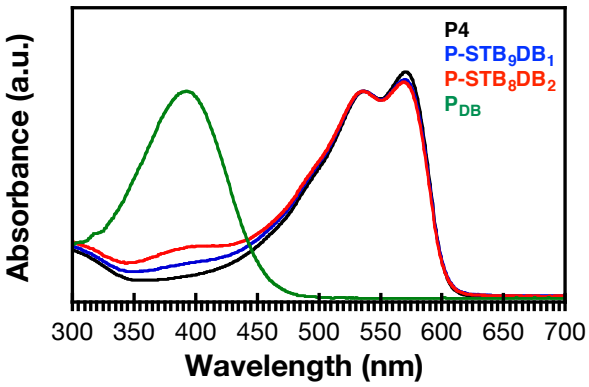

Figure 4-5. Absorption spectra of (black) **P4**, (blue) **P-STB$_9$DB$_1$**, (red) **P-STB$_8$DB$_2$** and (green) **P$_{DB}$**.

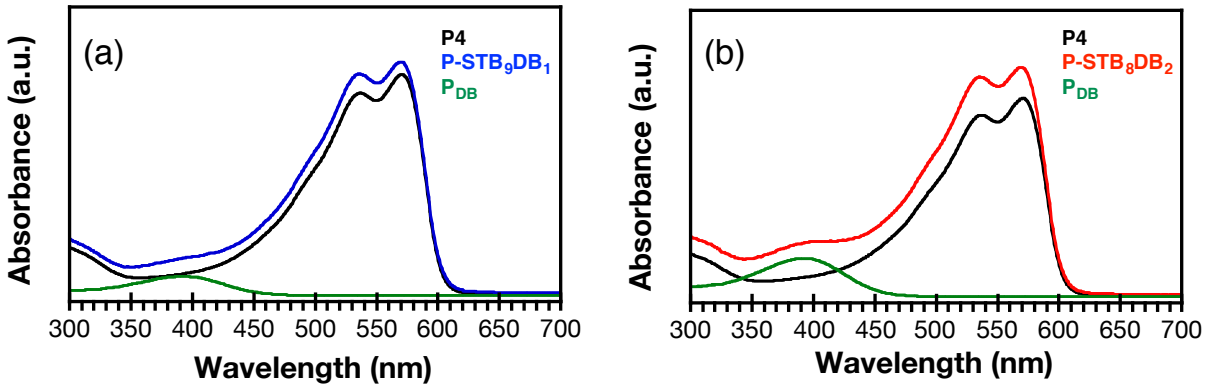

Figure 4-6. Absorption spectra of (blue) **P-STB$_9$DB$_1$** and (red) **P-STB$_8$DB$_2$**, which can be deconvoluted into the absorption spectra of (black) **P4** and (green) **P$_{DB}$**.

To directly visualize the expected structure of block copolymers, we observed the polymers using atomic force microscopy (AFM) measurement. Sample preparation was optimized so that a single polymer chain can be observed without aggregation; a very diluted solution of the polymer (2×10^{-7} mol/L) was spin-coated (3000 rpm) on a graphite substrate. As shown in Figure 4-2a, **P4** has a rigid and straight structure with the height of ~2 nm. While, as shown in Figure 4-7a, **P-STB$_8$DB$_2$** also consists of the rigid backbone, but thin linear structures are extended from both termini (Figure 4-7b). As such, we succeeded in confirming the block structure directly by AFM. Polymer length observed by AFM is not consistent with the molecular weight estimated by SEC. We assert that longer polymers, which tend to adsorb on the substrate during the spin-coating, were selectively observed by AFM. We also note that spin-coating may affect the backbone conformation by centrifugal stretching.

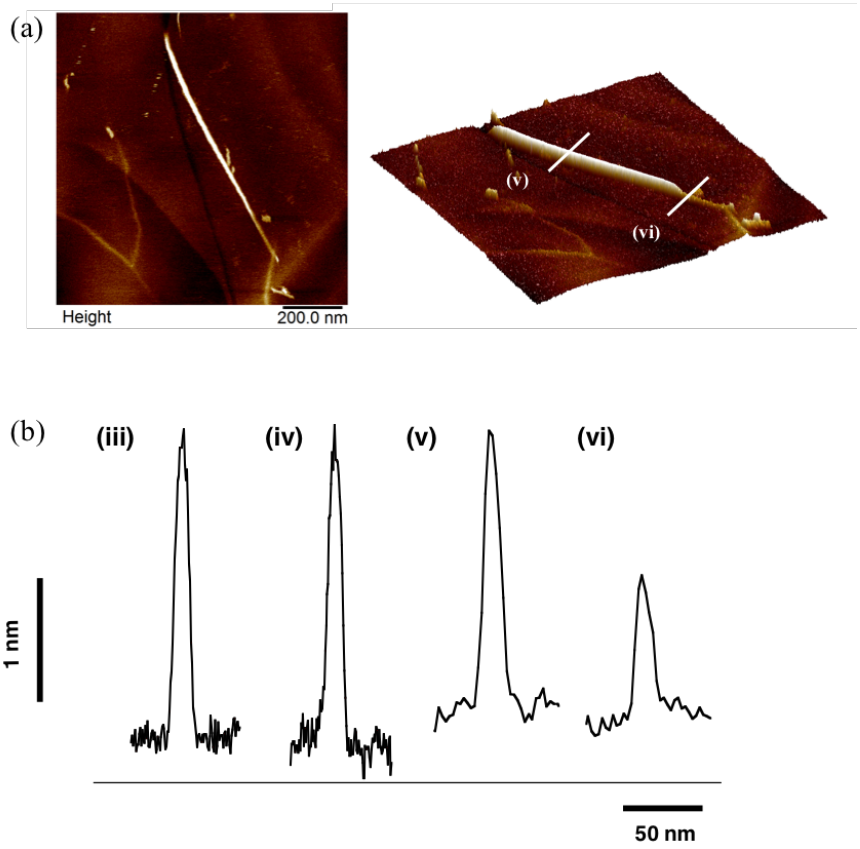

Figure 4-7. Typical AFM images of (a) **P-STB$_8$DB$_2$**. (b) Height profiles of **P4** and **P-STB$_8$DB$_2$** obtained along the white lines in the AFM images.

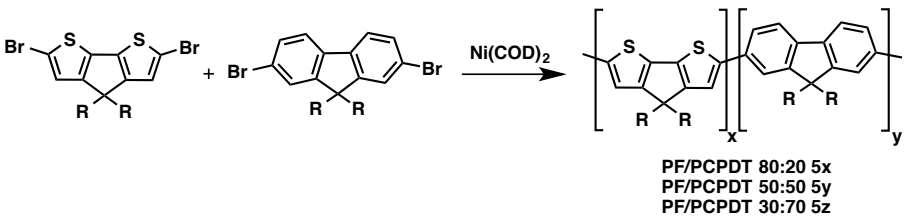

Scheme 4-7. Block copolymer synthesis through Yamamoto reductive polycondensation.

With the above results, we can conclude that copolymers were obtained through cyclopolymerization of $\mathbf{M_{STB}}$ and $\mathbf{M_{DB}}$ under common conditions. This behavior also observed by Scherf and co-workers. [18]. They synthesized block copolymers of poly(2,7-(9,9-dialkyl)fluorene) and poly(2,6-(4,4-dialkyl)-4*H*-cyclopenta[2,1-b:3,4-b′]dithiophene) using Yamamoto reductive coupling polymerization conditions despite

fact that propagation proceeds in the step-growth mechanism (Scheme 4-7). This remarkable polymerization was explained by the difference in the reactivity of both monomers with the nickel reagent. In our molecular design, as reported previously, the bithiophene backbone in $\mathbf{M_{STB}}$ is block planarized owing to the strapped structure[12], while that in $\mathbf{M_{DB}}$ is known to be twisted[19-20]. Because of the difference in planarity, $\mathbf{M_{STB}}$ and $\mathbf{M_{DB}}$ should have distinct electronic structures. In fact, absorption spectra (Figure 4-8), cyclic voltammetry (CV) (Figure 4-9), and differential pulse voltammogram (DPV) (Figure 4-10) showed that $\mathbf{M_{STB}}$ has better conjugation and lower oxidation potential in comparison with $\mathbf{M_{DB}}$. Therefore, we anticipated that these two monomers would have different reactivity in the reductive polycondensation.

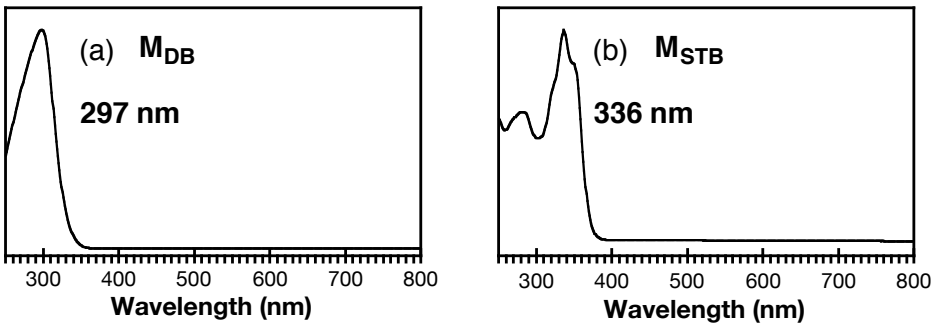

Figure 4-8. Absorption spectra of (a) $\mathbf{M_{DB}}$ and (b) $\mathbf{M_{STB}}$.

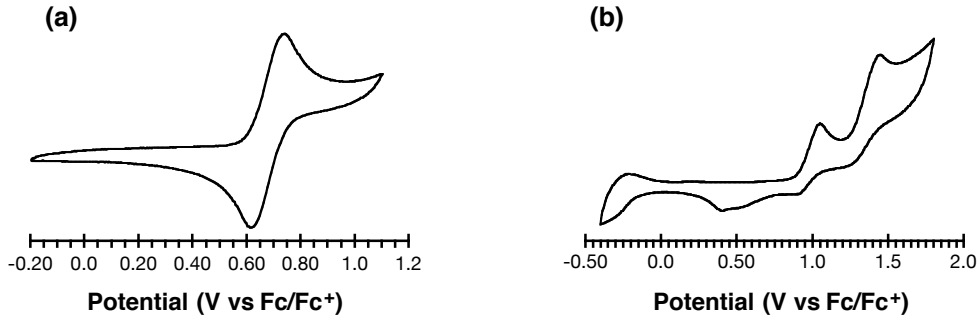

Figure 4-9. CV profiles of (a) monomer $\mathbf{M_{STB}}$ and (b) monomer $\mathbf{M_{DB}}$.

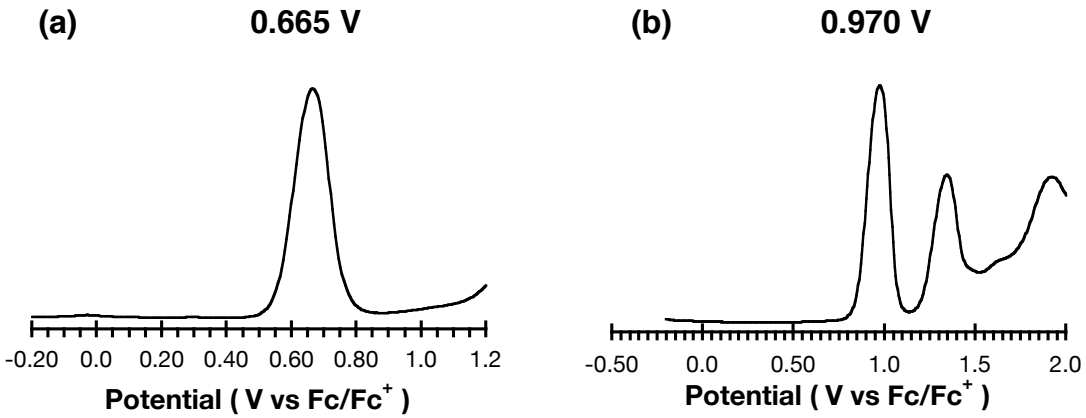

Figure 4-10. DPV profiles of (a) monomer $\mathbf{M_{STB}}$ and (b) monomer $\mathbf{M_{DB}}$.

4.2.4 Random copolymers

In order to obtain thiophene-based random copolymer in which structural defect can be intentionally incorporated. The monomers for Yamamoto reductive coupling copolymerization need to show similar reactivity. Thus, we designed new monomer ($\mathbf{M_{NDB}}$) for defect segment. (Scheme 4-8) We functionalized the 3,3'-dihexyl-2,2'-bithiophene and introduced the same self-threading bithiophene segment on the two head of this defect segment. By this new molecular design, the reactivity of two monomers would be close. The synthesis scheme towards $\mathbf{M_{NDB}}$ as shown in Scheme 4-8. After bromination reaction, compound **10** was obtained using compound **8** as starting material. Kumada–Tamao–Corriu coupling rather than Suzuki–Miyaura coupling or Stille coupling was used because forming Grignard reagent through *i*-PrMgCl is convincing. Furthermore, the polarity of the byproduct (dimer of compound **10**) and target are similar which result in the difficult on the separation through column chromatgraphy. Finally, Recycling GPC was applied to purify the resulting mixture. The combined columns YMC-GPC T2000 and T4000 were used.

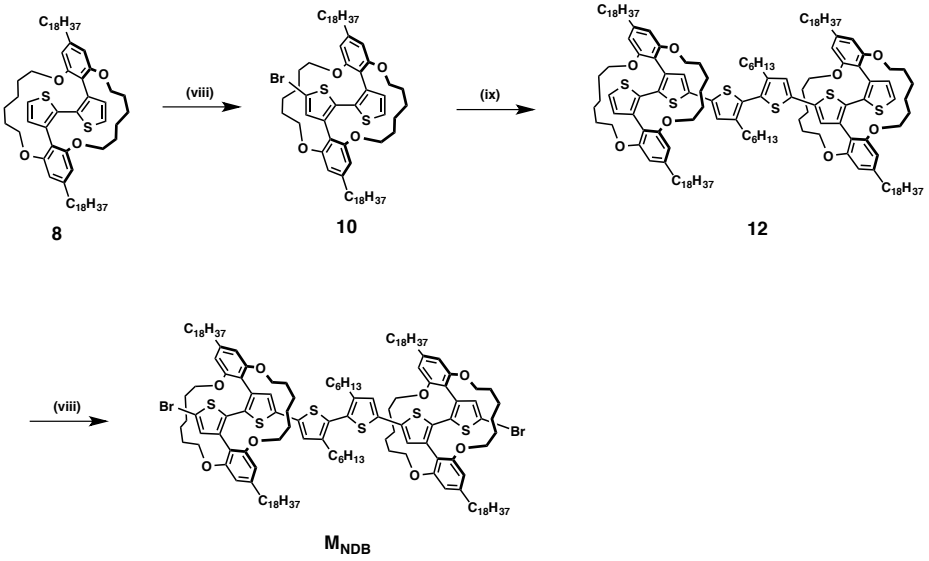

Scheme 4-8. Synthesis scheme towards new defect segment: $\mathbf{M_{NDB}}$. (viii) NBS, THF; (ix) *i*-PrMgCl, THF, 5,5'-dibromo-3,3'-dihexyl-2,2'-bithiophene, $Pd(dppf)Cl_2$, THF.

Random copolymerization of $\mathbf{M_{STB}}$ and $\mathbf{M_{NDB}}$ were performed under same conditions for block copolymers. Through tuning the ratio between $\mathbf{M_{STB}}$ and $\mathbf{M_{NDB}}$, defect copolymers with defect ratio of 0.0%, 0.96%, 2.27%, 4.17%, 7.14%, 9.38%, 12.50%, and 16.67% were obtained through Yamamoto reductive coupling copolymerization method. (Scheme 4-9) The obtained defect copolymers are hereafter referred to as $\mathbf{P_{DC\text{-}N}}$, in which the "N" indicate the defect ratio.

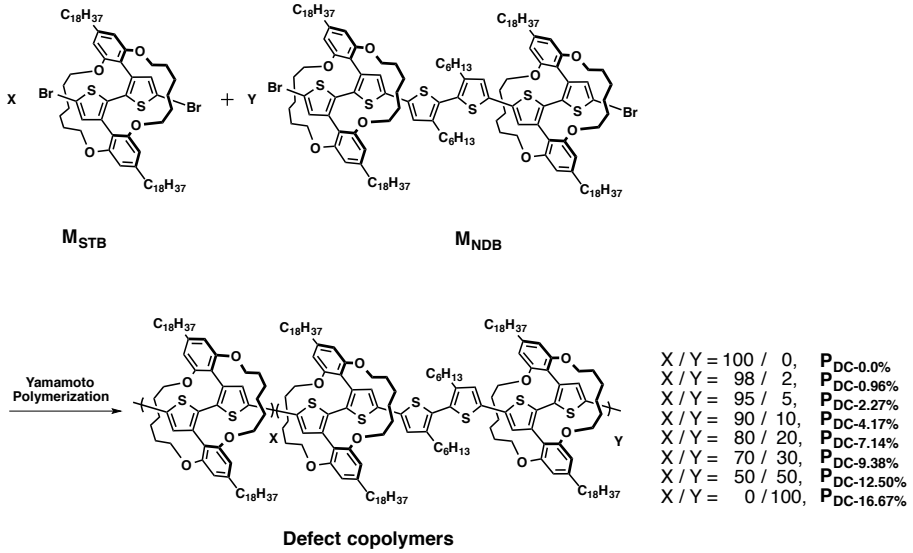

Scheme 4-9. Copolymerization scheme towards defect copolymers $\mathbf{P_{DC\text{-}N}}$, **N** (defect ratio) = 0.0%, 0.96%, 2.27%, 4.17%, 7.14%, 9.38%, 12.50% and 16.67%.

Size exclusion chromatography (SEC) profiles of the obtained polymers $\mathbf{P_{DC\text{-}N}}$ showed unimodal peaks (Figure 4-11), suggesting that the defect segments are connected in one polymer chain. These results indicate the formation of polymer chains consisting of defect segment. The number average molecular weight (M_n) of all defect copolymers determined to be over 50k by size-exclusion chromatography with polystyrene standard (Table 4-2).

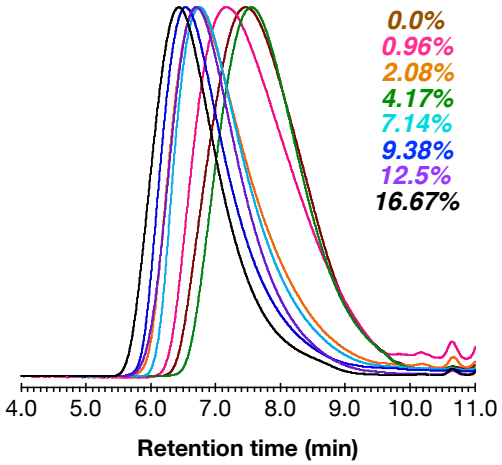

Figure 4-11. GPC profiles of $\mathbf{P_{DC\text{-}N}}$, **N** (defect ratio) = 0.0% (brown), 0.96% (pink), 2.27% (yellow), 4.17% (green), 7.14% (light blue), 9.38% (blue), 12.50% (purple) and 16.67% (black).

Table 4-2. Number-average molecular weight (M_n), weight-average molecular weight (M_w) and polydispersity index (PDI) of the defect copolymers

	Defect ratio	$\boldsymbol{M_n}$	$\boldsymbol{M_w}$	**PDI**
$\mathbf{P_{DC\text{-}0.0\%}}$	0.0 %	48 k	102 k	2.140
$\mathbf{P_{DC\text{-}0.96\%}}$	0.96 %	55 k	137 k	2.480
$\mathbf{P_{DC\text{-}2.27\%}}$	2.27 %	93 k	231 k	2.497
$\mathbf{P_{DC\text{-}4.17\%}}$	4.17 %	46 k	90 k	1.972
$\mathbf{P_{DC\text{-}7.14\%}}$	7.14 %	96 k	138 k	2.275
$\mathbf{P_{DC\text{-}9.38\%}}$	9.38 %	132 k	313 k	2.376
$\mathbf{P_{DC\text{-}12.50\%}}$	12.50 %	117 k	263 k	2.255
$\mathbf{P_{DC\text{-}16.67\%}}$	16.67 %	172 k	425 k	2.467

Figure 4-12a shows the absorption spectra of defect polymers measured in diluted $CHCl_3$ solution. Interestingly, as the defect ratio increases, the two absorption maxima, which represent transition energy E_{01} and E_{00}, shifted hypsochromically. This spectral change indicates the decrease of the effective conjugation length; even 1% structural defect deteriorates the electronic property of polythiophene. The change of absorption spectra also indicates the formation of random copolymers.

Figure 4-12b shows the absorption spectra of defect polymers in the film state. The identical spectra observed in solution and in films indicated that the defect copolymer backbone were isolated and interchain π–π interaction was effectively prevented. With successful synthesis of long polythiophenes with controlled amount of structural defect, the mechanism of charge carrier transport will be investigated in future.

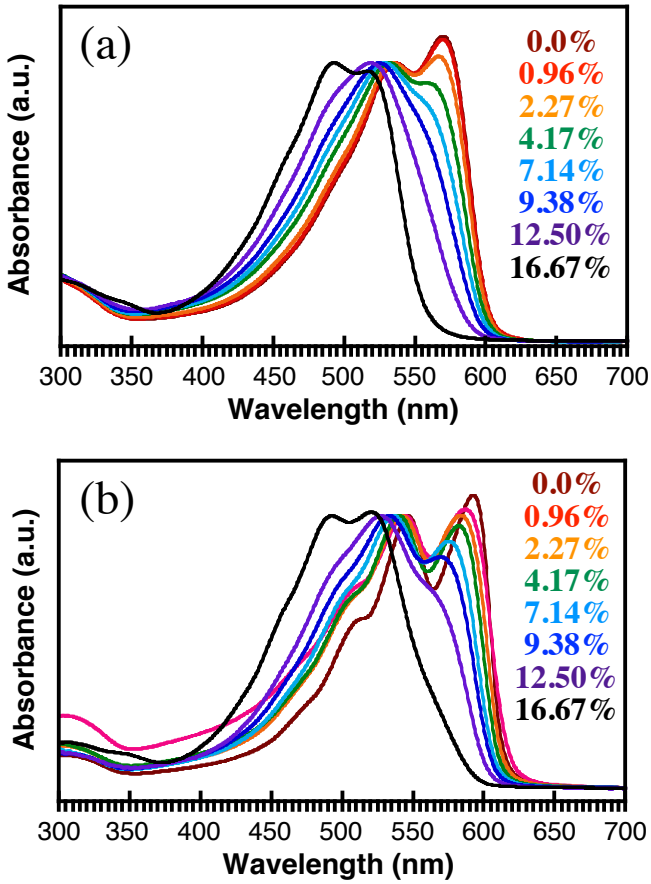

Figure 4-12. Absorption spectra of $\mathbf{P_{DC\text{-}N}}$, **N** (defect ratio) = 0.0% (brown), 0.96% (pink), 2.27% (yellow), 4.17% (green), 7.14% (light blue), 9.38% (blue), 12.50% (purple) and 16.67% (black) in (a) solution and (b) film state.

4.3 Conclusions

In conclusion, new self-threading polythiophenes in which the structural defect was intentionally introduced were synthesized successfully. The defect copolymer backbone was isolated and interchain π–π interaction was effectively prevented. Even 1% structural defect deteriorates the electronic property of polythiophene, which lead to the decrease of the effective conjugation length. Block copolymers were obtained despite using the polycondensation reaction.

4.4 Experimental sections

4.4.1 General

Air and water sensitive synthetic manipulations were performed under an argon atmosphere using standard Schlenk techniques. All chemicals were purchased from Aldrich, TCI, Kanto Chemical, or Wako and used as received without further purification. Column chromatography was performed on silica gel (KANTO Chemical silica gel 60N). ^{1}H NMR and ^{13}C NMR spectra were recorded on a JEOL ECS-400 spectrometer with tetramethylsilane (0 ppm for ^{1}H) or residual $CHCl_3$ (77 ppm for ^{13}C) as an internal standard. MALDI-TOF mass spectra were obtained with SHIMADZU AXIMA-CFR Plus station. UV-Vis absorption spectra were obtained on a JASCO V-670 spectrophotometer. Melting points were determined with a Yanako NP-500P micro melting point apparatus. Gel permeation chromatography was performed using a TOSHO GPC system (HLC-8320GPC EcoSEC) equipped with two TSK gel Super-Multipore HZ-M columns and a UV detector (254 nm), using THF as an eluent. Electrochemical measurements were conducted with an Eco Chemie AUTOLAB PGSTAT12 potentiostat, using a quasi-internal Ag/Ag+ reference electrode (Ag wire submersed in MeCN solution of 0.01 M AgNO3 and 0.1 M *n*-Bu3NPF6). Atomic force microscopy (AFM) was performed on a Bruker model MultiMode 8 atomic force microscope under ambient conditions in the scan assist analysis. AFM images were analyzed with Bruker Nanoanalysis.

4.4.2 Synthesis of monomer and polymers

a) Synthesis of monomer M_{STB}

Synthesis of compound 1: A 1 L three-neck round-bottom flask was charged with magnesium turnings (2.0 g, 82.9 mmol) and a small piece of iodine. The flask was evacuated and refilled with argon three times. After addition of dry THF (300 mL), 1-bromooctadecane (25.1 g, 76.0 mmol) was slowly added. The reaction mixture was stirred at room temperature for 3 hours, resulting in a Grignard solution. In another 2 L three-neck round-bottom flask, 1-bromo-3,5-dimethoxybenzene (15.0 g 69.1 mmol) and Pd(dppf)Cl_2 (505 mg, 0.7 mmol) were placed, and the flask was evacuated and refilled with argon three times. After addition of THF

(300 mL), the Grignard solution was slowly transferred to this flask. The mixture was stirred at 80 ºC overnight. Then, methanol was slowly added to quench the reaction. The mixture was washed with water and extracted with DCM three times. The organic layer was washed with brine and dried over $MgSO_4$. After solvent was evaporated, product was purified by column chromatography (silica gel, DCM / hexane = 1 / 5). Compound **1** was obtained as white solid (15.6 g, 90 %).

M.p.: 53.7 ºC. ^{1}H NMR ($CDCl_3$, 400 MHz, TMS, 298 K): δ 0.89 (t, J = 6.8 Hz, 3H), 1.27 – 1.42 (m, 30H), 1.61 (m, 2H), 2.55 (t, J = 8.0 Hz, 2H), 3.79 (s, 6H), 6.30 (t, J = 2.0 Hz, 1H), 6.35 (d, J = 2.0 Hz, 2H). ^{13}C NMR ($CDCl_3$, 100 MHz, TMS, 298 K): δ 14.24, 22.81, 29.47, 29.64, 29.71, 29.82, 31.42, 32.04, 36.42, 55.29, 97.59, 106.52, 145.51, 160.74. MALDI-TOF mass (Matrix: Dithranol): Found m/z = 391.6035, calculated ($C_{26}H_{46}O_2$) 390.35.

Synthesis of compound 2: A 1 L three-neck round-bottom flask was charged with compound **1** (16.0 g, 40.9 mmol), and evacuated and refilled with argon three times. After addition of dry diethyl ether (500 mL) and *N,N,N',N'*-tetramethylethylenediamine (TMEDA) (5.2 g, 45.0 mmol), *n*-BuLi (17 mL, 2.6 mol/L, 45.1 mmol) was slowly added at 0 ºC. The mixture was stirred at room temperature for 1 hour. Then, after addition of trimethyl borate (5.1 g, 49.2 mmol), the mixture was stirred at room temperature overnight. 1M HCl was slowly added to quench the reaction. The mixture was washed with water and extracted with $CHCl_3$. The organic layer was washed with brine and dried over $MgSO_4$. After solvent was evaporated, product was purified by reprecipitation ($CHCl_3$ / EtOAc = 1 / 4). Compound **2** was obtained as white solid (12.5 g, 70 %).

M. p.: 101.8 ºC . ^{1}H NMR ($CDCl_3$, 400 MHz, TMS, 298 K): δ 0.88 (t, J = 6.8 Hz, 3H), 1.25 – 1.32 (m, 30H), 1.62 (m, 2H), 2.60 (t, J = 8.0 Hz, 2H), 3.91 (s, 6H), 6.44 (s, 2H), 7.18 (s, 2H). ^{13}C NMR ($CDCl_3$, 100 MHz, TMS, 298 K): δ14.24, 22.79, 29.46, 29.60, 29.69, 29.80, 31.28, 32.02, 36.90, 56.01, 104.62, 149.09, 165.53. MALDI-TOF mass (Matrix: Dithranol): Found m/z = 434.5496, calculated ($C_{26}H_{47}BO_4$) 434.36.

Synthesis of compund 4: A 200 mL two-neck round-bottom flask was charged with 3,3'-dibromo-2,2'-bithiophene (2.4 g, 7.4 mmol), compound **2** (9.7 g, 22.2 mmol), K_3PO_4 (9.4 g, 44.4 mmol), $Pd_2(dba)_3$ (191.7 mg, 0.185 mmol) and 2-Dicyclohexylphosphino-2',6'-dimethoxybiphenyl (S-phos) (304 mg, 0.74 mmol). The flask was evacuated and re-filled with argon three times. After addition of dry toluene (4.4 mL), the mixture was stirred at 100 ºC overnight, and then, diluted by DCM, washed with water and extracted with DCM three times. The organic layer was washed with brine and dried over $MgSO_4$. After solvent was evaporated, product was purified by column chromatography (silica gel, DCM / hexane = 1 /2). Compound **4** was obtained as white solid (6.8 g, 97 %).

M. p.: 104.5 ºC . ^{1}H NMR ($CDCl_3$, 400 MHz, TMS, 298 K): δ 0.88 (t, J = 6.8 Hz, 6H), 1.22 – 1.35 (m, 60H), 1.64 (m, 4H), 2.57 (t, J = 8.0 Hz, 4H), 3.52 (s, 12H), 6.23 (s, 4H), 6.85 (d, J = 5.2 Hz, 2H), 7.09 (d, J = 5.2 Hz, 2H). ^{13}C NMR ($CDCl_3$, 100 MHz, TMS, 298 K): δ 14.25, 22.80, 29.47, 29.72, 29.83, 31.56, 32.03, 36.94,

55.39, 104.25, 111.79, 122.44, 130.17, 131.35, 134.19, 143.773, 157.88. MALDI-TOF mass (Matrix: Dithranol): Found m/z = 942.1617, calculated ($C_{60}H_{94}O_4S_2$) 942.66.

Synthesis of compound 5: A 200 mL two-neck round-bottom flask was charged with compound **4** (500 mg, 0.53 mmol), and evacuated and re-filled argon three times. After addition of dry DCM (11 mL), BBr_3 (2.12 mL, 1 mol/L, 2.12 mmol) was added slowly at 0 ºC. The resulting mixture was stirred at room temperature overnight, and then, washed with water and extracted with EtOAc. The organic layer was washed with brine and dried over $MgSO_4$. After solvent was evaporated, product was purified by column chromatography (silica gel, EtOAc / hexane = 1 / 2). Compound **5** was obtained as white solid (416 mg, 89 %).
M. p.: 129.0 ºC. MALDI-TOF mass (Matrix: Dithranol): Found m/z = 886.2784, calculated ($C_{56}H_{86}O_4S_2$) 886.60.

Synthesis of compound 6: A 30 mL two-neck flask was charge with compound **5** (300 mg, 0.34 mmol) and PPh_3 (709 mg, 2.70 mmol). The flask was evacuated and re-filled with argon three times. After addition of 3-buten-1-ol (195 mg, 2.70 mmol), THF (0.14 mL) and Diisopropyl azodicarboxylate (DIAD) (547 mg, 2.70 mmol), the mixture was sonicated for 1 hour. Then, after solvent was evaporated, product was purified by column chromatography (silica gel, DCM / hexane = 1 / 3). Compound **6** was obtained as white solid (116 mg, 31 %).
M. p.: 53.3 ºC . ^{1}H NMR ($CDCl_3$, 400 MHz, TMS, 298 K): δ. 0.89 (t, J = 6.8 Hz, 6H), 1.23 – 1.35 (m, 60H), 1.61 (m, 4H), 1.26 (m, 8H), 2.51 (t, J = 8.0 Hz, 4H), 3.65 (m, 4H), 3.75 (m, 4H), 4.97 – 5.04 (m, 8H), 5.70 (m, 4H), 6.12 (s, 4H), 6.82 (d, J = 5.2 Hz, 2H), 7.06 (d, J = 5.2 Hz, 2H). ^{13}C NMR ($CDCl_3$, 100 MHz, TMS, 298 K): δ 14.26, 22.82, 29.48, 29.74, 29.85, 31.54, 32.04, 33.81, 36.88, 67.35, 104.95, 112.38, 116.63, 121.66, 130.05, 132.21, 134.42, 134.93, 143.14, 156.99. MALDI-TOF mass (Matrix: Dithranol): Found m/z = 1102.0250, calculated ($C_{72}H_{110}O_4S_2$) 1102.78.

Synthesis of compound 7: A 1 L 3-neck bound-bottom flask was charged with compound **6** (1.2g, 1.1 mmol), and evacuated and re-filled with argon three times. After addition of dry DCM (540 mL), 2nd generation Grubbs catalyst (46.2 mg, 0.054 mmol) was added. The mixture was stirred at room temperature overnight, and then passed through short silica gel pad to remove catalyst. After solvent was evaporated, product was purified by column chromatography (silica gel, DCM / hexane = 1 / 2.5). Compound **7** was obtained as white solid (1.0 g, 88 %).
M. p.: 107.3 ºC . ^{1}H NMR ($CDCl_3$, 400 MHz, TMS, 298 K): δ 0.88 (t, J = 6.8 Hz, 6H), 1.22 – 1.36 (m, 60H), 1.68 (m, 4H), 2.15 (m, 8H), 2.67 (t, J = 8.0 Hz, 4H), 3.78 (m, 4H), 3.98 (m, 4H), 5.11 (t, J = 3.2 Hz, 4H), 6.54 (s, 4H), 6.73 (d, J = 5.2 Hz, 2H), 6.96 (d, J = 5.2 Hz, 2H). ^{13}C NMR ($CDCl_3$, 100 MHz, TMS, 298 K): δ 14.26, 22.81, 29.44, 29.47, 29.69, 29.83, 31.60, 32.04, 32.71, 36.79, 68.55, 107.96, 114.86, 122.55, 128.43,

129.39, 130.95, 133.86, 145.72, 158.49. MALDI-TOF mass (Matrix: Dithranol): Found m/z = 1046.1474, calculated ($C_{68}H_{102}O_4S_2$) 1046.72.

Synthesis of compound 8: A 500 mL two-neck bound-bottom flask was charge with compound **7** (2.1 g, 2 mmol), and evacuated and re-filled with argon one time. The flask was evacuated and re-filled with hydrogen gas one time. After addition of THF (70 mL), *tert*-Butanol (14 mL) and Wilkinson catalyst (185 mg, 0.2 mmol), the resulting mixture was stirred at room temperature three days, and then, passed through short silica gel pad to remove catalyst. After solvent was evaporated, product was purified by column chromatography (silica gel, DCM / hexane = 1 / 3). Compound **8** was obtained as white solid (2.0 g, 95 %).
M. p.: 114.5 ºC . ^{1}H NMR ($CDCl_3$, 400 MHz, TMS, 298 K): δ 0.88 (t, J = 6.8 Hz, 6H), 0.92 (m, 4H), 1.14 (m, 4H), 1.22 – 1.36 (m, 60H), 1.47 (m, 8H), 1.69 (m, 4H), 2.67 (t, J = 8.0 Hz, 4H), 3.73 (m, 4H), 4.02 (m, 4H), 6.52 (s, 4H), 6.75 (d, J = 4.8 Hz, 2H), 6.96 (d, J = 4.8 Hz, 2H). ^{13}C NMR ($CDCl_3$, 100 MHz, TMS, 298 K): δ 14.26, 22.81, 27.24, 29.44, 29.47, 29.68, 29.83, 30.34, 31.61, 32.03, 36.82, 69.76, 107.64, 114.76, 122.46, 129.61, 131.21, 133.66, 145.74, 158.62. MALDI-TOF mass (Matrix: Dithranol): Found m/z = 1050.1943, calculated ($C_{68}H_{106}O_4S_2$) 1050.75.

Synthesis of compound M_{STB}: A 50 mL brown flask was charged with compound **8** (600 mg, 0.57 mmol). After addition of THF (16 mL), NBS (203 mg, 1.14 mmol) was added at 0 ºC. The resulting mixture was stirred at room temperature for 3 hours, and then, washed with water and extracted with DCM. The organic layer was washed with brine and dried over $MgSO_4$. After solvent was evaporated, product was purified by column chromatography (silica gel, DCM / hexane = 1 / 3). Compound **M_{STB}** was obtained as white solid (600 mg, 87 %).
M. p.: 163.0 ºC . ^{1}H NMR ($CDCl_3$, 400 MHz, TMS, 298 K): δ 0.88 (t, J = 6.8 Hz, 6H), 0.99 (m, 4H), 1.20 – 1.41 (m, 64H), 1.52 (m, 8H), 1.69 (m, 4H), 2.67 (t, J = 8.0 Hz, 4H), 3.73 (m, 4H), 4.06 (m, 4H), 6.49 (s, 4H), 6.69 (s, 2H). ^{13}C NMR ($CDCl_3$, 100 MHz, TMS, 298 K): δ 14.26, 22.81, 27.60, 29.24, 29.48, 29.68, 29.77, 29.83, 30.41, 31.55, 32.04, 36.83, 69.75, 107.33, 110.57, 112.51, 131.58, 131.86, 134.70, 146.71, 158.43. MALDI-TOF mass (Matrix: Dithranol): Found m/z = 1206.9514, calculated ($C_{68}H_{104}Br_2O_4S_2$) 1206.57.

b) Synthesis of monomer M_{NDB}

Synthesis of compound 10: A 50 mL brown flask was charged with compound **9** (563 mg, 0.54 mmol). After addition of THF (15 mL), NBS (96 mg, 0.54 mmol) was added at 0 ºC. The resulting mixture was stirred at room temperature for 3 hours, and then, washed with water and extracted with DCM. The organic layer was washed with brine and dried over $MgSO_4$. After solvent was evaporated, product was purified by

column chromatography (silica gel, DCM / hexane = 1 / 3). Compound **10** was obtained as white solid (430 mg, 71 %).

M. p.: 119.5 ºC . ^{1}H NMR ($CDCl_3$, 400 MHz, TMS, 298 K): δ. ^{13}C NMR ($CDCl_3$, 100 MHz, TMS, 298 K): δ MALDI-TOF mass (Matrix: Dithranol): Found m/z = 1128.0431, calculated ($C_{68}H_{105}BrO_4S_2$) 1128.66.

Synthesis of compound 12: A two-neck 10 mL flask was charged with compound **10** (300 mg, 0.265 mmol), and evacuated and re-filled with argon three times. After addition of dry THF (2 mL), isopropylmagnesium chloride solution (^{i}PrMgCl) (0.133 mL, 2 mol/L, 0.265 mmol) was added at room temperature. The mixture was stirred at room temperature for 1 hour, and resulting in a Grignard solution. In another 30 mL two-neck flask, 5,5'-dibromo-3,3'-dihexyl-2,2'-bithiophene (65 mg, 0.133 mmol) and Pd(dppf)Cl_2 (5 mg, 0.0133 mmol) were placed. The flask was evacuated and re-filled with argon three times. After addition of dry THF (2 mL), Grignard solution was transformed to the flask slowly. The mixture was stirred at 80 ºC overnight, and then, washed with water and extracted with DCM three times. The organic layer was washed with brine and dried over $MgSO_4$. After solvent was evaporated, product was purified by column chromatography (silica gel, DCM / hexane = 1 / 3) and recycling GPC (Column: YMC T2000 + T400 + guard column, eluent: $CHCl_3$, detection: RI). Compound **12** was obtained as organic solid (162 mg, 52 %).

M. p.: 81.8 ºC . ^{1}H NMR ($CDCl_3$, 400 MHz, TMS, 298 K): δ 087 (m, 18H), 0.97 (m, 8H), 1.16 – 1.43 (m, 144H), 1.50 (m, 16H), 1.68 (m, 8H), 2.43 (t, J = 8.0 Hz, 4H), 2.66 (m, 8H), 3.75 (m, 8H), 4.05 (m, 8H), 6.51 (s, 4H), 6.54 (s, 4H), 6.73 (s, 2H), 6.77 (d, J = 5.2 Hz, 2H), 6.85 (s, 2H), 6.98 (d, J = 5.2 Hz, 2H). ^{13}C NMR ($CDCl_3$, 100 MHz, TMS, 298 K): δ 14.25, 22.75, 22.81, 27.40, 29.10, 29.32, 29.41, 29.48, 29.68, 29.83, 30.41, 30.76, 31.62, 31.82, 32.04, 36.79, 36.84, 69.77, 107.38, 107.49, 114.22, 122.98, 123.70, 126.41, 126.69, 129.59, 131.56, 132.01, 132.93, 133.27, 133.38, 138.00, 142.82, 145.92, 146.12, 158.54, 158.64. MALDI-TOF mass (Matrix: Dithranol): Found m/z = 2431.6352, calculated ($C_{156}H_{238}O_8S_6$) 2431.65.

Synthesis of compound M_{NDB}: A 100 mL brown flask was charged with compound **12** (330 mg, 0.14 mmol). After addition of THF (8 mL), NBS (46 mg, 0.26 mmol) was added at 0 ºC. The resulting mixture was stirred at room temperature for 3 hours, and then, washed with water and extracted with DCM. The organic layer was washed with brine and dried over $MgSO_4$. After solvent was evaporated, product was purified by column chromatography (silica gel, DCM / hexane = 1 / 3). Compound **M_{NDB}** was obtained as organic solid (250 mg, 71.2 %).

M. p.: 125.2 ºC . ^{1}H NMR ($CDCl_3$, 400 MHz, TMS, 298 K): δ 087 (m, 18H), 1.00 (m, 8H), 1.25 – 1.40 (m, 144H), 1.52 (m, 16H), 1.69 (m, 8H), 2.42 (t, J = 8.0 Hz, 4H), 2.67 (m, 8H), 3.74 (m, 8H), 4.07 (m, 8H), 6.50 (s, 4H), 6.52 (s, 4H), 6.72 (s, 2H), 6.73 (s, 2H), 6.82 (s, 2H). ^{13}C NMR ($CDCl_3$, 100 MHz, TMS, 298 K): δ MALDI-TOF mass (Matrix: Dithranol): Found m/z = 2587.3320, calculated ($C_{156}H_{238}Br_2O_8S_6$) 2587.48.

4.5 Reference:

[1] Perepichka, I. G.; Perepichka, D. F. *Handbook of Thiophene-Based Materials: Applications in Organic Electronics and Photonics* (John Wiley & Sons, Ltd., **2009**).

[2] Roncali, J. *Chem. Rev.* **2009**, 92, 711.

[3] McCullough, R. D. *Adv. Mater.* **1998**, 10, 93.

[4] Mishra, A., Ma, C. Q.; Bäuerle, P. *Chem. Rev.* **2009**, 109, 1141.

[5] Bao, Z.; Dodabalapur, A.; Lovinger, A. *J. Appl. Phys. Lett.* **1996**, 69, 4108.

[6] Sirringhaus, H.; Brown, P. J.; Friend, R. H.; Nielsen, M. M.; Bechgaard, K.; Langeveld-Voss, B. M. W.; Spiering, A. J. H.; Janssen, R. A. J.; Meijer, E. W.; Herwig, P.; de Leeuw, D. M. *Nature* **1999**, 401, 685.

[7] McCulloch, I.; Heeney, M.; Bailey, C.; Genevicius, K.; MacDonald, I.; Shkunov, M.; Sparrowe, D.; Tierney, S.; Wagner, R.; Zhang, W.; Chabinyc, M. L.; Kline, R. J.; McGehee, M. D.; Toney, M. F. *Nature Mater.* **2006**, 5, 328.

[8] Bronstein, H.; Chen, Z.; Ashraf, R. S.; Zhang, W.; Du, J.; Durrant, J. R.; Tuladhar, P. S.; Song, K.; Watkins, S. E.; Geerts, Y.; Wienk, M. M.; Janssen, R. A. J.; Anthopoulos, T.; Sirringhaus, H.; Heeney, M.; McCulloch, I. *J. Am. Chem. Soc.* **2011**, 133, 3272.

[9] Zhang, X.; Bronstein, H.; Kronemeijer, A. J.; Smith, J.; Kim, Y.; Kline, R. J.; Richter, L. J.; Anthopoulos, T. D.; Sirringhaus, H.; Song, K.; Heeney, M.; Zhang, W.; McCulloch, I.; DeLongchamp, D. M. *Nature Commun.* 2013, 4, 2238.

[10] Noriega, R.; Rivnay, J.; Vandewal, K.; Koch, F. P. V.; Stingelin, N.; Smith, P.; Toney, M. F.; Salleo, A. *Nature Mater.* **2013**, 12, 1038.

[11] Venkateshvaran, D.; Nikolka, M.; Sadhanala, A.; Lemaur, V.; Zelazny, M.; Kepa, M.; Hurhangee, M.; Kronemeijer, A. J.; Pecunia, V.; Nasrallah, I.; Romanov, I.; Broch, K.; McCulloch, I.; Emin, D.; Olivier, Y.; Cornil, J.; Beljonne, D.; Sirringhaus, H. *Nature*, **2014**, 515, 384.

[12] Sugiyasu, K.; Honsho, Y.; Harrison, R. M.; Sato, A.; Yasuda, T.; Seki S.; Takeuchi, M. *J. Am. Chem. Soc.* **2010**, 132, 14754.

[13] Shomura, R.; Sugiyasu, K.; Yasuda, T.; Sato, A.; Takeuchi, M. *Macromolecules* **2012**, 45, 3759.

[14] Pan, C.; Sugiyasu, K.; Aimi, J.; Sato, A.; M. Takeuchi, *Angew. Chem. Int. Ed.* **2014**, 53, 8870.

[15] Frampton, M. J.; Anderson, H. L. *Angew. Chem. Int. Ed.* **2007**, 46, 1028.

[16] Pan, C.; Zhao, C.; Takeuchi, M.; Sugiyasu, K. *Chem. Asian J.* **2015**, 10, 1820.

[17] Woo, C. H.; Thompson, B. C.; Kim, B. J.; Toney, M. F.; Fréchet. J. M. J. *J. Am. Chem. Soc.* **2008**, 130, 16324.

[18] Asawapirom, U.; Scherf, U. *Macromol. Rapid Commun.* **2001**, 22, 746.

[19] Osaka, I.; McCullough, R. D. *Acc. Chem. Res.* **2008**, 41, 1202.

[20] Kim, J.-S.; Kim, J.-H.; Lee, W.; Yu, H.; Kim, H. J.; Song, I.; Shin, M.; Oh, J. H.; Jeong, U.; Kim, T.-S.; Kim, B. J. *Macromolecules* **2015**, 48, 4339.

Chapter 5 Conclusions and Perspectives

5.1. Conclusions

In this thesis, a series of thiophene-based conjugated polymers were described: (1) twisted poly(3-substituted thiophene)s; (2) picket-fence polythiophenes; and (3) self-threading polythiophenes. Through those molecular design, we can establish and control the structural parameters: dihedral angle, dielectric constants, and regioregularity. Upon extensive characterization of the physical and electrical properties of these unique polymers, the structure-properties relationships were clearly demonstrated.

In chapter 2, twisted poly(3-substituted thiophene)s were synthesized through cyclopolymerization. This is the first attempt of polythiophene synthesis through cyclopolymerization. One important structural parameter, the dihedral angle, can also be dictated by monomer design. As a consequence, photophysical properties of polythiophene could be modulated.

In chapter 3, new picket fence polythiophenes based on a 7-spiro(9-fluorenyl)-cyclopentadithiophene (SFT) framework were synthesized. Despite the bulky side chains, well-developed conjugation was achieved as demonstrated by the oligomer studies. The dielectric sheaths can be altered in this new molecular design, thereby allowing the properties of the charge carriers generated in IMWs to be modulated. A highly doped state of insulated polythiophene can be stabilized using sheaths with a high dielectric constant even in the absence of interchain delocalization.

In chapter 4, new self-threading polythiophenes in which the structural defect was intentionally introduced were synthesized successfully. The defect copolymer backbone were isolated and interchain π–π interaction was effectively prevented. Even 1% structural defect deteriorates the electronic property of polythiophene, which lead to the decrease of the effective conjugation length. Block copolymers were obtained despite using the polycondensation reaction.

The study on these thiophene-based materials not only improves the understanding on the nature of charge carriers, but also paves the way to new molecular design around polythiophene backbone for device application.

5.2. Perspectives

5.2.1 Polaronic ferromagnetism

In 1986, Fukutome *et al.*[1] deisgned a class of ferromagnetic conjugated polymers. These polymers have no built-in radicals, but spins are generated by doping. The structure of a polymeric ferromagnet may be conceptually broken down into two components: spin containing units (SC) and ferromagnetic coupling units (FC) that ensure high-spin interactions between SCs (Figure 5-1).

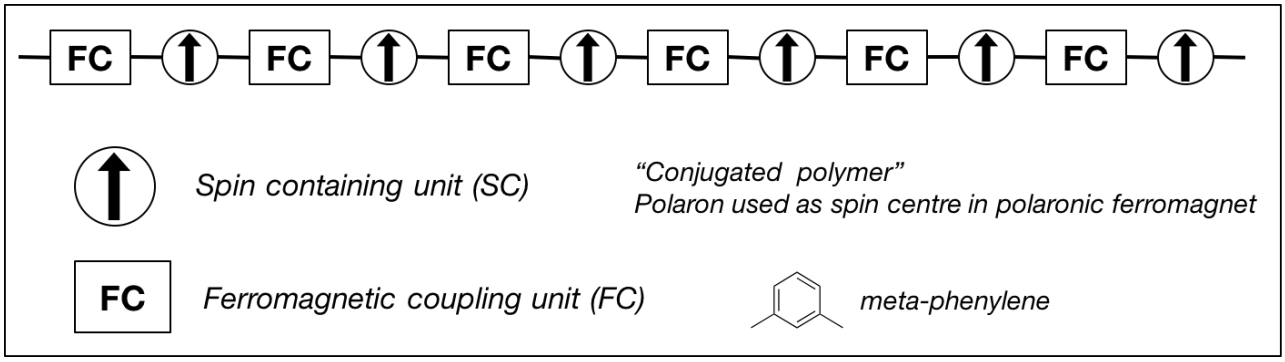

Figure 5-1. Schematic design for high-spin polymers. In the polaronic ferromagnet the SC is a polaron.

As is well known, polythiophenes (PTs) are stable under both doped state and undoped state. PTs are good candidate for the polaronic ferrimagnetism material. In 1994, Dougherty *et al.*[2] designed and synthesized many different PTs that are considered one-dimensional prototypes for the polaronic ferromagnet. They found that interchain interactions limit the high spin properties. He suggested that to "insulate" the chains from one another by adding bulky groups. In 1998, Tanaka *et al.*[3] also designed and synthesized PT for polaronic ferromagnet. They found their oxidized PT is suitable as a ferromagnetic polymer at least without consideration of interchain antiferromagnetic coupling. Therefore, polaron generation and limited interchain interaction should be satisfied in one molecule. To this end, we designed new insulated polythiophenes as polaronic ferromagnetism material (Scheme 5-1).

According to our study, we using insulated molecular wire method to isolated the polymer backbone. We observed the forming process of polaron, polaron pair, bipolaron by other PTs. Through controlled over doping level, we can selectively to form polaron. Due to the insulated layer, the interchain interactions are greatly limited. Therefore, polaron will be stable in insulated PT wire.

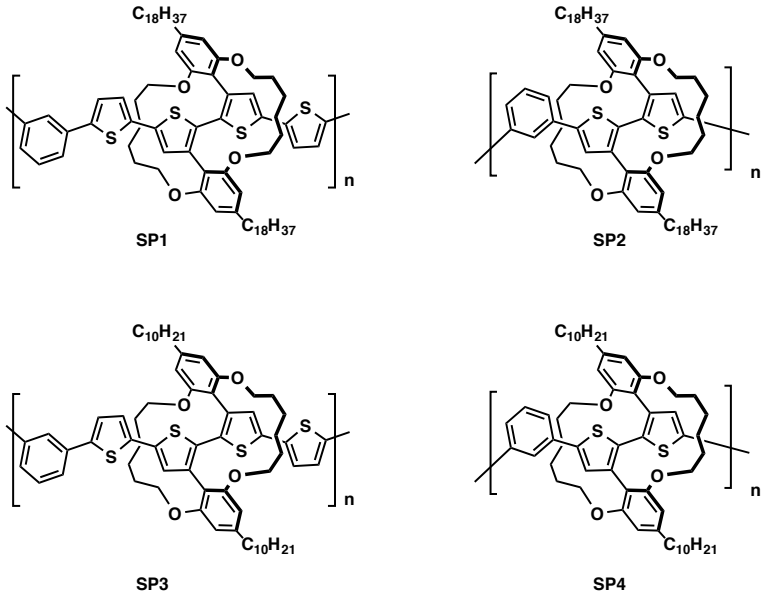

Scheme 5-1. Chemical structure of polaronic ferromagnetic polythiophenes.

Through Suzuki–Miyaura coupling polymerization method, different polaronic ferromagnetism polythiophenes were obtained. According to GPC results, molecular weight of **SP3** and **SP4** are relatively low (PS as standard). This may due to the steric hindrance caused by bukly insulated layers. By comparsion, **SP1** and **SP3** showed good molecular weight.

With those polymers in hand, magnetic properties can be characterized in future. And new molecules for polaronic ferromagnet were under design.

5.2.2 Molecular wire with unsheathed heads

Insulated molecular wires (IMWs) are conjugated polymers which are molecularly sheathed with an insulating layer, thus structurally analogous to electric power cord in nanoscale.[4,5] To employ IMW in molecular electronics, its termini have to be unsheathed for contacts (Figure 5-2a). In scanning tunneling microscopy (STM) break junction,[6,7] the unsheathed thiophene moieties at both ends were used as anchoring points to the electrodes, thus enabling the single molecule conductance measurements. However, in the case of polymer structures, such a precise molecular design is synthetically challenging.

Here, in our study, we succeeded in the synthesis of IMWs of which both the termini are unsheathed (Figure 5-2b). The synthetic protocol is straightforward to achieve the block copolymer structures despite using the polycondensation reaction. As these termini are expected to have a better contact to electrodes, and each block could be distinguished by AFM, our future challenge is now directed to characterize this IMW, for example, by using multiprobe STM technique.

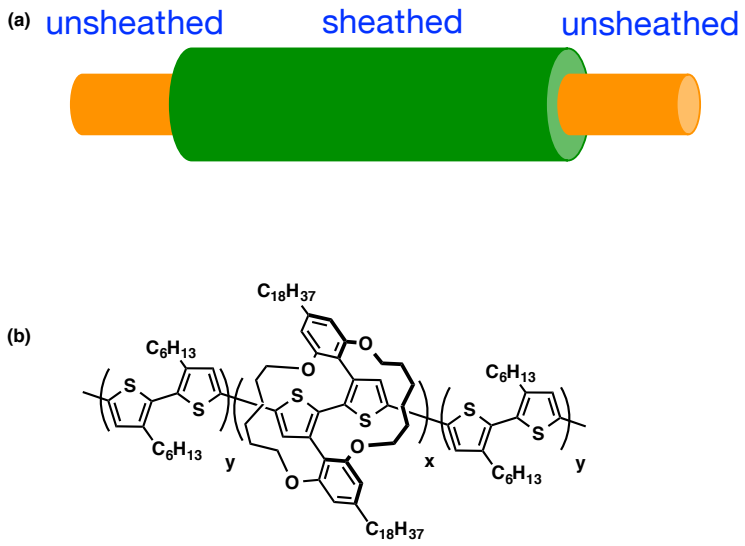

Figure 5-2. (a) model of unsheathed insulated molecular wire. (b) chemical structure of unsheathed insulated molecular wire

5.3 References

[1] Fukutome, H.; Takahashi, A.; Ozaki, M. *Chem. Phys. Lett.* **1987**, 133, 34.

[2] Murray, M. M.; Kaszynski, P.; Kaisaki, D. A.; Chang, W.; Dougherty, D. A. *J. Am. Chem. Soc.* **1994**, 116, 8152.

[3] Sato, T.; Hori, K.; Tanaka, K. *J. Mater. Chem.* **1998**, 8, 589.

[4] Frampton, M. J.; Anderson, H. L. *Angew. Chem. Int. Ed.* **2007**, 46, 1028.

[5] Pan, C.; Zhao, C.; Takeuchi, M.; Sugiyasu, K. *Chem. Asian J.* **2015**, 10, 1820.

[6] Kiguchi, M.; Ohto, T.; Fujii, S.; Sugiyasu, K.; Nakajima, S.; Takeuchi, M.; Nakamura, H. *J. Am. Chem. Soc.* **2014**, 136, 7327.

[7] Yamada, R.; Kumazawa, H.; Noutoshi, T.; Tanaka, S.; Tada, H. *Nano Lett.* **2008**, 8, 1237;

Major achievements of this thesis are as follows

List of Publications

[1] "Conjugated Oligomers and Polymers Sheathed with Designer Side Chains"
C. Pan, C. Zhao, M. Takeuchi,* and K. Sugiyasu* *Chem. Asian J.* 2015, 10 (9), 1820-1835.
Focus Review, **Highlighted as Frontispiece of the issue**

[2] "Twisting poly(3-substituted thiophene)s: cyclopolymerization of gemini thiophene monomers through catalyst-transfer polycondensation"
C. Zhao, K. Nagura, M. Takeuchi,* and K. Sugiyasu* *Polymer J.* in press

[3] "Stabilization of Charge Carriers in Picket-Fence Polythiophenes Using Dielectric Side Chains"
C. Zhao, T. Sakurai, S. Yoneda, S. Seki,* M. Sugimoto, C. Oki, M. Takeuchi,* and K. Sugiyasu* *Chem. Asian J.* in press

[4] "Synthesis of Unsheathed Insulated Molecular Wires"
C. Zhao, M. Takeuchi,* and K. Sugiyasu* *Chem. Lett.* accepted for publication.

Presentations at Conferences

[1] "Twisting Polythiophene Backbone through Cyclopolymerization of Gemini Thiophene Monomers"
C. Zhao, K. Sugiyasu,* and M. Takeuchi*
NIMS Conference 2013, Tsukuba, Jul. 1st – 3rd 2013, **Poster**

[2] "Stabilizing charge carriers in dielectric picket-fence polythiophenes"
C. Zhao, K. Sugiyasu,* and M. Takeuchi*
The 11th International Conference on Advanced Polymers via Macromolecular Engineering (APME 2015), Yokohama, Oct. 18th- 22nd 2015, **Poster**

Acknowledgments

The author would like to express his deepest respect and appreciation to Professor Masayuki Takeuchi for his financial support, advice, and encouragement throughout this study. The author also would like to express his great respect and appreciation to Associate Professor Kazunori Sugiyasu for his advice, encouragement in the past four years.

The author would like to thank committee members, Professor Kazushi Miki, Professor Masanobu Naito, Professor Yohei Yamamoto for reviewing my thesis and their constructive suggestions.

The author would like to thank Professor Shu Seki, Dr. Tsuneaki Sakurai at Kyoto University and Mr. Satoru Yoneda at Osaka University for their cooperation on conductivity measurements. The author would like to thank Associate Professor Manabu Sugimoto at Kumamoto University and Dr. Kazuhiko Nagura at National Institute for Materials Science (NIMS) for their cooperation on electronic structure calculations. The author would like to thank Dr. Akira Sato, and Dr. Yoshitaka Matsushita at NIMS Materials Analysis Station for crystal structure analysis. The author would like to thank Mr. Choji Oki at Nagaoka University of Technology for his effort on the synthesis of polythiophenes. The author would like to thank Dr. Takashi Minowa, Dr. Taro Takemura and Dr. Jie Li at NIMS Molecule & Material Synthesis Platform for their help and NMR measurements.

The author would like to thank Dr. Takashi Nakanishi, Dr. Yuka Kobayashi, Dr. Junko Aimi, Dr. Atsuro Takai, Dr. Fengniu Lu, Dr. Krishinan K. Kartha at NIMS and Dr. Chengjun Pan at Shenzhen University for their constructive suggestions and valuable discussions in research field. The author also would like to thank all the members in Molecular Design & Function Group at NIMS for their kind help and discussions.

Finally, the author would like to express his deepest appreciation to his family, Mr. Kuangru Zhao, Ms. Jiujiu Zeng, for all their support, help and love.

August 2016

Tsukuba, Japan

Chunhui Zhao

Doctoral Program in Materials Science and Engineering

Graduate School of Pure and Applied Sciences

University of Tsukuba